INTERCONNECTION OF SOLAR POWER TO THE GRID THROUGH THE POWER PLANT AUXILIARY SYSTEM

Nkululeko Mazibuko

In fulfillment of the Masters in Electrical Engineering
College of Agriculture, Engineering and Science,
University of KwaZulu-Natal

31 July 2015

Akshay Kumar Saha

As the candidate’s Supervisor I agree/do not agree to the submission of this thesis.

Akshay Kumar Saha……..

Date……

DECLARATION 1 - PLAGIARISM

I …Nkululeko Ntuthuko Mazibuko.., declare that

1. The research reported in this thesis, except where otherwise indicated, is my original research.

2. This thesis has not been submitted for any degree or examination at any other university.

3. This thesis does not contain other persons' data, pictures, graphs or other information, unless specifically acknowledged as being sourced from other persons.

4. This thesis does not contain other persons' writing, unless specifically acknowledged as being sourced from other researchers. Where other written sources have been quoted, then:

a. Their words have been re-written but the general information attributed to them has been referenced

b. Where their exact words have been used, then their writing has been placed in italics and inside quotation marks, and referenced.

5. This thesis does not contain text, graphics or tables copied and pasted from the Internet, unless specifically acknowledged, and the source being detailed in the thesis and in the References sections.

Signed

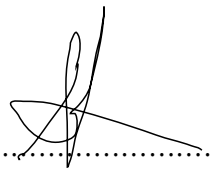

……

DECLARATION 2 - PUBLICATIONS

DETAILS OF CONTRIBUTION TO PUBLICATIONS:

Publication:

N. Mazibuko and A. Saha "Interconnection Of Photovoltaic Sources Into The Eskom Power Station Auxiliaries - Modelling And Perfomance Analysis," in *SAUPEC*, Johannesburg, 29 January 2015

N. Mazibuko and A. Saha " Dynamic analysis of photovoltaic plant using custom modelled pv system," in *SAUPEC*, vaal, 26-28 January 2016

N. Mazibuko and A. Saha “modelling and simulation of grid-connected photovoltaic systems," in *SAUPEC*, vaal, 26-28 January 2016

N. Mazibuko and A. Saha “study of photovoltaic intregration impact on eskom power station distribution system using custom modelled pv system," in *SAUPEC*, vaal, 26-28 January 2016

Signed:

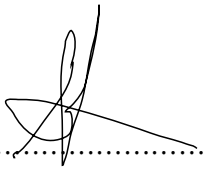

……

ACKNOWLEDGEMENTS

I wish to extend my gratitude to:

- My supervisor Dr Saha for providing me with the opportunity to pursue my Masters Degree and for the constant support, honest opinion and guidance throughout this research period.
- Eskom for the opportunity given to me to pursue a Masters Degree
- All my friends and colleagues especially N Masela & G Dumakude for the encouragements.
- My family for their support, patience and their best wishes.
- My son Ntokozo giving me inspiration to work harder each day
- Most of all, the one above for his wisdom and making everything possible.

ABSTRACT

In this thesis, an improved mathematical model based on classical equations and control approach for the photovoltaic system is developed and implemented using a pulse width modulation as the interfacing. The functionality of the developed model with the inclusion of a maximum power point tracking is verified against the generic model in Power Factory library which is constrained by assumptions, such as: no maximum power point tracking and uses static generator as the interfacing converter but gives an acceptable basic understanding of photovoltaic operation. The new improved mathematical model characterizes the solar cell with sufficient degree of precision with a percentage error of 0.03% measured in comparison with experimental data. The developed photovoltaic system under established control fulfils the operational requirements for a grid-connected photovoltaic system according to the South African Grid Code. Based on the developed mathematical model, various studies are performed, such as: steady-state and transient analysis to ascertain the impact of photovoltaic system integration with the power station reticulation system. The effects are analyzed with the photovoltaic system connected on the 11 kV bus bar which is the closest point to the generator to simulate an extreme circumstance. Case studies to demonstrate the photovoltaic effect on the reticulation system are evaluated for voltage stability and local generator behavior. Apparent features of the photovoltaic system such as the rapid power variation due to atmospheric changes (irradiance and temperature), tripping the photovoltaic system and simulating an electrical fault are implemented with various photovoltaic penetration levels. The results provided practical insight on the feasibility of interconnecting photovoltaic system to power station auxiliary network. Results illustrated at steady state the benefits of the generation capacity to be reduced relatively to photovoltaic penetration level and reactive power control which assist in supporting voltage during voltage dips at the point of connection and lastly the photovoltaic inverter presented the ability to limits/control fault current to about 1.5 p.u. which is lower than the 4 - 10 p.u. fault current typically caused by rotating machines. Transient studies discovered that the changes in atmospheric conditions do not impose stability threats but increased photovoltaic penetration level will increases the risk of generator becoming unstable during abnormal situations.

Table of Contents

List of Figures

List of tables

NOMENCLATURE

PV	Photovoltaic
DC	Direct current
AC	Alternative Current
SWH	Solar Water Heating
MPPT	Maximum Power Point Tracking
IncCond	Incremental Conductance
P&O	Perturbation & Observation
SAGC	South African Grid Code
DSL	DigSilent Simulation Language
EMF	Electron Motive Force
PLL	Phase Locked Loop
THD	Total Harmonic Distortion
CSI	Current Source Inverter
VSI	Voltage Source Inverter
PWM	Pulse Width Modulation
LF	Low Frequency
HF	High Frequency
UPS	Uninterrupted Power Supply
RPPS	Renewable Power Plants
DS	Distribution System
TS	Transmission System
SO	System Operator
POC	Point Of Connection
PF	PowerFactory
STC	Standard Test Condition
PS	Power Station
NIPS	National Interconnected Power Systems

CHAPTER 1
INTRODUCTION

1.1 Background

In the last decade, solar energy has emerged as a promising resource of green energy alternative to non-renewable energy resources. Solar energy is probably the strongest growing electricity generation technology, demonstrating recent annual growth rates of around 23% and worldwide production of 32-34 GW in 2012 and in 2013 an addition of more than 39 GW production which resulted a total exceeding 139 GW consisting of both grid-connected and off-grid remote power supplies [1]. Photovoltaic is starting to play a substantial role in electricity generation in some countries, particularly in Europe, while lower prices are opening new markets from Africa and the Middle East to Asia and Latin America [2].

Global warming awareness is the main drive in renewable energy sources and has brought about policy agreements that have been signed by countries (i.e. Kyoto, Copenhagen and Durban) to reduce the global warming. Policy targets accelerated the development of renewable energy technologies [3]. Renewable energy targets take many forms, although the majority continues to focus on the electricity sector, targets for renewable heating and cooling in South Africa is to provide fully subsidized Solar Water Heating (SWH) to low-income households, and aims to award contracts through competitive tendering for the manufacturing of 650,000 individual SWH by 2015. Moreover, target for transportation is becoming an important tool for policymakers. Other forms of targets include renewable shares of primary and final energy, as well as capacities of specific renewable technologies or their energy output. Targets more often focus on a specific future year for expanding energy access. While some countries have met targets for the year 2013, others have failed to meet their targets by years end. A goal target set by South Africa to generate 10,000 GWh of renewable electricity by the year 2013 was not achieved and postponed to 2015 [2].

Most areas in South Africa average more than 2 500 hours of sunshine per year, and average solar-radiation levels range between 4.5 and 6.5 kWh/m^2 in one day. The Southern African region, and in fact the whole of Africa, has sunshine all year round. The annual 24-hour global solar radiation average is about 220 W/m^2 for South Africa compared with about 150 W/m^2 for

parts of the USA, and about 100 W/m^2 for Europe and the United Kingdom. This makes South Africa's local resource one of the highest in the world.

The use of solar energy is the most readily accessible resource in South Africa and it is readily available for a number of potential uses more so because the country's solar-equipment industry is developing.

Annual photovoltaic (PV) panel-assembly capacity totals 5 MW [4]. The PV technology is one of the best ways to harvest the solar energy since PV requires very little maintenance and is capable of giving output from microwatts to megawatts.

However, it is worth noting that each energy technology whether renewable, alternative or traditional has both advantages and disadvantages which are mentioned below for solar cell.

Advantages of Solar Energy

Solar energy fuel source is sunlight which is free and it is indefinite thus reliable. Solar panels require little maintenance and do not require any type of mechanical parts that can fail. Solar panels produce zero emissions of carbon dioxide, other greenhouse gas emissions or conventional pollutants.

Disadvantages of Solar

The obvious disadvantage of solar power is that it cannot be created during the night and to utilize battery storage is an expensive solution considering battery maintenance and life cycle. The power generation is also reduced or fluctuates during cloudy days. The efficiency of the solar is relatively low and this means a large amount of surface area is required to produce adequate electricity.

1.1.1 Photovoltaic system

1.1.1.1 Solar cell characterization

Solar cell is simply a p-n junction diode, where a diode is formed by forming a junction between the n-type and p-type region. As sunlight strikes a solar cell, the incident energy is converted directly into electrical energy [5]. The illuminated solar cell generates excess electron-holes pairs throughout the semiconductor material; hence dc current will flow [6].

1.1.1.2 Grid connected PV system

Directly connecting a PV array to the grid has compatibility problems with grid frequency. Therefore an interface mechanism to convert dc output from PV to ac output synchronized with the grid is necessary. The interface mechanism is a typical DC-AC converter (inverter) which inverts the DC output current from the PV array into a synchronized sinusoidal waveform [7]. Another challenge is the matching of power extraction from sun with the load. PV array is a nonlinear system that is influenced by solar irradiation and weather conditions. To match the nonlinear output, a maximum power point tracking (MPPT) technique is implemented and it keeps the grid-connected system to operate at maximum power point. The MPPT algorithm is applied inside the inverter controls; therefore, the grid-connected PV system efficiency is increased [7].

1.1.1.3 Inverters

Depending on the demand of load, rating of PV system, selecting a proper inverter for a particular application also depends on the waveform requirements of the load and the efficiency of the inverter. Inverter selection will also depend on whether the PV system is grid-connected system or a stand-alone. Further discussions of available inverters are found as the thesis progresses.

1.1.1.4 Maximum power point tracker

As mentioned earlier the PV has a non-linear property which varies with the atmosphere, load and altitude, considering these variations, there is necessity to identify and track the P-V characteristics of a PV generator at the point where maximum power is transferred. A reliable technique to track the maximum power point irrespective of the environmental conditions is necessary. The tracking system operates by adjusting the inverter voltage reference and the dc voltage at the output of the PV array to achieve maximum output power (refer to P-V curve). A number of MPPT techniques have been developed and a few will be discussed in the literature, such as popular ones being incremental conductance and P&O (Perturbation & Observation method).

1.2 Purpose of investigation

Eskom's strategy to go green is diversification of the generation-mix to lower carbon emitting technologies, increasing efficiency by measures to reduce demand, greenhouse gas and other emissions through the adoption of renewable technology. Therefore, it is important to

integrating renewable sources (photovoltaic plants, hydro turbine and wind) into the Eskom power station electrical auxiliary system. The potential of renewable sources to be integrated to Eskom power stations require research or studies to confirm the hypothesis of improving the reliability, availability and optimize the operation of local generation to which will reduce emissions. The power generated by a solar photovoltaic is strongly dependent on climate conditions. For this reason, a system operator needs a good understanding of the PV response due to solar irradiance and temperature variations, therefore study models to accurately simulate the instability associated with the renewable sources needs to be developed and evaluated to determine the impact on the utility. Currently Eskom does not have renewable energy data base in Digsilent software to perform system studies, and therefore the impact to the power station operation and associated risks are not fully known. This research will evaluate the integration impact of PV system with the hypothesis of optimizing generation efficiency to reduce emissions and thus improving the reliability and availability of Eskom's auxiliary network. The following key questions are to be addressed:

- What will be the impact of integrating renewables into the power station auxiliary network (negative & positive) in terms of plant operation, protection & maintenance?
- How will the variation problems of solar & wind energy affects the stability of the power station auxiliary network?
- What are the associated risks?

1.3 Objectives of this Thesis

- Conduct a literature review of photovoltaic system, MPPT & Inverter.
- Develop an improved accurate photovoltaic model that can be used to accurately simulate PV connected to power station reticulation network.
- Verify and test the model controls for grid compliance
- Determine and analyze the impact of connecting the PV system to the power station reticulation taking into account plant operation & control.
- Perform steady state and transient studies on existing power station reticulation system with various solar PV system ratings from 100 KW to 50 MW.
- Study the impact of voltage stability, reactive power control, and local generator behavior.

The developed PV model is to be connected to a typical Eskom power station to supply the power station auxiliary network. Various studies are to be performed, such as: steady-state and

transient analysis to ascertain the behavior of PV system at various disturbances to identify any stability risks. Impact studies such as fault analysis, voltage fluctuation, frequency and atmospheric changes of irradiance and temperature are performed. The voltage & reactive power control will be developed which will comply with SAGC requirement. Evaluation of a suitable rating of PV system and point of connection will be carried out.

1.4 Scope of Work

The equation to describe the solar cell characteristic is nonlinear thus; numerical techniques to solve for I-V curve have been implemented to be able to extract accurately the unknown data for generalized solar cell under varying weather conditions. Simulation tools such as INSEL & PVsyst etc. are excellent in solving PV circuit network which are dedicated software tools unlike conventional power system engineering software available for Eskom: PowerFactory DigSilent software does not solve simultaneous nor iterations equations but it is flexible providing a coding feature DigSilent Simulation Language (DSL) which will be utilized to characterize PV cell. A user defined model of PV module interfacing with PWM converter and control are to be established.

A mathematical model of a photovoltaic system that is interfaced with power station electrical auxiliary network is modelled based on basic theory and modelling methods reviewed, and is implemented in simulation tool. The supporting system to the PV; MPPT and inverter are implemented based on discovered theory from reviewed literatures. The grid integration requirements influence the control part of the developed PV model in order for the PV to be successfully connected thereby internal & external controls are established in line with these requirements. The different methods used to model the PV system are verified mathematically and then implemented in PowerFactory. Various tests and evaluations are displayed to measure the PV system accuracy to ensure reliability of results. Further testing of the developed PV system is done for grid compliance in accordance to South African Grid Code (SAGC). The impact of the PV system is modelled connected to the Kendel power station electrical auxiliary network, the following are studies accomplished; load flow, fault level and contingency analysis and stability. The connecting bus is the 11 kV busbar of the reticulating system which is the closest bus to the generator. Thus power deviation of the PV system will have an effect on the power flow stability of the power station auxiliary network. Therefore, impact studies of rapid power variation of the PV system due to changes of irradiance and temperature, tripping the PV system and simulating three phase fault accomplished to give an understanding of connecting

the PV system. The dynamic analysis illustrated the stability impact of the PV system and the responses indicate penetration level of the PV system has a great effect on stability.

1.5 Limitations

In the thesis, due to the broadness of the subject, several limitations are outlined:

- No study is carried out in determining suitable choice of an inverter according to the PV systems arrangement.
- The PV inverter is single-stage; there is no DC-DC boost converter involved and no studies done concerning double-stage inverters.
- No power quality studies (e.g. harmonics) are performed.

1.6 Project outline

Chapter 2 gives an overview of PV system; MPPT, Inverters and auxiliary network. The general photovoltaic systems as well as electrical characteristics of PV cell are discussed considering mathematical modelling options based on a number of proven techniques. The available MPPT techniques are discussed and compared. The different classification of inverter configurations with respect to power output and the internal topology (CSI & VSI) is discussed and finally typical power station auxiliary network is shown and discussed along with requirements for the PV integration to the grid.

Chapter 3 is dedicated to explaining in detail the modelling of the PV plant. Modelling methodology based on solar cell equivalent circuit and equation is discussed. Implementation of the developed model and further validation is done in simulation tool in this case PowerFactory by various case studies with suitable controls.

Chapter 4 discusses the modelling of two MPPT controls namely P&O and IncCond. The compliance of the PV controls is tested against SAGC. Steady state and dynamic analysis are done to evaluate the PV system behaviour standing alone and when integrated to the auxiliary network studying different cases.

Chapter 5 is assigned for dynamic analysis looking at various PV penetration levels and analysing different cases such as irradiance change, PV system tripping and during fault scenarios and the results of the generator power, Load angle, frequency and PV power output are obtained to determine the stability.

Chapter 6 summarizes the discussion and conclusion drawn from this research project and it also outlines the possible future work.

CHAPTER 2

OVERVIEW OF GRID-CONNECTED PHOTOVOLTAIC SYSTEM

This chapter introduces a mathematical model of a photovoltaic system that is interfaced with power station electrical auxiliary network. A basic theory and modelling methods of photovoltaic are reviewed based on the equivalent circuit and scientific equations. The supporting system to the PV system such as MPPT and inverter will be reviewed and discussed. The grid integration has requirements that will influence the control part of the developed PV model in order for the PV to be successfully connected therefore, grid requirement is outlined. Later on further chapters the derived model will be evaluated under arbitrary environmental operational conditions.

2.1 Operating principle of photovoltaic effect

The solar cell operating principle is based on the photovoltaic effect [6]. In general the photovoltaic effect means the generation of potential different at the P-N junction, as the photons are absorbed, hole-electron pairs may be formed, when these charge carriers reach the P-N junction the electric field in the depletion region will push the holes into the p-side and push electrons to the n side as shown in Figure 2-1 [6] [8]. When light is absorbed by matter, photons are given up to excite electrons to higher energy states within the material (the energy difference between the initial and final states is given by ***h***+) as shown in Figure 2-1 [9], which shows the internal field. Particularly, this occurs when the energy of the photons making up the light is larger than the forbidden band gap of the semiconductor [9] [10]. But the excited electrons relax back quickly to their original or ground state. In a photovoltaic device, there is a built-in asymmetry (due to doping) which pulls the excited electrons away before they can relax, and feeds them to an external circuit. The extra energy of the excited electrons generates a potential difference or electron motive force (EMF). This force drives the electrons through a load in the external circuit to do electrical work as shown in Figure 2.1 [6]. The summarized processes of photovoltaic effect are [11]:

- Generation of the charge carriers due to absorption of photons in the material that forms a junction,
- Subsequent separation of the photon generated charge carriers in the junction,
- Collection of the photo-generated charge carriers at the terminals of the junction.

Basically in layman's terms light knocks loose electrons from silicon atoms and freed electron get energy then gets pushed by the internal electric field to the terminals creating current flow and this phenomenon is known as photovoltaic effect and never run out of electrons as shown in Figure 2-1 [6] [8] [9] [10].

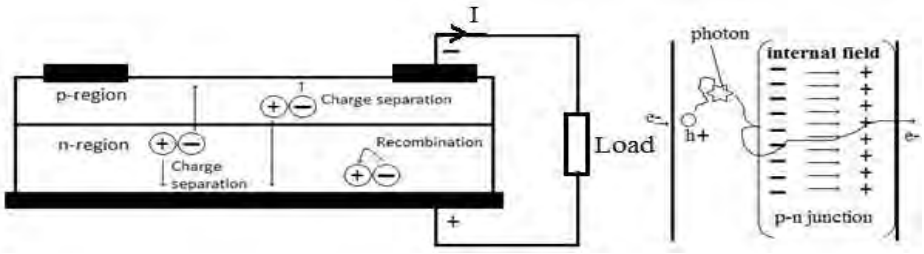

Figure 2-1: Process in an irradiated solar

2.2 Electrical characteristics of Photovoltaic

Photovoltaic models can be classified into various types as shown in Figures 2-2 & 2-3 the simplest one being the single diode model shown in Figure 2-2 (a). It is described with a single diode which the modified Shockley diode equation is incorporating n (the ideality factor) to account for the recombination mechanism that occurs in the P-N junction, represented as anti-parallel diode to the current source [6]. The simplicity of this model compromises the accuracy of PV cell especially at maximum point [12]. The evolved model with the added series resistor improves the model to (4-p). The equivalent solar characteristic is shown in Figure 2-3 b) but the (4-p) model accuracy is not adequate for the intended study [13]. Thus, further evolution of the single diode model to a (5-p) model is shown on Figure 2-3 c) which is described by equation (2.1) [6] [13] [14], and it is the commonly used model for conducting studies as it is fairly accurate in comparison to experimental data [14]. Review summaries of the equivalent models are further described below and reasoning to justifying a model to be implemented used in this thesis.

$$I = I_{ph} - I_d - I_p = I_{ph} - I_0\left(e^{\left(\frac{V+IR_s}{nV_t}\right)} - 1\right) - \frac{V+IR_s}{R_p} \qquad (2.1)$$

2.3 Electrical description of solar cell

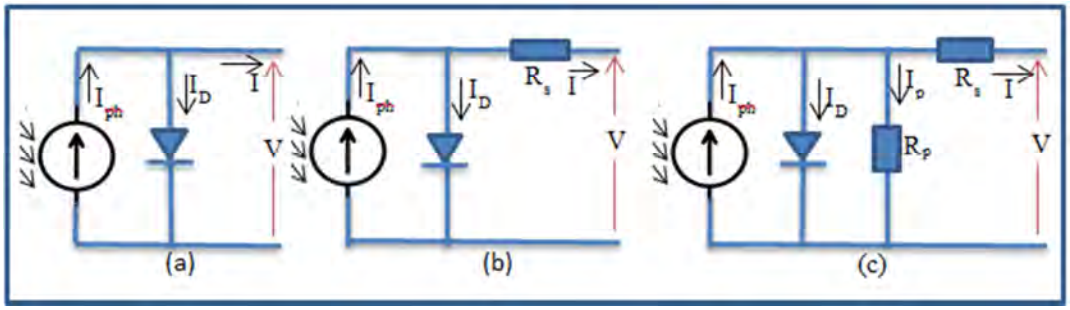

Figure 2-2: The equivalent circuit of a solar cell: a) ideal single diode model b) 4-p model c) 5-p models

2.3.1 Ideal model

An ideal PV cell is modelled as an ideal current source and a diode connected anti parallel. Based on the Shockley theory, recombination in the space-charge zone can be ignored and therefore the second diode can be omitted [15]. This is the simplest form which does not take into account the internal electrical losses of series and parallel resistance [16]. Based on the Shockley and Queisses diode equation, the mathematical model of this ideal PV cell is shown by equation (2.2) [16].

$$I = I_{ph} - I_d = I_{ph} - I_0\left(e^{V/V_t} - 1\right) \tag{2.2}$$

where I_{ph} is the photocurrent, I_d is the diode current given by equation (2.3) [15] [16] , V is the input voltage imposed on the diode,

$$I_d = I_0\left[e^{\left(\frac{V}{nV_t}\right)} - 1\right] \tag{2.3}$$

2.3.2 4-p model

One diode (4-p) model is shown in Figure 2-2 b) [17] [18], in which the parallel resistance is assumed as infinite and is not considered. The four parameters from which its name is obtained having four unknown parameters*:* I_{ph}, I_0, n & R_s. The 4-p model can be obtained by Equation (2.4) [19] [20] as follows:

$$I = I_{ph} - I_d = I_{ph} - I_0\left[e^{\left(\frac{V+IR_s}{nV_t}\right)} - 1\right] \tag{2.4}$$

From previous studies [20] & [21] have explored the 4-p model which neglects the parallel resistance has been discovered to be inadequate compared with experimental data from I-V and P-V curve. Further in [22] the 4-p model was proposed and implemented into a transient simulation program TRNSYS [23]. And the two models the 4-p and 5-p models were compared in [19] [20] [24] and it was learned that the 4-p model demonstrated unsatisfactory results compared to experimental results, the comparison results showed the 5-p model to display an improved accuracy compared to 4-p model.

2.3.3 5-p model

The five parameters from which it gets the name are: I_{ph}, I_0, n, R_s & R_p. The equivalent circuit for one diode 5-p model is shown on Figure 2-3 c), applying Kirchhoff law yield equation (2.4) [19] [20].

$$I = I_{ph} - I_d - I_p = I_{ph} - I_0\left(e^{\left(\frac{V+IR_s}{nV_t}\right)} - 1\right) - \frac{V+IR_s}{R_p} \tag{2.4}$$

The 5-p model is the widely used PV cell model as its accuracy is fairly precise to measured characteristics with only a small percentage error [24]. The improved accuracy lies with the included parallel resistance. It has been widely discussed that the series and parallel resistance influence the characteristics of a PV cell, where the parallel resistance reduces the output current and the series resistance reduces the output voltage of PV cell [6]. This illustrates that the single diode 5-p model is a sufficient model to consider in this thesis but further development of the model in order to achieve accurateness of model is reviewed below comprising a second diode.

2.3.4 Two- diode models

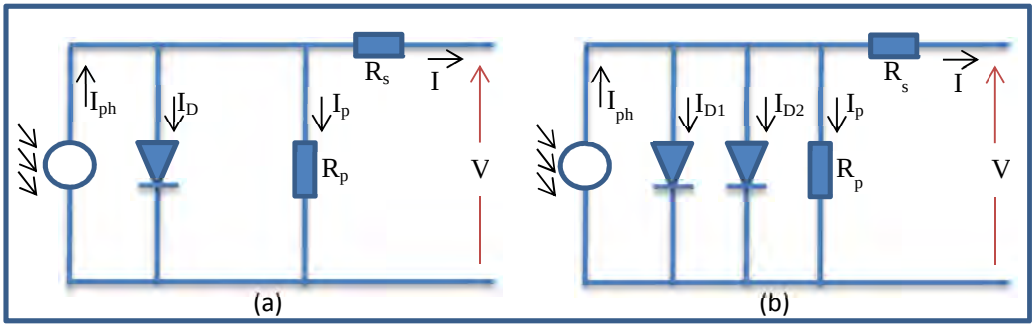

Figure 2-3: Equivalent PV cell circuit: a) one diode model b) two diode model

The double diode model shown in Figure 2-3 b), shows a second diode added to the single diode (5-p) model shown in Figure 2-3 a), which further characterizes the charge diffusion for diode one and recombination for diode two in the space charge layer [25] therefore the I_0 can be considered as the contribution of two Shockley effects represented on equation (2.5) [15] [26]. This photovoltaic model is accurate since it considers all the effects of the reverse saturation current contributed by the two mechanisms namely diffusion and recombination in the space charge [25], and this model has been proposed and supported by many [25] [27] [28].

$$I = I_{ph} - I_{d1} - I_{d2} - I_p = I_{ph} - I_{o1}\left(e^{(V+IR_s/V_{t1})} - 1\right) - I_{02}\left(e^{(V+IR_s/V_{t2})} - 1\right) - \frac{V+IR_s}{R_p} \qquad (2.5)$$

The addition of the second diode increases the number of parameters to be computed to seven unknowns (I_{ph}, I_{01}, I_{02}, n_1, n_2, R_s, R_p) [27] and having to derive solving equations from equation (2.5) which is having non-linear with more than one exponential term will be challenging and time consuming resulting in slow convergence time. A study by [25] attempted to extract the unknown parameters and made use of Levenberg/Marquardt, Newton-Raphson methods incorporated with cell samples at different ranges of irradiance and temperature and n (ideality factor) held constant to simplify the calculation. The extraction defined successfully results but a vast of computation is required and data acquisition. Other attempts by [29] reduced the double diode model from seven variables to four parameters to be computed therefore, achieving more accuracy faster but still requires lot of PV data and assumptions.

In comparison of the two diode and single diode model of Figure 2-3 a) & 2-3 b) respectively exhibit similar results displayed by [27] with only one exception where at low voltages and lower irradiance the double diode model tends to be more accurate than the single diode model

[29] [30]. In this thesis the developed model will be evaluated as a solar module for power source and implemented at large voltages. Thus, the single diode model is adequate for use in this thesis and considering that only five parameters are to be computed (I_{ph}, I_0, n, R_s, R_p) increasing convergence time. Once the model to be used is determined then the next challenging factor is extracting the unknown parameters which will be discussed in chapter 3.

2.4 Electrical characteristic of PV system

The equation (2.1) represents electrical characteristics of solar cell and shows the output current is a function of cell voltage and the series resistance is representing a voltage drop at the P-N junctions, diode reverse current is for the recombination in space charge and the parallel resistance represents the leakage currents at the cell edges [6] [31].

The PV equivalent circuit (5-p model) described by equation (2.1) is complex and has no explicit solution for neither voltage nor current. But one can plot the I-V curve by spreadsheet incrementing the diode voltage and a corresponding current value is found [8]. A plot obtained this way is shown in Figure 2-4 [6] I-V curve (red). Also shows the product of voltage and current that is power delivered by the PV cell P-V curve (blue).

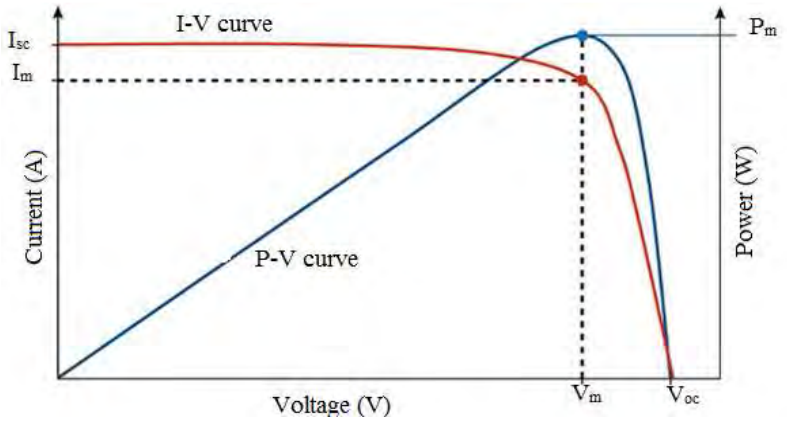

Figure 2-4: I-V curve (red) and P-V curve (blue)

From the Figure 2-4 three main points can be noted namely the maximum power point P_m made up by (I_m,V_m), Short Circuit current labelled I_{sc} and Open Voltage V_{oc} measurement these are normally given by the manufacturer at standard test condition (STC) of (E_{stc}=1000W/m^2, T_{stc}=25^{0}C, AM=1.5). [6] [8].

The maximum power point is around the knee of the I-V curve at which the product of current and voltage gives the maximum power (V_m & I_m), this is the most efficient point to operate the photovoltaic system for a given irradiance and temperature [18]. The Open circuit voltage point

can be taken as a huge loading and producing zero power ($V=V_{oc}$, $I=0$) as the load decreases the operating point of voltage decreases while current starts to flow and increases thus power increases until the operating point reaches the maximum operating power ($V=V_m$,$I=I_m$). Decreasing load beyond this point decreases voltage and current slightly increases but power decreases until power output is zero again ($V=0$,$I=I_{sc}$) [6] [11].

2.4.1 From Cell to Module to Array

Since a single cell produces around 0.5 Volts, it is not so useful for application therefore the cells are cascaded in series to increase the voltage and connected in parallel to increase the current output. [6] [8]. A basic building block is the PV module which consists of a number of series connections of solar cell typically 36 cells designated for 12 Volts, but for grid connected modules many solar cells are connected to meet the required voltage.

A module connection is in series therefore according to Kirchhoff's law current in series connection current stays the same but voltage is added therefore total voltage is given by equation (2.6) [6] [21]:

$$V = \sum_{i=1}^{n} V_i \tag{2.6}$$

A parallel connection of modules according to Kirchhoff's current law increases current to get a desired power output described by equation (2.7) [6] [21] below can be used;

$$I = \sum_{i=1}^{n} I_i \tag{2.7}$$

Parallel connection not often used then the series connection for reasons associated with higher transmission losses [6]. Modules connected in series to increase voltage and parallel to increase current make up an array. In this way the desired I-V curve is generated. Below it can be seen in Figure 2-5 [8] [21] [32] the effect of series and parallel connections of module.

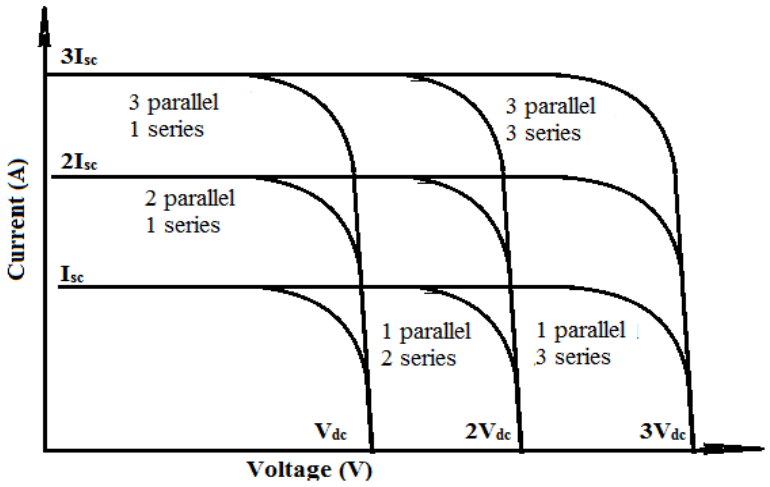

Figure 2-5: Effect of interconnection of modules on the I-V curve

The series and parallel connection builds up an array as shown in Figure 2-6 (d). [15] [32]

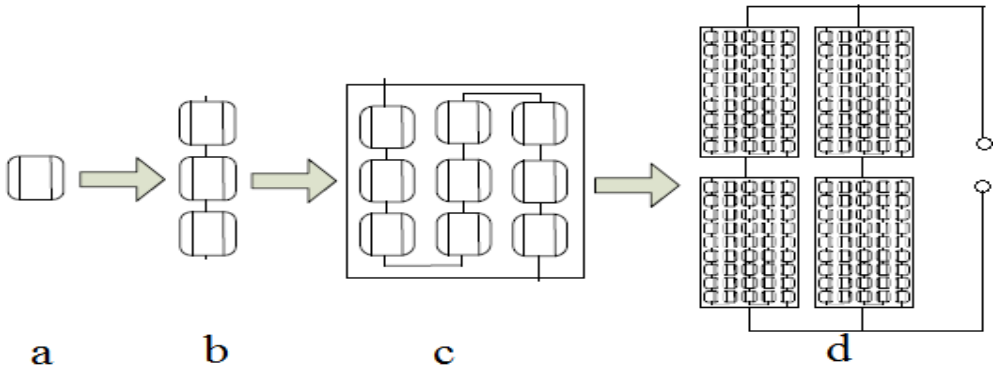

Figure 2-6: (a) Photovoltaic cell, (b) cell series string, (c) cell module & (d) PV array

Therefore for a PV module or PV array a mathematical model can be deduced where N_s is number of series connected cells which multiplies the output voltage and N_p is the number of parallel connections multiplying output current as shown below: [15] [26].

$$I = N_p I_{ph} - N_p I_0 \left(e^{\frac{1}{V_t}\left(\frac{V}{N_s}+\frac{I}{N_p}R_s\right)} - 1 \right) - \frac{N_p}{R_p}\left(\frac{V}{N_s}+\frac{I}{N_p}R_s\right) \tag{2.8}$$

The delivered power by photovoltaic can be calculated by multiplying equation (2.1) by V_{dc} and deduce;

$$P_{pv} = N_p I_{ph} V_{dc} - N_p I_0 V_{dc} \left[\exp\left(\frac{qV_{dc}}{nKT_{cell}} \right) - 1 \right] - \frac{N_p}{R_p} \left(\frac{V_{dc}}{N_s} + \frac{I_{ph}}{N_p} R_s \right) V_{dc} \quad (2.9)$$

From equation (2.9) it shows that the power delivered by the photovoltaic is a function of photo current and voltage across the solar cell circuit [26] [33].

2.4.2 Irradiance and temperature effect

The I-V & P-V curve in Figure 2-4 show typical output characteristics of solar cell to be non-linear but the solar cell is crucially dependent on solar radiation, temperature and load condition [15] [34]. The current source is dependent on irradiation and temperature and equation (2.6) describes that photo current is proportional to the radiation and linear to temperature [35] [33]. Plots on Figure 2-7 [8] [31] show the effect of irradiance; and effects of temperature is partly influence the current as seen in Figure 2-8

$$I_{ph} = \left[I_{sc} + k_i (T - T_{STC}) \right] \frac{E}{E_{STC}} \quad (2.6)$$

where I_{ph} is the photo current, I_{sc} short circuit current and K_i is the temperature coefficient of I_{sc}, T and T_{STC} is the operational temperature and STC temperatures (25^0C) respectively and E & E_{STC} is the operational irradiation and STC irradiation (1000 W/m^2) respectively.

The open circuit voltage shown in equation (2.7) describes that V_{oc} is a linear function of temperature [36] [32]. Plots on Figure 2-6 [8] [31] show the effect of temperature on V_{oc};

$$V_{oc} = V_{oc\_STC} + k_v (T - T_{STC}) \quad (2.7)$$

where V_{oc} & V_{oc_STC} is the operational and STC open circuit voltage respectively and K_v is the temperature coefficient for voltage and T & T_{STC} are the operational temperature and STC temperatures (25^0C) respectively.

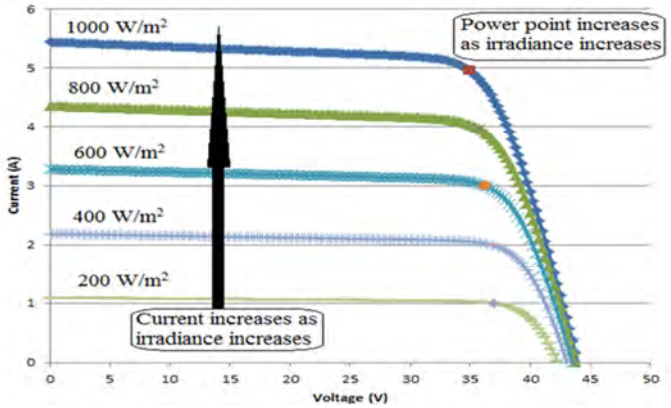

Figure 2-7: PV system effect for temperature with constant irradiance

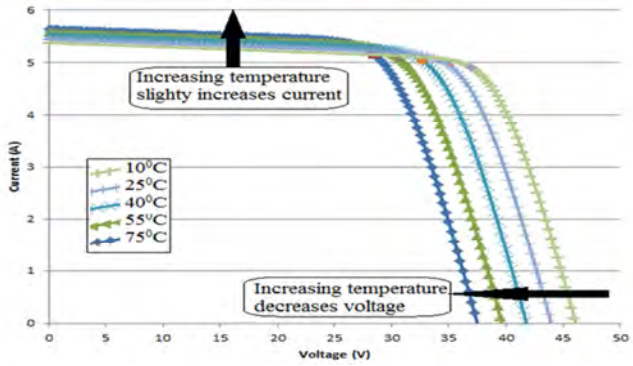

Figure 2-8: PV system effect for irradiance with constant temperature

Figures 2-7 & 2-8 show characteristics of the typical response of a photovoltaic system for a given irradiance and temperature. The voltage output is highly influenced by temperature whereas current is highly influenced by irradiance. The irradiance and temperature vary every minute in atmosphere which has a great consequence for solar which in-turn will change the maximum power point (MPP) every minute [34] [32]. Therefore, the atmospheric fluctuations reduce the efficiency of the overall PV system; therefore a mechanism to track the maximum point is essential known as the maximum power point tracker in order to operate efficiently and to deliver maximum possible power.

2.5 Maximum Power Point Tracking MPPT

Maximum power point tracking is a control mechanism which regulates the DC voltage in such a way that maximum possible power output is delivered with respect to the weather conditions [18] [33]. An MPPT is fully an electronic system that varies the operating point of the modules to achieve optimal operating point and is embedded inside the inverting interface. [37]

There are several MPPT algorithms available for use, implementing different techniques. Some of these techniques will be discussed based on references [33] [38] [39] [40] [41] [42] [43]

2.5.1 Perturb and Observe

The Perturb and Observe technique is simple to implement period, Figure 2-4 (blue curve) has a maximum power point and for a given operating voltage P&O algorithm will be perturbed periodically by adjusting the voltage in a direction to climbing the P-V curve in small changes of ΔV, the direction of the change is determined by the measured power P_n subtracting P_{n-1} previously measured and if it happens that dp/dV > 0 this means the gradient is positive which is climbing up the P-V curve towards the maximum power point, therefore the P&O will continue to perturb in the same direction. But if dp/dV < 0 negative gradient that means the maximum power point is passed and the P&O needs to reverse it direction therefore perturb backwards. The problem with P&O is of oscillations around the maximum point during steady state operations and can also track incorrectly under rapid change of irradiance or temperature. These two disadvantages cause power loss. The oscillations can be minimized by reducing the perturbation step size but this will slow down the MPP tracking system [44] [45]. The problem of miss tracking MPP during rapid change of environment conditions can be solved by introducing a third reference $V_{dc}(n+3)$ [46] [47].

Three conditions are identified:

i. dp/dV>0 increase $+\Delta V_{dc}$
ii. dp/dV_{dc}<0 decrease $-\Delta V_{dc}$
iii. dp/dV_{dc}=0 (at MPP)

2.5.2 Incremental conductance

The incCond algorithm is based on the observation that the equation (2.12) holds at maximum power point.

$$di_{pv}/dv_{pv} + i_{pv}/v_{pv} = 0 \qquad (2.12)$$

The algorithm starts the first cycle by obtaining measurements of current values of $I_{pv}(n)$ and $V_{dc}(n)$ and corresponding values $I_{pv}(n-1)$ and $V_{dc}(n-1)$ and the changes are approximately $\Delta I_{pv}=I_{pv}(n)-I_{pv}(n-1)$ and $\Delta V_{dc}=V_{dc}(n)-V_{dc}(n-1)$ and these changes dI_{pv}/dV_{dc} are equated in equation (2.12) $(dI_{pv}/dV_{dc}+I_{pv}/V_{dc})$ and if this equation yields a negative value means the operating point on the P-V curve is to the right of the maximum power point and the voltage V_{dc} will be

increased in steps towards maximum point and if yields positive value then operating point is to the left of the maximum point therefore the voltage V_{dc} will be decreased in step towards the maximum point. Two more checks in the algorithm to detect whether a control adjustment is required when the maximum point has been previously been reached *($dV_{dc}=0$),* checking if *($dI_{pv}\neq 0$)* for the purpose of checking change in environment and if *($dI_{pv}\neq 0$)* then a search for new maximum position by changing V_{dc} or else bypass the perturbation step.

Practically the condition $dI_{pv}/dV_{dc}=-I_{pv}/V_{dc}$ seldom occurs because of the approximations made in calculations dI_{pv} and dV_{dc} , therefore an absolute value ε which determines the sensitivity of the MPPT to reduce potential oscillations. The trade-off for the problem of not operating exactly at maximum point and possible oscillation is if the absolute value is high will cause operating point to move away from maximum point and too low it can cause oscillations therefore a suitable value is to used can be determined by hit and trail. Therefore maximum is assumed when $\left|\frac{di_{pv}}{dv_{pv}}+\frac{i_{pv}}{v_{pv}}\right|<\varepsilon$. The voltage increment step ΔV which determines the algorithm speed.

This algorithm performs well under rapidly changing environmental conditions but requires two sensors to measure instantaneous voltage and current which results in high cost and complex system [48].

2.5.3 Constant voltage

This algorithm makes use of the fact that the maximum power point voltage changes slightly with varying irradiance but dependent on temperature levels. The ratio *k* as seen in equation (2.13) depends on the solar cell parameters but it is around 71%-78% for different irradiance and temperature levels. In this algorithm the MPPT momentary disconnects PV array to allow measurements of the arrays open circuit voltage. Then the operating voltage V_m is the multiple of the ratio and open circuit voltage V_{oc}. The disadvantage about this algorithm is energy is wasted every time the MPPT disconnects and the operating point is not always between 71%-78% of the arrays open circuit voltage [49]. To prevent the momentary disconnections [50] suggested the use of pilot cells from which V_{oc} can be obtained.

$$V_m \approx kV_{oc} \tag{2.13}$$

This algorithm is simple and only requires one measurement and is suitable for use where the optimal operation is not required. It more suitable to measure the open circuit voltage at start up and set the operational voltage V_m.

2.5.4 Fractional Short-Circuit Current

Fractional I_{sc} described by equation (2.14) is very similar to constant voltage technique with the constant k_1 generally found to be between 0.78 and 0.92. Measuring I_{sc} during operation is problematic. An additional switch usually has to be added to the power converter to periodically short the PV array so that I_{sc} can be measured using a current sensor [51].

$$I_m \approx k_1 I_{sc} \tag{2.14}$$

where k_1 is a proportionality constant. Power output is not only reduced when measuring I_{sc} but also does not always operate between 78%-92% [42].

2.5.5 MPPT performance

The important factors of an efficient MPPT is the tracking speed and the tracking accuracy, ideally less steps (tracking accuracy) and higher frequency (tracking speed) should work perfectly since small duty cycle will decrease oscillation and high frequency will increase the speed but from [42] [45]it is not practical to operate the MPPT due to noise and time delay. In the case of a rapid change in atmospheric conditions the MPPT will be less efficient especially on cloudy days. Therefore it is important to set the duty cycle step low but also allow system to reach new steady state first before perturbation.

2.5.5.1 Efficiency of MPPT algorithm

The efficiency of the different algorithms is compared in [38] and the results are tabled below Table2-1;

Table: 2-1 Efficiency of different MPPT algorithms

	P&O	IncCond	CV
Array	96.5%	98.2%	88.1%
Simulator	97.2%	98.5%	92.7%

As expected the constant voltage has the lowest efficiency followed by the P&O algorithm and IncCond has a better efficiency. Similar studies were done in [33] & [41] and both show incCond has a higher efficiency then P&O and last the constant voltage with a lower efficiency. The P&O and incCond have quite close efficiencies relatively but the incCond has more

complexity then the P&O. In the thesis both (IncCond & P&O) MPPT techniques will be implemented for comparison reasons and implemented in the DigSilent PowerFactory.

2.6 PV Inverter

The basic inverter function is to convert the DC power produced by the PV system to AC power interfacing the PV array power to the grid. Extra functionalities such as maximum power point tracking to ensure maximum power is extracted, synchronization with the grid which is performed aided by phase locked loop (PLL) or zero crossing detector etc., power flow control mechanism for real and reactive power control and protection settings such as the anti-islanding protection these functionalities are all implemented by the PV inverter. [52] [53]. Photovoltaic inverters operate at rated power for only few hours per year due to the weather fluctuations. Therefore it is important to use high efficient inverters and do not oversize the ratings as it will contribute to the losses. The inverter efficiency characteristics for module and central inverters are shown on Figure 2-9 [6].

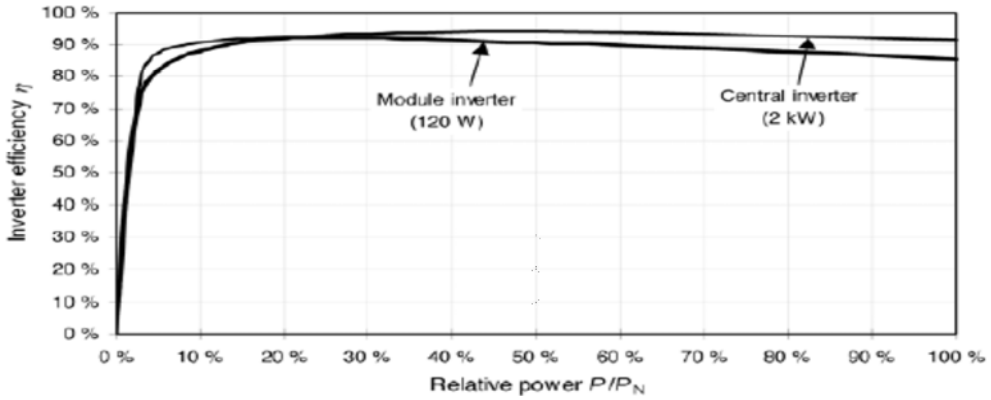

Figure: 2-9 Efficiency of photovoltaic generation powers

The efficiency of the inverters is important to note as it affects the energy yield, one way to evaluate the overall efficiency of the inverter is European efficiency standard given by equation (2.15) [54] which takes in consideration the amount of time (in percentage) that the inverter is expected to work. Even though the standard is valid for irradiance levels in Europe it is sufficient to compare different inverters. [54]

$$\eta_{EURO} = 0.03\eta_{5\%} + 0.06\eta_{10\%} + 0.13\eta_{20\%} + 0.1\eta_{30\%} + 0.48\eta_{50\%} + 0.2\eta_{100\%} \quad (2.15)$$

where η is the efficiency and the subscript percentage is the operating percent of the rated capacity. The numbers in front of the η are weighting coefficients (they add up to 1 for 100%).

For a specified peak power the ideal energy yield E_{ideal} of a photovoltaic is given by equation (2.16).

$$E_{ideal} = A_{pv}\eta_{pv}E_{irradiation} \tag{2.16}$$

For A_{pv} being the area of photovoltaic, η_{pv} module efficiency and $E_{irradiation}$ is irradiance. But in reality they are other effect such as inverter failure, MPP tracking problems, soiling, shading and high temperatures which lower the energy yield and the consideration of these losses is described by performance ratio (PR) as shown in equation (2.17) [6]. Good systems have a PR greater than 0.8 and problematic give PR less than 0.6.

$$E_{real} = PR \cdot E_{ideal} \tag{2.17}$$

For a specified peak power rating the real energy yield is given by equation (2.16);

$$E_{real} = P_{array\_STD} \times f_{temp} \times f_{mm} \times f_{dirt} \times H_{tilt} \times \eta_{pv\_inv} \times \eta_{inv} \times \eta_{inv-sb} \tag{2.16}$$

2.6.1 PV inverter configuration

Inverters are categorized in four types namely central inverters, string inverters, multistring inverters and module inverters as shown in Figure 2-10 and these are discussed below referenced from [6] [55] [56]. The available type of inverter in Digsilent PowerFactory is central inverter and will be discussed in details in the next chapter.

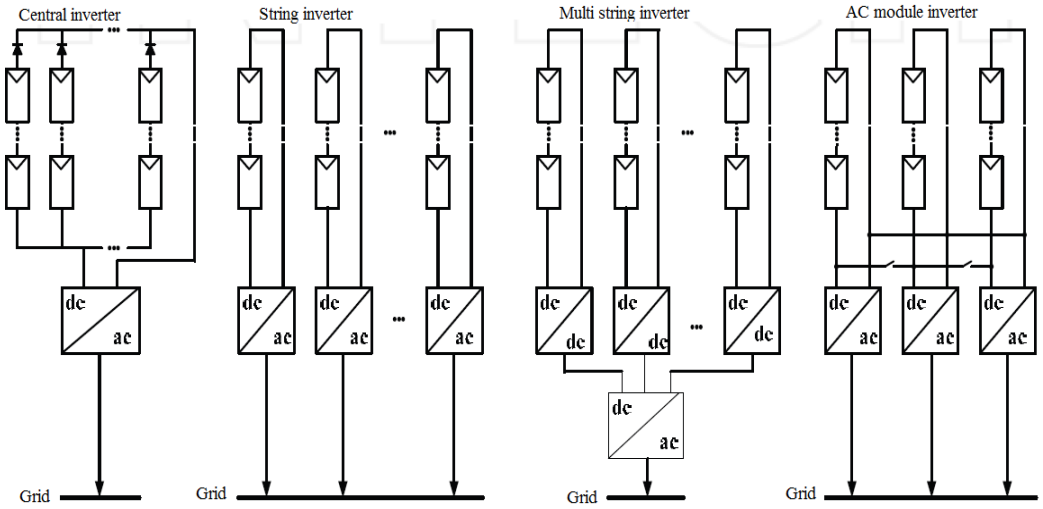

Figure: 2-10 PV array inverter configuration

2.6.1.1 Central inverters:

PV modules strings are connected in parallel and series to achieve desired output power and connected to the DC side of the inverter. This kind of inverter can connect voltages of up to 1 kV on the DC side therefore there is no need for DC-DC converter to boost the voltage. The available rating for this inverter ranges from 1 kW to 1 MW. The advantages of central inverters is the efficiency is high at low cost per watt and low total harmonic distortion (THD) but disadvantages are its reliability problem if the inverter trips the whole generation is disconnected from the system and shading effect does not suit this inverter well.

2.6.1.2 **String inverters**:

This configuration can accommodate different physical shape orientations of modules to suit the different shading conditions. Each module string is connected to an inverter and having its own MPPT control therefore the reliability is improved should one equipment trip the other equipment will remain connected generating. The available ratings range from 0.4kW to 2kW. The cost per kW is higher than that of central inverters.

2.6.1.3 Multi-string inverters:

This type has an additional converter, DC-DC converter which introduces an element of flexibility in terms of module voltage input to the main DC-AC inverter. This arrangement gets more efficient since each inverter has own MPPT control but the disadvantage will be the losses with many power conversions occurring. It ranges from 1kW to 6kW.

2.6.1.4 AC module inverter:

The PV inverters are set up in parallel and the main advantage is that it has multiple DC-AC inverters increasing the reliability. And no DC wiring is necessary and risks of electric arc and firing is eliminated, but has low efficiency at high costs and its life time does not reach that of PV module.

The next topic the different structures and topologies of grid connected inverters are reviewed and discussed.

2.6.2 Grid interfacing

They are two topologies that can be implemented to provide single stage DC-AC conversion. The Current Source Inverter (CSI) and the Voltage Source Inverter (VSI) are illustrated in Figure 2-11 (a) & Figure 2-11 (b). [57] [58].

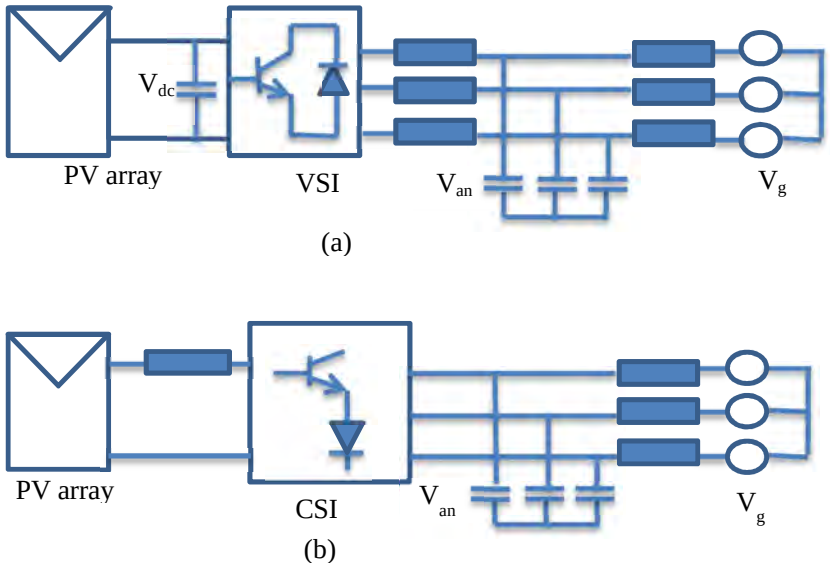

Figure 2-11: Main circuit (a) voltage source inverter and (b) current source inverter

The basic difference between the inverters is on the dc-link side a voltage source inverter is fed by a dc-link capacitor, whereas the current source inverter is fed by a current source. The Capacitive energy storage is more efficient and cost effective than inductive energy storage in low and medium power application [57] [58]. The DC side of VSI has a constant DC voltage and the output current varies with the load. The DC side of CSI has constant current output and the voltage is varying with the load, the protection filter is a capacitance in parallel with DC source [57] [58]. An advantage of the CSI is the switching losses are lower than in the VSI

which leads to lower total power losses at a high switching frequency. The grid connection is done through an inductance as to not supply with infinitely when there is not phase voltage match between inverter and grid [58] [59]. Table 2-2 [60] summarizes the comparisons between the VSI and CSI. Both topologies achieve the main target of an AC output integrated onto the grid with controlled magnitude, phase and frequency from a dc source. The selection of the inverter depends on the application, economical consideration, and its performance with varying environments. The used inverter will be subject to steady state and transient conditions, therefore VSI show good performance with this regard therefore, VSI topology is used in the study,

Table 2-2 Comparison of VSI and CSI [61]

Comparing criteria	**VSI**	**CSI**
Cost and sizing dc component	DC capacitor is small, cheap and efficient energy storage.	DC inductor is bulky, expensive and contributes more losses.
Steady state and transient response	Good steady-state performance. Excellent response during transient with small overshoot.	Good steady-state performance. However, takes longer time to reach steady-state. Satisfactory performance during transient.
Power semiconductor losses	High switching loss but low conduction loss. Thus, total power loss is low. At high switching frequency, the total loss is higher than CSI.	Low switching loss but high conduction loss. Thus, the total power loss is high. However at high switching frequency, the total loss is lower than VSI.
Efficiency Full power	97.7%	95.7%
Efficiency Lower power	97.8%	89.9%
Input Power Harmonics	Low, meets IEEE 519	High, requires isolation / filter

2.6.2.1 Pulse Width Modulation

PWM is the process of controlling the voltage magnitude and the frequency. The control is within the inverter itself. A fixed dc voltage is fed to the inverter and a controlled AC voltage is obtained by adjusting the on and off periods of the inverter components [59]. The inverters function takes the input voltage and outputs AC controlling the magnitude and frequency.

There are different PWM techniques that pulse-width modulation can be implemented and listed below.

(a) Single-pulse modulation

(b) Multiple pulse modulations

(c) Sinusoidal pulse width modulation

A commonly used technique is sinusoidal-PWM, the manner the sinusoidal waveform is obtained is done by a comparator for which at a specific frequency a sinusoidal control signal at the specific frequency is compared with a triangular waveform shown by Figure 2-12 [62]. The inverter then uses the frequency of the triangle wave as the switching frequency.

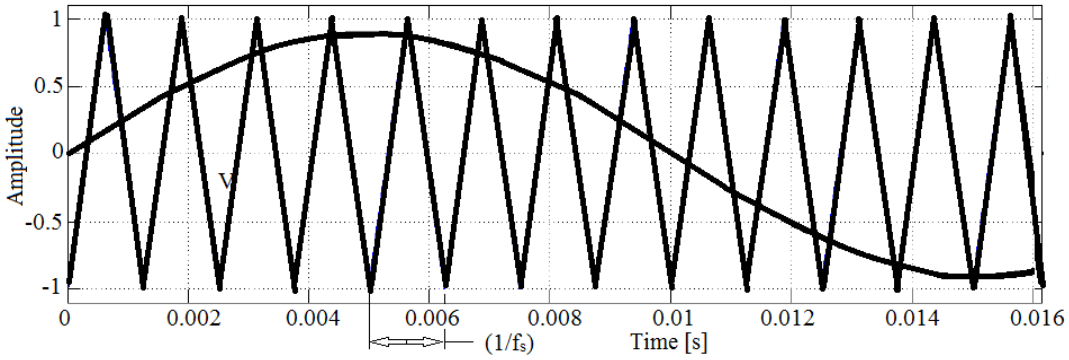

Figure 2-12: Reference voltages, frequency compared with a triangular waveform

In order to control PWM it is necessary to define some parameters, the amplitude modulation *m* and frequency modulation m_f.

$$m = \frac{V_{control}}{V_{tri}} \tag{2.17}$$

$$m_f = \frac{f_s}{f_1} \tag{2.18}$$

where V_{tri} is the triangle waveform, $V_{control}$ is the peak amplitude where the control signal $V_{control}$ is used to modulate the switch duty ratio at frequency f_1. This is the fundamental frequency of the inverter voltage output, f_s is switching frequency controlling the speed which the inverter

switches are turned on and off. The duty cycle of the inverter switches is called the amplitude modulation ratio, *m*. [55].

A good switching frequency and frequency-modulation ratio, m_f, is usually considered to be better higher than lower. This is due to the fact that it is easier to filter out the harmonics at higher frequencies. The main disadvantage is the switching losses in the inverter switches increases proportionally with the switching frequency f_s. In many inverter applications the switching frequency is taken to be either less than 6 kHz or greater than 20 kHz, which is out of the audible range. Therefore, it is well suited for an inverter with low input voltage such as a fuel cell, battery, or solar cell input

2.6.3 Converter topology

The converters described above on section 2.6.1 have the same topology, the fundamental PV converter topologies are described by the DC-AC inverter, DC-DC converter and transformer (galvanic isolation) referenced from [63] [64] [65] summarized below:

2.6.3.1 Transformer (galvanic isolation) and transformerless PV inverters

The major function of the transformer is to amplify the voltage, gain isolation between PV array and the grid and to also avoid circulation of DC current on the AC side that causes saturation and overheating of power distribution transformers. The isolation transformer also provides flexibility of grid tie options. The two basic ways to connect the transformer is by embedding Low Frequency (LF) transformer or high frequency (HF) transformer DC-DC converter. The (LF) transformer in conventional PV converter design is responsible for additional losses and accounts for the largest part of the inverter's weight and volume whereas the high frequency transformers are small and lightweight. The galvanic isolation also assists to properly ground the PV system by connecting the negative terminal to ground and for a design without a transformer the grounding becomes a problem. A transformerless topology is cheaper, more efficient and lighter then (LF) transformer which introduces about 2% losses of peak efficiency. But the transformerless design is constrained due to system ground and ground leakage currents therefore, requires more electronics and control to provide protection. The transformerless topology needs more research in order to limit the leakage current and ensure safety and panel reliability. In modern converters there is an inclination towards using HF transformers.

2.6.3.2 DC-DC converter

DC-DC converters have a wide range of uses and are becoming more important in everyday use. DC power supplies are the major use of the converters which are much more compact and efficient. There are three basic types of DC-DC converters from which Cuk converters and Full bridge converters are derived from these converters [66];

- The boost converter as a step-up converter is used for cases in which a higher output voltage than input is required;
- A buck converter as a step-down converter is used for cases in which a lower output voltage than input is required; and
- A buck-boost converter, which reduces or increases the voltage ratio with a unit gain
- For a duty ratio of 50%.

DC-DC converter will convert the low and varying voltage from the PV array through the input capacitor C_{pv}. The choice of DC-DC converter depends on the use of (HF) transformer and amplification range. When there is no transformer, a buck, boost, buck-boost can be used and if a (HF) transformer is used, a forward, push-pull, flyback, half-bride, full-bridge can be applied. In comparison amongst the variants the Full-Bridge DC-DC is more suitable for applications with higher input voltages and it has capabilities of power handling capabilities, stability, and symmetry [65]. The control is accomplished by using Pulse Width Modulation (PWM) control. The available switching power devices in this converter are either IGBTs or MOSFETs. For high power applications and output voltage rating higher than 150V, the IGBT is used as power device. In spite of its lower on-state voltage drop, higher power density and lower cost respect to the MOSFET, the IGBT has higher switching losses and limited switching frequency. In particular, the turn-off switching loss is very high because of the IGBT current tail phenomena [67].

2.6.3.3 DC-AC converter

In this thesis single stage full bridge inverter is used. This is the final stage in a power electronic circuit that converts DC power into AC power at desired output voltage and frequency. The full-bridge inverter can produce an output power twice that of the half-bridge inverter with the same input voltage. Thus used at high power levels and requires less paralleling devices. The three phase full bridge topology is shown in Figure 2-13.

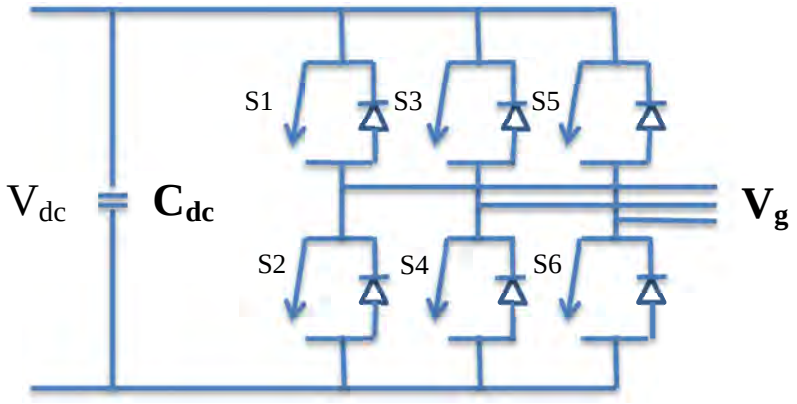

Figure 2-13: Three phase full bridge

2.6.3.3(a) Single stage inverter

The single-stage handle all tasks itself, i.e., MPPT, grid current control and voltage amplification. This is the easiest way to interface a large number of PV modules. The single-stage topology shown in Figure 2-14 (a) presents the most reliable and cost effective topology but with the operational limitation of minimum PV voltage being larger than the peak ac grid voltage in order to avoid the over-modulation. The unwanted large series connection of PV panels from the optimal operation point of view can be attenuated by connecting to a line frequency transformer. The disadvantage associated with this topology is it's less efficient. The AC output power ripple which has double fundamental frequency oscillation unavoidably introduces the double-line-frequency voltage ripple. To minimize the DC voltage ripple and also enhance the solar energy transfer efficiency, a large value DC-link capacitor is normally employed, which however cannot fully eliminate this problem and leads to the increase of system size and cost.

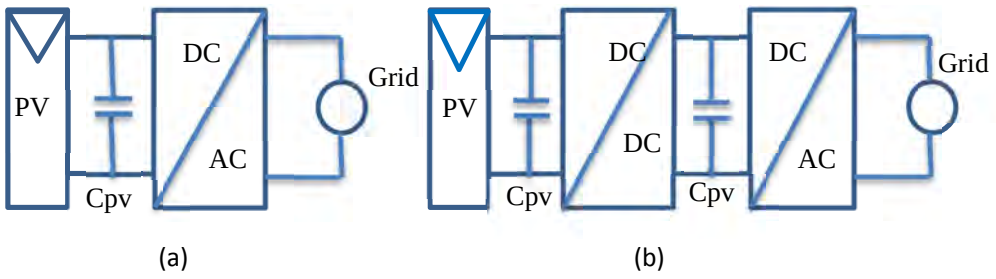

Figure 2-14: Single and double topology with coupling capacitor

2.6.3.3(b) Energy storage in single stage PV inverters

The bus link capacitor is used in DC to AC inverters to decouple the effects of the inductance from the DC voltage source to the power bridge. The bus link capacitor provides a low impedance path for the ripple currents associated with a hard switched inverter. The ripple currents are a result of the output inductance of the load, the bus voltage and the PWM frequency of the inverter [68]. The ripple currents have been the primary factor in sizing the electrolytic bus link capacitor. A lot of work has been done into reducing the DC-link capacitance of inverters in order to replace electrolytic capacitors with the more reliable capacitors.

The comparison of electrolytic capacitor and film capacitor is summarized by [58] and reveals the high temperature on the electrolytic capacitor is the main contribution to reduced life time of the electrolytic capacitor and the film capacitors displayed ability to operating at a wide temperature range for a long life time. But film capacitors are more expensive than the electrolytic ones in term of cost per farad and hence the size of the capacitance has to be smaller to keep the price of the capacitor acceptable [69]. However, smaller capacitance would weaken the power decoupling ability of the DC-link capacitor which may cause DC-link voltage fluctuations that lead to distortion of the inverter output current to the grid [56].

Power decoupling is normally achieved by means of an electrolytic capacitor as stated above. This component is the main limiting factor of the lifetime thus; it should be kept as small as possible and preferably substituted with film capacitors [56] [70]. The capacitor is placed in parallel with the PV modules and the size of the decoupling capacitor can be expressed as:

$$C = \frac{P_{PV}}{2w_{grid}U_c^2\Delta u_c} \tag{2.19}$$

where P_{pv} is the nominal power of the PV module, U_c is the mean voltage across the capacitor and Δu_c is the amplitude ripple.

2.7 Harmonic mitigation

Injection of power from the PV system to the grid is done through a VSI at 50Hz sinusoidal. Harmonics in the output voltage of the inverter is removed by connecting a filter between the VSI and the grid in order to comply with the power quality requirements.

The most common filters used for this purpose are tabled below referenced by [71]. [72] [73]:

- Line reactor
- DC chokes
- Passive harmonic filters

2.7.1 Line reactor

The AC line reactor is the simplest and cheapest mean of mitigating harmonics. It is connected in series with the mains. The impedance rating of the line reactor indicates the per unit impedance relative to its rated full load current [71]. The percent impedance, relative to a given load, is the voltage drop across that impedance caused by the fundamental load current flowing though the impedance as shown by equation (2.20):

$$R_L = \sqrt{3}.I_f.X_f / V_{L-L} \tag{2.20}$$

where I_f is the fundamental load current, X_f is the reactance at the fundamental frequency and $V_{L\text{-}L}$ is the line to line voltage (RMS).

2.7.2 DC chokes

Harmonic mitigation by using DC reactors which is simply a series inductance installed on the DC link of the inverter. The harmonic mitigation is achieved and comparable with the AC side but harmonic reduction is greater for the 5th and 7th harmonics.

2.7.3 Passive harmonic filters

One of the most effective methods for control of harmonics in the industry is the use of passive filtering techniques that simply makes use of combinations of inductances, capacitances and resistances to form a trap for specific harmonic orders. Passive filters can be classified, according to their connections, into single-tuned, damped and high pass filters. Passive filters are designed to provide a band-pass that can filter harmonics over a certain frequency bandwidth thus preventing the flow of these harmonic currents into the electrical system.
Mitigation of harmonics summarized some comparisons between most various harmonics mitigation techniques highlighting the pros and cons of each technique to enable the design selecting the optimum harmonic mitigating technique [74]. Mitigation of harmonics is very important in the industrial applications in order to increase system reliability, enhance operation economics and avoid equipment failure and process downtimes [75].

Table 2-3: Harmonic mitigation devices pros and cons [71].

Harmonic mitigation devices	Advantage	Disadvantages
Line reactor	Cheap, simple, provides protection for inverter rom line voltage transients & provides damping for the short circuit faults.	Additional voltage drop across the reactor, not reduce harmonic levels to below IEEE519-1992 guidelines & produce large heat during operation.
DC chokes	Cheap, integrated within the inverter & provides less voltage drop than ac equivalent line reactor.	Provide less line voltage protection than AC line reactor, may not reduce harmonic levels to below IEEE 519-1992 guidelines, DC choke cannot be installed at site because it must be installed by the manufacturer only.
Passive harmonic filters	Cheap, simple circuitry, easy maintenance, provides power factor correction & a single filter can compensate for multiple drives	Require harmonic studies using specialized software for identifying the harmonics, may not reduce harmonic levels to below IEEE 519-1992 guidelines, Separate mounting and protective device required, Care is needed in filter's components sizing to avoid overloading & during light loading conditions, the passive filter may lead to leading power factors.

2.8 Types of PV systems

PV systems can be very simple e.g. a PV array connected to load, such as direct powering of a water pump motor, or more complex connected to the grid. Thus depending on the PV system configuration, there are three main types of PV systems namely: stand-alone, grid-connected, and hybrid. For all cases, the basic PV system principles and elements remain the same. Systems can be modified to meet particular energy requirements by varying the type and quantity of the basic elements, such as PV panels can always be expanded, as power demands increases.

2.8.1 Stand-alone systems

The stand-alone system can be for domestic or non-domestic application, where PV modules can provide electrical power in locations where it would be inconvenient or expensive to use conversional grid supplies. They often charge batteries to ensure continuity of power. Off grid domestic application usually are of 1 KW in size and can provide electricity for lighting, refrigeration, and non-domestics such as PV parking meter, navigation buoy and telemetry system. In many developing countries electricity grids are often nonexistence or rudimentary, particularly in rural areas, and all form of energy is usually expensive. Here photovoltaic can be highly competitive with other forms of energy supply, especially in countries with high radiation levels. Stand-alone system can be turned into a more reliable system when combined with wind turbines, diesel generators, battery storage etc. to form the hybrid systems and is implemented in several applications [53].

2.8.2 Grid connected PV system components

Grid-connected PV systems have become increasingly popular as building integrated application. They are connected to the grid through inverters, and do not require batteries because the grid can accept all of the electricity that a PV generator can supply. Alternatively they are used as power stations [76]. A grid connected system can be divided into two major sections which is the solar power conversion unit and the interfacing unit as shown in Figure 2-15. The interfacing system will be connected to the low or medium voltage transformer grid through an LV/HV transformer. The LV/HV transformer acts as an isolation transformer and can be used for voltage adjustment if required [53]. The impact of PV modules to the grid is to be considered according to the South African Grid Code.

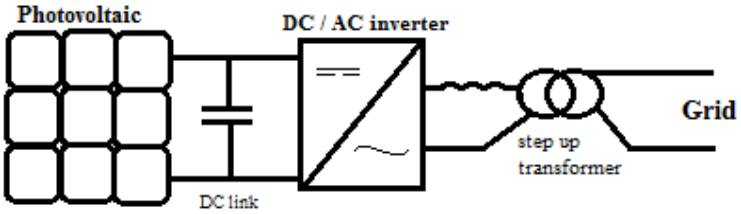

Figure 2-15 Grid connected PV system

2.9 Power station auxiliary network

Eskom power plant layouts slightly vary from station to station. In this thesis one power station electrical auxiliaries will be looked and analyzed independently as power stations auxiliary network topology have more or less same configuration. In a high level all power stations electrical auxiliaries have the same objectives described below.

Power plants need to have an extensive auxiliary power system that supplies power to the power station electrical auxiliary network to provide reliable power to all of the support equipment in the power plant. It is similar to the distribution system in an industrial plant, but it has certain special requirements and limitations. When the unit is generating, it can supply power to its own auxiliaries, when not generating, it must be provided with an external power source [77] [78]. This source must also be capable of supplying the cold start. The main function of the power station electrical auxiliary system is to supply electrical power to the equipment and auxiliaries needed to generate electrical power [77] [78].

The power is distributed on various voltage levels that are associated with the function of the system. The typical Eskom auxiliary power is distributed with voltages of 11 kV, 6.6 kV and 400 V as seen in Figure 2-16. The control and protection is normally supplied by a DC supply (e.g. 24 V, 220 V DC) and 400 V for UPS. When the normal supply fails an AC essential board (e.g. 400 V) is backed up by a diesel generators and DC essential boards (e.g. 220 V DC) kick in which are supplied from battery banks which are normally charged at normal operations. The backup supplies are used to provide power to the equipment that is primarily used for safety, protection and the safeguarding of major primary plant [77] [78].

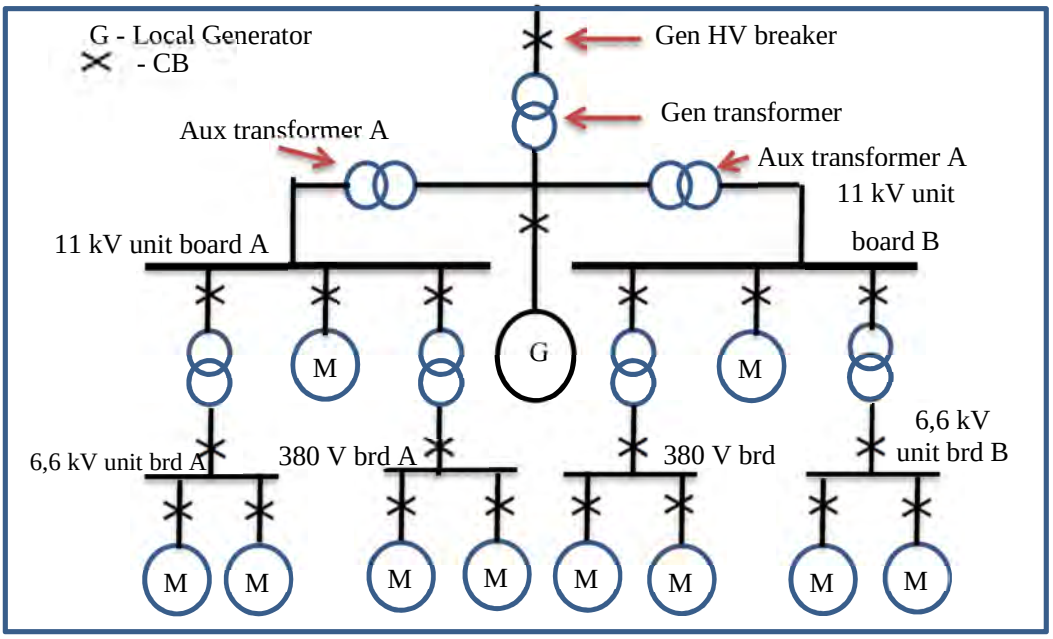

Figure 2-16: Single line diagram for power plant distribution network

In this study the connection of renewable source photovoltaic system will be analyzed for all results connected at 11 kV busbar board A & B. This is the closest point to the local generator thus maximum impact of the PV will be attained from carrying steady-state and transient analysis. Identification of an optimal point of connections is evaluated for suitable rating of PV system and compliance to the grid according the South African Grid Code (SAGC) is determined.

2.10 South African Grid Code (SAGC)

For renewable source to connect to the South African grid a documented procedure is to be followed titled “Grid Code For Renewable Power Plants (RPPs) Connected to the Electricity Transmission system (TS) or The distribution System (DS) in South Africa”. This document specifies the minimum technical and design requirement to support grid operations and stability. The PV system to be allowed connect to the Power station distribution network must be able to meet the minimum requirements as listed by the SAGC [79]

2.10.1 Listed the requirements to be met are listed taken straight from the SAGC.

Table 2-4RPPs group categories

Category	Rated Power Range
A1	0 to 13.8 kVA
A2	>13.8kVAto <100 kVA
A3	100kVA to < 1MVA
B	1MVA to < 20MVA
C	20 MVA upwards

2.10.1.1 Tolerance of Frequency and Voltage Deviations:

- The RPP shall be able to withstand frequency and voltage deviations at the POC under normal and abnormal operating conditions described in this grid connection code while reducing the active power as little as possible.
- The RPP shall be able to support network frequency and voltage stability in line with the requirements of this grid connection code.

2.10.1.2 Frequency response

- In case of frequency deviations in the *NIPS*, *RPPs* shall be designed to be capable to provide power-frequency response in order to stabilise the grid *frequency*. The metering accuracy for the grid frequency shall be at least ±10mHz.

2.10.1.3 Reactive power capability

- RPPs of category A shall be designed with the capability to supply rated power (MW) for power factors ranging between 0.95 lagging and 0.95 leading, available from 20% of rated power, measured at the Point Of Connection (POC).
- The RPP of category A shall be designed to operate according to a power factor characteristic curve, which will be determined by the Network Service Provider (NSP) or the System Operator (SO).
- The RPP of category A default power factor setting shall be unity power factor, unless otherwise specified by the NSP or the SO.
- RPPs of category B shall be designed with the capability to operate in a voltage (V), power factor or reactive power (Q or Mvar) control modes as described in SAGC

section 8. The actual operating mode (V, power factor or Q control) as well as the operating point shall be agreed with the NSP.

- RPPs of category B shall be designed to supply rated power (MW) for power factors ranging between 0.975 lagging and 0.975 leading, available from 20% of rated power, measured at the POC. This is illustrated in Figure 2-12.
- In addition the RPP of category B shall be designed in such a way that the operating point can lie anywhere within the hatched area in Figure 2-12 & 2-13.
- With regard to Figure 2-12, point A is equivalent (in MVar) to –5% rated MW output and point B is equivalent (in MVar) to 5% rated MW output, and point C is equivalent (in MW) to 5% rated MW output.

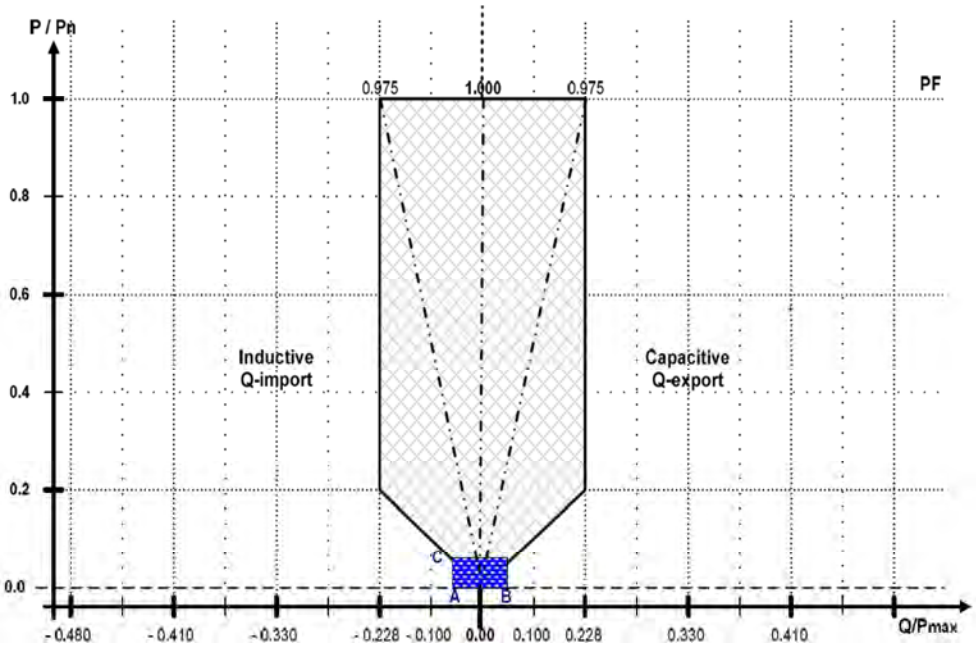

Figure 2-17 Reactive power requirement for category B RPPs

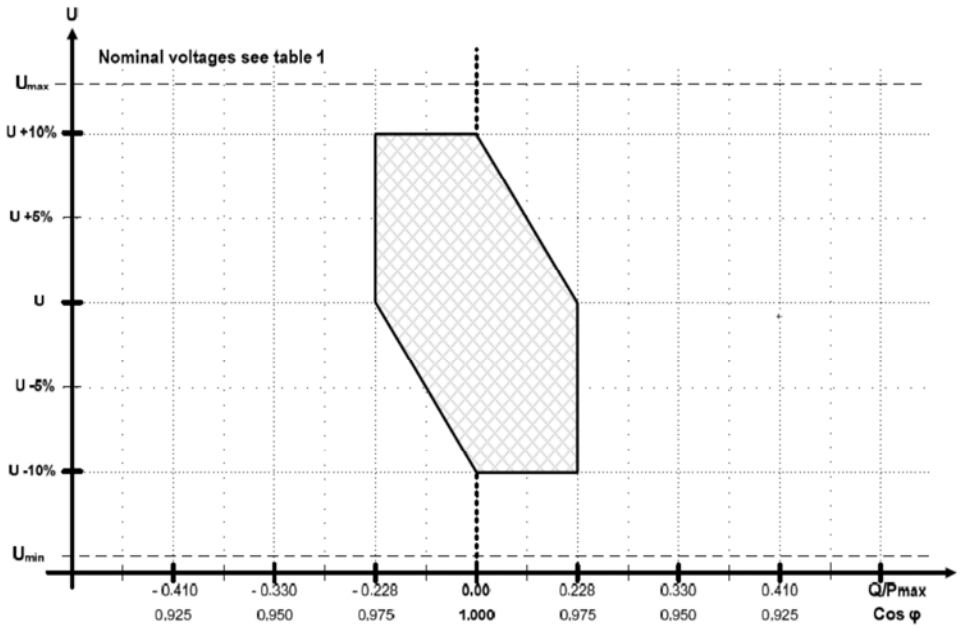

Figure 2-18 Requirements for voltage control range for category B

2.10.1.4 9. Power Quality

- The following requirements shall apply to all *categories* of *RPPs*.
- *Power quality* and voltage regulation impact shall be monitored at the *POC* and shall include an assessment of the impact on *power quality* from the *RPP* concerning the following disturbances at the *POC:*
    i. Voltage fluctuations:
    ii. High-frequency currents and voltages:
    iii. unbalanced currents and voltages:
    iv. *RPP* will generally follow the supply network frequency:

In summary the PV system must participate in steady state conditions controlling voltage to keep the voltage changes within acceptable limits, by means of reactive power control by injecting reactive power and support grid voltage.

During abnormal conditions dynamic network support: The PV system must not disconnection off the grid as grid may collapse. During a fault the PV system must stay connected to the grid and inject short circuit current

The PV systems in this thesis will be connected to the LV and MV busbar of the Power station Distribution network. Therefore, the studies only focus on network stability at LV & MV networks at the POC looking at the following:

- Active power control for change in frequency
- Static voltage support with reactive power
- Voltage support in the presence of a fault

A detailed discussion and testing of the developed model against these requirements will be gradually revealed in further chapters.

CHAPTER 3
PHOTOVOLTAIC SYSTEM MODELLING

This chapter presents a comparative study of four methods for extracting solar cell parameters of the 5-p single diode model. The five-parameter model accomplishes analytically characterizing the electrical behaviors of a photovoltaic module for outdoors operating condition of temperature and solar irradiance. It involves the determination of five parameters, namely, photocurrent I_{ph}, diode saturation current I_0, ideality factor n, series and shunt resistances R_s and R_{sh} respectively. The method to be implemented in PowerFactory (PF) aided by DigSilent Simulation Language (DSL) is chosen based a good compromise between simplicity and accuracy. The established model will be compared with the generic model (four-parameter model) which replicates the electrical behaviors of PV modules based on assumptions to simplify the mathematical model. However, these assumptions cause some inaccuracies, and hence inaccurate stability analysis and unrealistic economic returns are predicted. Various tests and evaluations will be observed to measure the PV system accuracy and reliability of results. The developed model is expected to improve the simple generic DigSilent PV model.

3.1 PV cell

In this thesis the one diode model, 5-parameter was chosen for modelling the PV cell with intent to improve the accuracy of the simple (4-p) simulation model in PowerFactory Digsilent as seen in Figure 3-1 (a) [80]. The equivalent circuit of one diode 5-parameter is described by Figure 3-1 (b). The (5-p) model discussed earlier on section 2.3.3 shows that much research has been carried out in developing the 5-pmodel results demonstrate acceptable levels of accuracy [81] [82] [19] [83] [84] [85] [86].

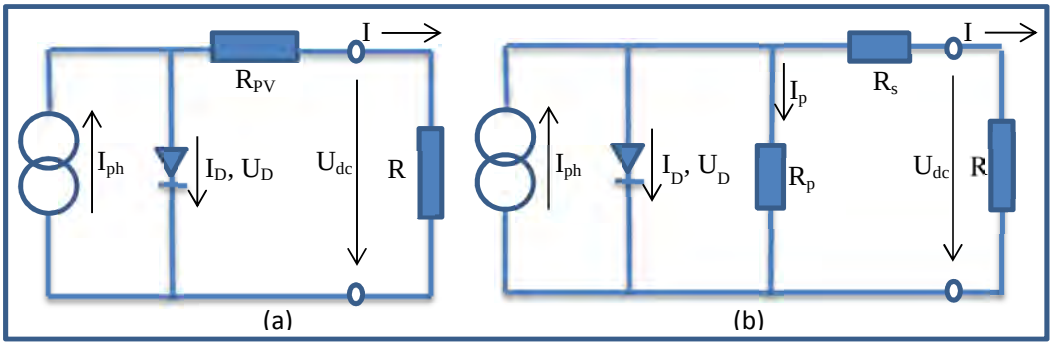

Figure 3-1: Equivalent photovoltaic circuit (a) PowerFactory model, (b) developed model

The (5-p) model requires five parameters (I_{ph}, I_0, n, Rs, Rp), and determining the unknown model parameters is challenging, as the simultaneous equations are non-linear and comprises of exponential terms. Mathematical techniques have been developed to extract the unknown parameters. In determining the most suitable extracting method depends on the degree of complexity and accuracy. Many studies have been conducted attempting to solve the above equation (3.1). Essentially calculating the unknown model parameters, analytical and numerical methods are used [82] [87].

3.2 Methodology

Various formulating methods which characterize and dimension the solar cell arrays are reviewed and presented. Derivation of the current-voltage relationships is expanded from a single solar cell to a PV module and finally to an array. Development of the current-voltage relationship is based on a five-parameter model, which requires datasheet typically provided by the manufacturer. The model accurately predicts (I-V) curves, (P-V) curves, maximum power point (MPP), short-circuit current and open-circuit voltage for a range of irradiation levels and cell temperatures. The model can be applied for any size of PV array and implemented to simulation circuitry. Accuracy of the model was validated by relating the available techniques against each other, which have been validated through a series experiments performed outdoors for different configurations of a PV array.
Overall activities completed in this chapter:

- A review of PV array model suitable for computer simulations.
- Development of an I-V relationship for a PV array.
- Development of a datasheet based parameter determination method.
- Demonstration of the model and validation of results in comparison with other available methods.
- Implementation of PV model in PF for further verification.

3.3 Modelling PV characteristic

3.3.1 PV parameters at general conditions

The PV system is exposed to various levels of wind speed, temperature and irradiance which affect the performance of the PV system which are everyday operating conditions of the PV system [21], and these operating conditions are inputs to the PV system operations and must be considered in calculations in order to predict PV performance accurately at all operating

conditions. The deriving equations to calculate the unknown parameters are at STC and must consider for outdoors operating condition of temperature and solar irradiance [88]. Since the model parameters change with operating conditions it is important to consider the environmental influence in the equations to generalize the model to other operating conditions of irradiance and temperature and in order to make sense and utilize the PV model practically and be interpreted by PowerFactory the following expressions are implemented [5].

Equation (3.1) describe the open circuit voltage with, the open circuit voltage $V_{oc\text{-}STC}$ is at STC and V_{oc} is at solar cell operating temperature, K_v temperature coefficient for open circuit voltage provided by the manufacture, at operating conditions of different temperatures is expressed as follows:

$$V_{oc} = V_{oc-STC}\left[1 + k_v\left(T - T_{STC}\right)\right] \tag{3.1}$$

The photo-current I_{ph} depends on solar irradiance and cell temperature and is expressed as shown below by equation (3.2):

$$I_{ph} = I_{ph-STC}\left[1 + k_i\left(T - T_{STC}\right)\right]\frac{E}{E_{STC}} \tag{3.2}$$

where $I_{ph\text{-}STC}$ is photo current at STC and K_i temperature coefficient of short circuit current. K_i is basically the change of short circuit current with respect to temperature.
The saturation diode current is proportional to the temperature raised by power of three as shown by equation (3.3) below [89] [90]:

$$I_0 = AT^3 e^{\left(\frac{-E_g}{nkT}\right)} \tag{3.3}$$

where A is temperature coefficient and E_g is the band energy in eV defined below as [91]:

$$E_g = 1.16 - 7.02e^{-4}\frac{T^2}{T - 1108} \tag{3.4}$$

The ideality factor is shown by [92] as a unit less parameter defining the extent to which the solar cell acts as an ideal diode. The ideality factor is not affected by the weather conditions therefore n at STC is the same at operating conditions [92].

The temperature of the cell is a function of ambient temperature, solar irradiance, the module back-surface temperature and cell temperature is shown below:

$$T_c = T_m + \Delta T \frac{E}{E_{STC}} \tag{3.5}$$

where T_c is the cell operating temperature in ^{0}C, T_m is the collected back-surface operating temperature of module in ^{0}C and ΔT is a constant temperature between cell and module back-surface and is 3^0C [81].

The thermal voltage is influenced by temperature as shown in equation (3.6):

$$V_t = V_{t-STC} \frac{T}{T_{STC}} \tag{3.6}$$

The parallel resistance which represents the leakage current as mentioned in chapter 2 is affected by the irradiance proportionality defined by [93] [89] used in this thesis shown in equation (3.7) but in [83] the proportionality is inverse.

$$R_p = \frac{R_{p-STC}}{E/E_{STC}} \tag{3.7}$$

And lastly the series resistance was concluded by [89] [90] that it is better it not influenced by operational weather conditions which will simplify the calculation process. But in this thesis the series resistance is analytically established from the other four parameters obtained under various operating conditions.

3.3.2 Photovoltaic cell model

The selected model one diode (5-p) model as described by Figure 3-1 (b) expressed in equation (3.1) is an implicit non-linear equation and can be solved using different methods. There are basically two approaches to calculate the model parameters. One is numerical, in which the parameters are calculated iteratively, and the second approach involves the extraction of the parameters analytically [93] [84]. The latter approach is used for extracting the model parameters since it offers simpler but good enough solutions and can be easily implemented in PF. The five parameters I_{ph}, I_0, n, R_s and R_p making up equation (3.8) are to be extracted at STC from the following given parameters (V_{oc}, I_{sc}, V_m, I_m, k_v & k_i) open circuit voltage, short circuit current, maximum power point voltage, maximum power point current, the temperature

coefficients for open circuit voltage and short circuit current respectively. The equivalent photovoltaic circuit is described and written as:

$$I = I_{ph} - I_0\left(e^{\frac{V_{dc}+IR_s}{nV_t}} - 1\right) - \frac{V_{dc}+IR_s}{R_p} \tag{3.8}$$

where I_{ph} and I_0 are the photo current and the reverse saturation current respectively, V_t = $nNskT/q$ is the thermal voltage of the module with a number of Ns cells connected in series, q represents the electron charge, k is the Boltzmann constant, T means the temperature of the P–N junction and n represents the ideality factor of the diode. I is the output current from the cell and V is output voltage of the cell. The implicit transcendental equation is usually solved by iterative method such as Newton–Raphson, which is very complex. Simpler methods to achieve overlapping results with an experimental curve, proper values of these five parameters must be determined. One way to do this is described below.

Five equations, containing the five unknowns, are needed. By solving the equations simultaneously, the desired parameter values are obtained. These equations will be derived from three points, open circuit voltage, short circuit current and maximum power points from equation (3.1) [93] [5] [94].

With the following substitutions in (3.8), the first of the five needed equations is derived from open circuit voltage at STC i.e. I=0 and $V_{dc}=V_{oc}$ yielding [93] [5] [94]:

$$0 = I_{ph} - I_0\left(e^{\frac{V_{oc}}{V_t}} - 1\right) - \frac{V_{oc}}{R_p} \tag{3.9}$$

At the short circuit point i.e. $I=I_{sc}$ and $V_{dc}=0$ substituting in equation (3.8), the second needed equation from short circuit current at STC, yield [93] [5] [94]:

$$I_{sc} = I_{ph} - I_0\left(e^{\frac{I_{sc}R_s}{V_t}} - 1\right) - \frac{I_{sc}R_s}{R_p} \tag{3.10}$$

To obtain the next three equations the measured current and voltage at the maximum power point at STC is substituted onto equation (3.8) and the third equation is obtained for i.e. $I=I_m$ and $V=V_m$ yields [93] [5] [94]:

$$I_m = I_{ph} - I_0\left(e^{\frac{V_m + I_m R_s}{V_t}} - 1\right) - \frac{V_m + I_m R_s}{R_p} \tag{3.11}$$

Forth equation is obtaining by derivative of power with respect to voltage which is equal to zero. $\partial P/\partial v\big|_{P=P_{\max}} = 0$ [93] [5] [94].

$$\left.\frac{dP}{dV}\right|_{P=P_m} = \left.\frac{d(IV)}{dV}\right|_{\substack{V=V_m \\ I=I_m}} = I + V\frac{dI}{dV} = 0 \tag{3.12}$$

i.e.

$$\frac{I_m}{V_m} = -\left.\frac{dI}{dV}\right|_{\substack{V=V_m \\ I=I_m}} \tag{3.13}$$

But the original equation which is a circular type equation can be rewritten as function of current and voltage [93] [5] [94].

$$I = f(I,V) \tag{3.14}$$

Differentiating equation (3.14) gives [93] [5] [94]:

$$dI = df(I,V) = dI\frac{\partial f(I,V)}{\partial I} + dV\frac{\partial f(I,V)}{\partial V} \tag{3.15}$$

$$\frac{dI}{dV} = \frac{\dfrac{\partial f(I,V)}{\partial V}}{1 - \dfrac{\partial f(I,V)}{\partial I}}$$

(3.16)

Substituting equation (3.16) into equation (3.13) and solving deduce the forth equation (3.17) below [93] [5] [94]:

$$\frac{I_m}{V_m} = -\left.\frac{dI}{dV}\right|_{\substack{V=V_m \\ I=I_m}} = -\left.\frac{\dfrac{\partial f(I,V)}{\partial V}}{1 - \dfrac{\partial f(I,V)}{\partial I}}\right|_{\substack{V=V_m \\ I=\mathrm{Im}}} = \frac{\dfrac{I_0}{V_t}e^{\frac{V_m + I_m R_s}{V_t}} + \dfrac{1}{R_p}}{1 + \dfrac{R_s}{V_t}I_0 e^{\frac{V_m + I_m R_s}{V_t}} + \dfrac{R_s}{R_p}} \tag{3.17}$$

The solar cell series and parallel resistances affect the I-V curve before and after the maximum point (knee point) respectively. Therefore the 4th and 5th equations can be derived from equation (3.14) at points ($I=I_{sc}$,$V=0$) and ($I=0$,$V=V_{oc}$) as seen in Figure 3-2) [93] [5] [94].

$$\left.\frac{dI}{dV}\right|_{\substack{I=I_{sc}\\V=0}} = -\frac{1}{R_p} = \frac{\frac{I_0}{V_t}e^{\frac{I_{sc}R_s}{V_t}} - \frac{1}{R_p}}{1+\frac{R_s}{V_t}I_0 e^{\frac{I_{sc}R_s}{V_t}} + \frac{R_s}{R_p}} \tag{3.18}$$

Similarly the relationship for 5th equation [93] [5] [94]:

$$\left.\frac{dI}{dV}\right|_{\substack{I=0\\V=V_{oc}}} = -\frac{1}{R_s} = \frac{\frac{I_0}{V_t}e^{\frac{V_{oc}}{V_t}} - \frac{1}{R_p}}{1+\frac{R_s}{V_t}I_0 e^{\frac{V_{oc}}{V_t}} + \frac{R_s}{R_p}} \tag{3.19}$$

On the other hand, [5] proposed another solution to develop the firth equation based on the temperature coefficient of the open circuit voltage provided by the manufacturer. The V_{oc} at operating temperature is expressed as $V_{oc}[1 + k_v(T-T_{STC})]$,therefore yields:

$$0 = I_{ph} - I_0\left(e^{\frac{V_{oc}\left[1+k_v\left(T-T_{STC}\right)\right]}{nV_t}} - 1\right) - \frac{V_{oc}\left[1+k_v\left(T-T_{STC}\right)\right]}{R_p} \tag{3.20}$$

Using the combination of equation (3.18) & (3.20) was found to be the most suitable fifth equation as the result can fit the module's I-V characteristic at short circuit point and voltage thermal performance simultaneously. The above determination equations are transcendent and nonlinear, making it almost impossible to separate all unknowns and solve them analytically. This implicit non-linear equation can be solved with numerical iterative methods which require powerful mathematical tools that also require a close approximation of initial parameter values to attain convergence.

3.4 Available extracting methods

Many studies have been conducted attempting to solve the above equations. Basically, to calculate the model parameters, analytical and numerical methods are used. A few methods employed by several authors are discussed as follows.

Numerical methods use powerful mathematical tools and iterative methods to solve the non-linear equations such as of PV cell model. These methods are widely used in engineering as they offer good accuracy [95] for the extracting of PV cell parameters. To mention a few available numerical methods such as the non-linear least squares optimization algorithm based on Newton model is used in [87] to evaluate PV model parameters incorporated into microcomputer-based data acquisition software. Author [89] & [96] uses historical data of solar radiation, cell temperature and information from the manufacture together with semi-empirical equations to predict the I-V curve aided by equation solver, and author [97] uses short term historical environmental data as input to analyze the system and predict the PV system instantaneous power output of PV systems. Author [88] proposed the combination of numerical methods and analytical to determine the PV parameters in Matlab using Levenberg-Marquardt algorithm. And the optimization algorithm Lambert W function is implemented in [98] to convert I-V implicit equation to an explicit equation; the method forms combination of an algebraic equations system with an optimization algorithm in order to obtain the required parameters of the model, minimal set of experimental data is required. The Gauss-Newton algorithm is used in [93], the least squares fitting method in [84] and the bisection method in [99] . All these methods yield positive results with insignificant inconsistencies. Simulation tools have been developed such as PVsyst software which employs one diode model to calculate CSi modules developed by University of Geneva in Switzerland, INSEL software developed in Germany by Doppelintegral GmbH which uses two diode model to analyze and characterize the module and PVSET 1.0 to characterize the performance and dynamic behavior of PV system is established in [100]. The proposed numerical methods all require powerful and dedicated software tool to achieve a solution and most cannot be implement in conventional power system engineering tools. In order to simplify the process, the parameters are extracted by means of analytical methods discussed in the next section proposed in [101] [102] [19] [85] [90] [82] [86] & [103] which implemented systematic solution method to obtain the five parameter model and [90] [82] [86] [103] is be further discussed below.

3.4.1.1 Proposed modelling model

The modelling/extracting technique proposed for the study is created from author [82]. The method provides a good balance of accuracy and complexity. Methods that give good accuracy often require greater amount of information and in some cases require laboratory calculations and some statistical processes. The referenced technique [82] shows a percentage error of 0.03%

measured in comparison with experimental data and simulation results. Three more methods are briefly discussed and reviewed in the following section and a comparison study is conducted.

3.4.2 Summary of method approach

In this section the performance and accuracy of the method developed is accessed. To do so, the results is compared with other existing methods with similar objectives to obtain unknowns parameters I_{ph}, I_0, n, R_s and R_p. The different methods discussed are also based on data provided by the manufacturer to obtain the parameters of the equivalent circuit.

3.4.2.1 Car11 extracting method

The proposed method uses a simplified procedure that allows the estimate of the ideality factor and the loss resistances of any PV cell. The method uses the five parameter model and information from the manufacture as input namely the three points on the I-V curve as input (open circuit voltage, short circuit current, maximum power point) which greatly simplifies the data acquisition process. To ensure the convergence of the iterative process the derived equations do not containing exponential terms and, the values that the ideality factor can take is limited in order for the values of the loss resistances to overlap with those presented by the actual PV cell generator, which is not always guaranteed by other methods. The initial conditions are obtain through the developed equations which make the iteration process efficient, at most four iterations give an accuracy at the maximum point that differs by 0.03% from experimental results therefore fast convergence and quite a good accuracy [82].

3.4.2.2 Pha84 extracting method

This method derives the analytical expressions to extract solar cell single diode from experimental data or good initial guess. The method evaluates and derives equations from equation (3.1) to give explicit non–linear equations. The derivations of the analytical expressions include many assumptions therefore neglecting some significant equation terms which influence the accuracy of the model. The validation of the method was done using PV cell characteristic obtained by developed analytical expressions and compared with the actual values used in generating the characteristic. The differences were expressed in terms of percentage errors and plotted in a grid of *Rs* and *Rsh* values. The results presented where the 1% and 5% error contours for parameters *n, Is, Rs* and *Rsh* are drawn in an *Rs*-*Rsh* grid. The results showed that the analytical expressions for all four parameters are accurate to within 1% provided *Rs* is in the range of 1 mΩ to 150 mΩ and *Rsh* is in the range of 30 Ω to 3000 Ω. For

5% errors, the range of validity is even wider, and would include most solar cells. The assumptions incorporated in the derivations of the analytical expressions introduced errors in the final results. But a plus for this method is it does not involve iteration processes therefore rapid convergence [86].

3.4.2.3 MAd02 extracting method

The method evaluates a simple analytical method that extracts parameters involved in the photovoltaic module behavior equation. Based on a series of experimental voltage–intensity curves obtained under various temperature and irradiance conditions, R_{so} and R_{sho} values are obtained to extract the model parameters. The values at data point's short circuit current, open circuit voltage and voltage at maximum power point and in the entire I-V curve yield errors that are less than 1%. The values for series and parallel resistance are initially assumed, which are not given by manufacture specifications. The challenge involved with this method is obtaining a sufficient number of data points that are near the points of intersection with the axes, to obtain the slope, as required for the analytical calculation of the parameters, but this can be overcome by assigning fixed values for series and parallel resistance. If the fixed assigned values are properly selected, the adjustment errors between experimental curves under different temperature and irradiance conditions and the theoretical model become less than 1%. The sensibility of the model to the value of parallel resistance is minor but is particularly sensitive to thermal voltage *n* value [90].

3.4.2.4 Cub13 extracting method

This method presents an analytical method that easily calculates the equivalent circuit parameters from the data that manufacturers usually provide. The analytical approximation is based on a new methodology which uses four boundaries at open circuit voltage, short circuit current and maximum power point at (I_m, V_m) but only four equations can be derived from four boundaries and these are not enough for five unknowns therefore the fifth parameter has to be estimated and in this method the ideality factor is estimated according to [104] ranging from 1-1.5 for a single junction solar cell. The method is simple, non-iterative and straightforward. The accuracy of the results compared with experimental results is less than 1% in terms of current around the maximum power point. However the *RMSE* (root-mean-square error) to the experimental results is computed to improving the fitting of the I-V curve and accuracy.

3.4.3 Validation and analyses of model results

The data characteristic of solar panel from a typical manufacture datasheet is shown on Table 3-1 [105] and the results obtained after implementing the different methods are tabled on Table 3.2. All the methods have agreed closely with each other. The different is the computation time, degree of complexity and assumptions to create boundaries. The chosen method used in the paper has the advantage of not having to assume any initial values, thus, it is fast and simple to implement and has good accuracy of 0.03% at maximum power point in comparison with the experimental results. The other methods have the shortfall that they require an initial value to be assumed indicated by asterisk "*" on Table 2 and leads to further iterations to improve the assumed value and they achieve at most an accuracy less than 1% with attached conditions mentioned.

Table 3-1: Parameter of the KC200GT solar array at 25^0C, 1.5AM, 1000W/m^2

Characteristics	Value
Open-Circuit Voltage (V_{oc})	32.9 V
Voltage at maximum power point (V_m)	26.3 V
Short-Circuit Current (I_{sc})	8.21 A
Current at maximum power point (I_m)	7.61 A
Maximum Power at STC (P_m)	200.1 W
Number of cells connected in series	54
Temperature coefficient of I_{sc} (alpha)	3.2 mA/C
Temperature coefficient of V_{oc} (beta)	-123 mV/C

The simulation results of the different models were compared under different solar radiation levels. Figure 3-2 & Figure 3-3 presents the I-V curves and the P-V curves respectively for solar radiation of 600W/m^2 & 1000W/m^2 when the cell temperature is 25 ^{0}C. It can be seen that only a slight difference between the models is in the knee of the curves, which may result from the ideality factor being less than one for Car11 and greater than one for Cub13. Other curves agree well. The graphic results illustrate that the simulation model results of this study agree well with those from other methods models which validates the simulation model allowing it to be used for PV performance prediction.

Table 3-2: Extracted parameters using different methods

Method	Iph	I0	n	Rs	Rsh
[Car11]	8.25	1.65E-14	0.702	0.454	90.88
[Cub13]	8.23	3.22E-09	1.1*	0.126	44.29
[MAd02]	8.25	2.97E-13	0.767	0.414*	90*
[Pha84]	8.26	9.95E-20	0.662	0.459	90

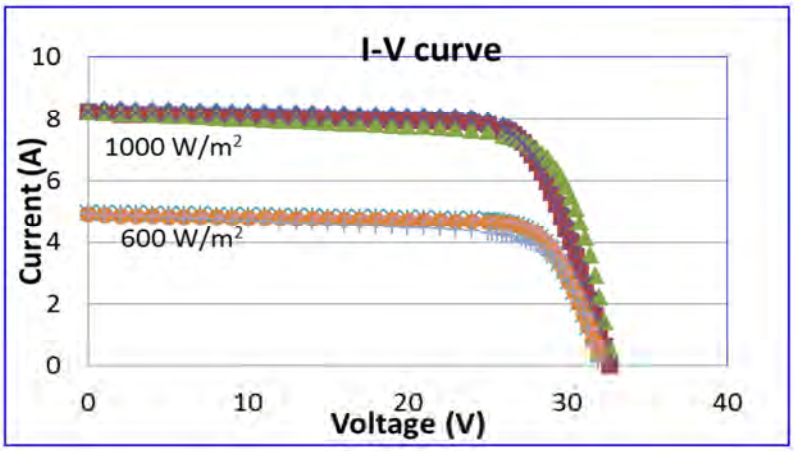

Figure 3-2: I-V model for Method [used],[1],[2]&[3] for 600 & 1000 W/m2

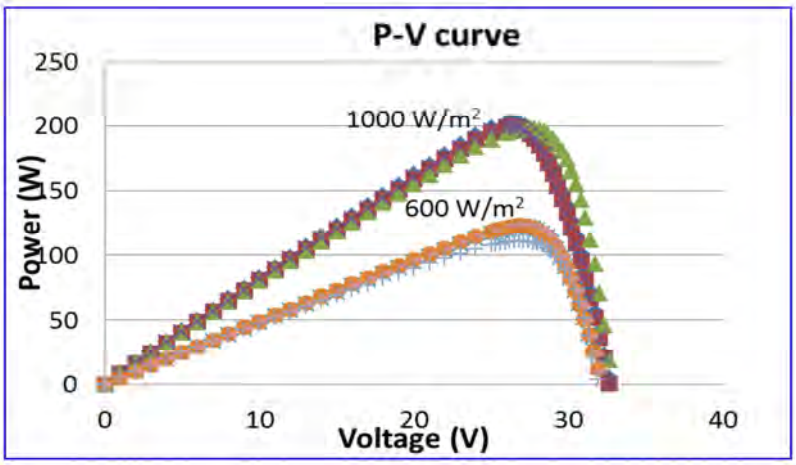

Figure 3-3: P-V model for Method [used],[1],[2]&[3] for 600 & 1000 W/m2

3.5 PowerFactory Photovoltaic generation modelling

The modelling method chosen is further implemented in PowerFactory DigSilent aided by the DSL function available to perform dynamic modelling. The DSL functions allow creation, initialization and testing of dynamic models for use in time-domain power systems simulations [106]. The PV model in DigSilent can be represented in two configurations either in static generator or PWM converter. The static generator configuration is the generic model in DigSilent as shown in Figure 3-4 (a) and PV system as a whole is represented in the control frame modelled using DSL codes. If the interface is PWM converter shown in Figure 3-4 (b the PV array is represented with a constant current source connected to a DC busbar in parallel with DC link capacitor. In paper the latter is used. The elements in DigSilent are noted as DC source current (ElmDci), Pulse Width Modulation converter (ElmVscmono) and compensation shunt capacitor (ElmShnt).

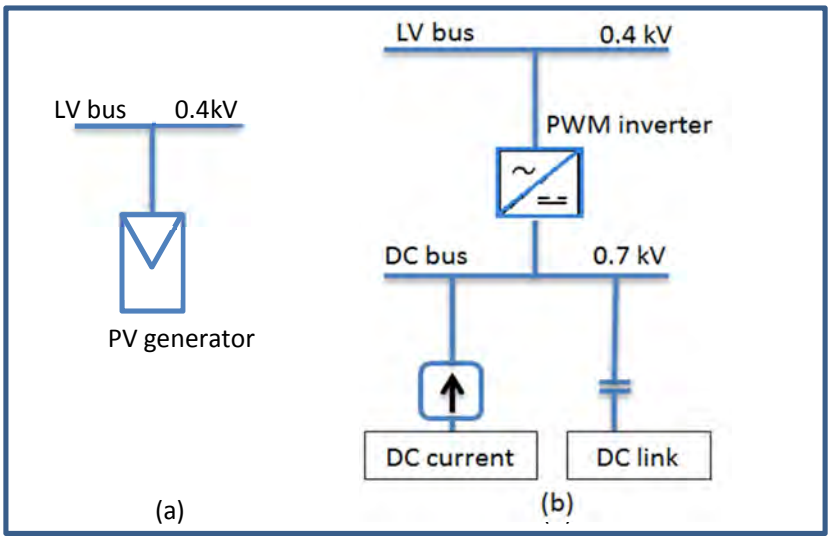

Figure 3-4: DigSilent PV model (a) static generator, (b) PWM converter PV

3.5.1 Static generator

The PV generator in DigSilent is simple to use and has variety of functions and grid interfacing is via static generator [80]. The generic PV template consists of modelling, controls and interfacing blocks shown in Figure 3-5 [80]. The static generator is an easy-to-use model of any kind of static, functioning as a photovoltaic generator. The PV generation system modelling and support system is shown on Figure 3-5. With photovoltaic array model described by PV array block; dc capacitor is modelled as DC bus and capacitor and *Vdc* feeding controller model

which is the important part providing output current reference values *id* and *iq*. Phase measurement provides the grid voltage angle for static generator.

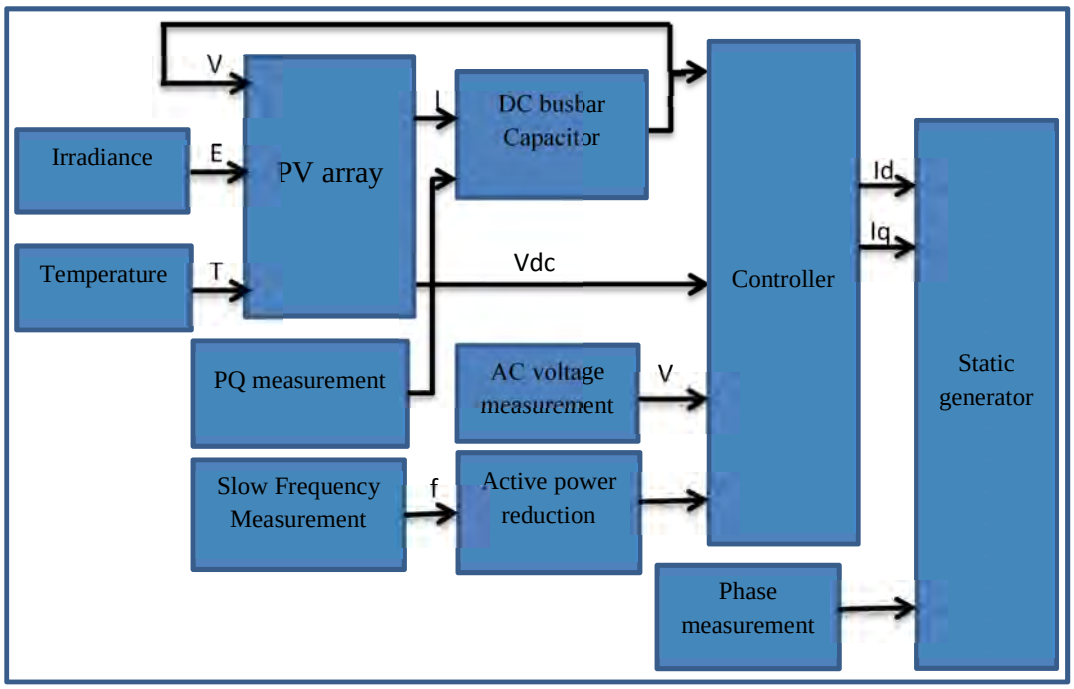

Figure 3-5: Static generator PV model

The interconnectivity of the blocks is summarized below

The control frame of the generic PV system shows the connectivity of the build-up blocks of the PV system with three inputs being temperature (ElmDsl) & irradiation (ElmDsl) from the atmospheric conditions and the DC voltage of the PV system. The Photovoltaic model (ElmDsl), DC busbar and Capacitor model (ElmDsl), Controller (ElmDsl), Active Power Reduction block (ElmDsl) are modelled using DSL function. The Power Measurement (StaPQmea*), Slow Frequency Measurements (ElmPhi*), AC Voltage (StaVmea) & Phase Measurement (ElmPhi*) are measuring blocks. The MPPT block is not available in the generic control frame and this will be included in the developed PV system.

3.5.2 Developed model

The developed PV model in PowerFactory DigSilent rules out some assumptions considering the modelling uses referenced scientific modelling equations thereby, improving prediction accuracy of the PV cell power output. The developed model will incorporate two types of

MPPT Perturb & Observation and Incremental Conductance not discussed here which will be shown in the next chapter.

3.5.2.1 The developed PV frame

The control schematic for the developed PV system is shown in Figure 3-6 Calculation and measurement block is showing the PV array block with temperature, radiation and voltage as inputs modelled using DSL function and the measuring blocks and feeding the controller which controls the input information and processed to the inverter block as shown.

3.5.2.1(a) Summary of the control frame blocks developed.

The controller block is the block which determines the active and reactive power outputs of the PV system from the DC side. The four inputs are DC voltage from busbar, DC voltage reference from the MPPT block, the measured AC voltage and the grid loading power (Hz). Pi controllers are used to regulate changes. The output of the controller is fed to the PWM inverter which is the interfacing block to the grid. These outputs are in d-axis and q-axis components of the reference current *id_ref* & *iq_ref* respectively.

Power control schematic

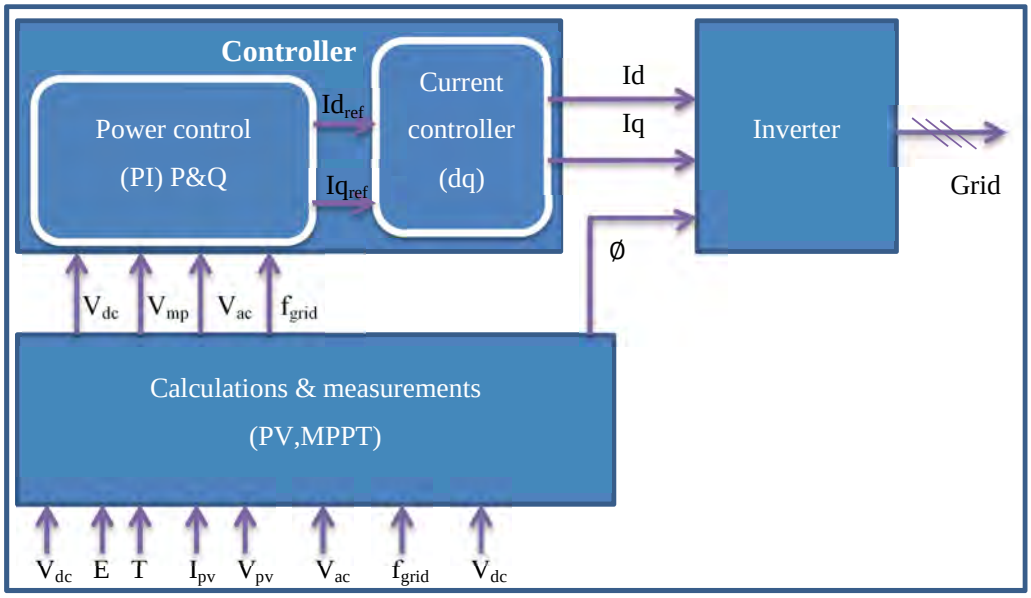

Figure 3-6 : Overview of PV control

The calculation & measurements block measures the DC voltage from the dc bus, irradiance and temperature from atmosphere, grid side voltage & frequency. From measured inputs PV block outputs the PV array current I_{pv} and voltage V_{pv} fed to the MPPT. The dc-link voltage V_{dc} is used for tracking the maximum power point of the PV array. The phase locked-loop (PLL) block generates a signal synchronized in phase to the grid-side voltage to provide the reference phase angle ∅ used for the abc to dq transformation. In the power control mini block the synchronous dq reference frame, the real and reactive power of the inverter can be controlled separately by the q-axis current Iq and d-axis current Id of the inverter [106] [107]. When Iq is positive the inverter consumes reactive power, and generates for negative Iq. For Id the inverter generates real power and limited to zero for absorbing power. The MPPT block generates V_{mp} which is the desired value of dc-link voltage, which is compared to the actual value V_{dc} and the error between the two values is processed as Id through a PI controller. The measured and set point grid voltage at the POC is also compared and similarly the error between the desired and actual value V_{ac}, is processed into Iq and the relative reactive power is achieved. The d-axis current reference is limited to the range between Id_min=0 and Id_max=1 to protect the inverter from excessive heating and reverse current flow through the PV array. The q-axis reference limits of Id_min=-1 and Id_max=1 may be set by considering the q-axis current range and the inverter thermal rating [107].

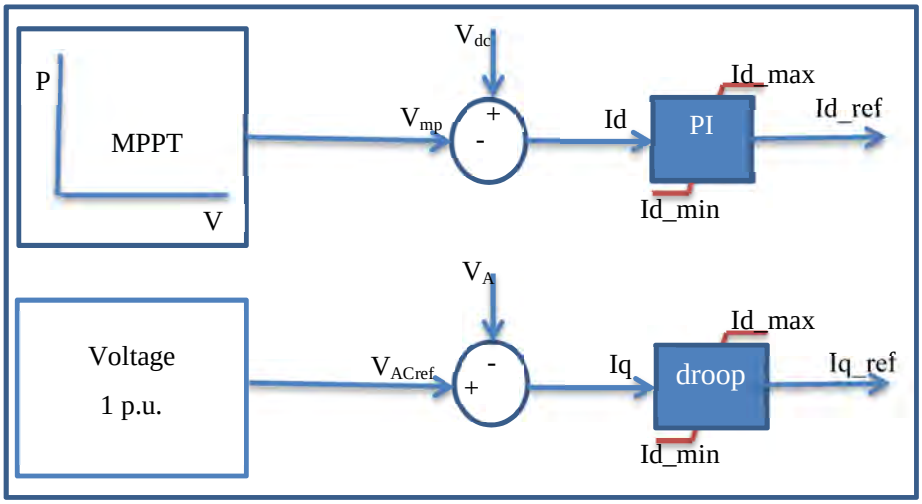

Figure 3-7: Power control block

3.5.2.2 Inverter

The PWM converter is the interfacing inverter which connects the DC power by inverting it to AC power in order to connect to the grid. The inverter can have constant voltage as input which in this case it is named voltage source inverter (VSI) which has the ability to control magnitude of voltage & frequency etc. if the DC input is constant current then the inverter is known as the current source inverter (CSI) which controls the output current.

The (VSI) is the widely used in industry and will be used in this thesis as it has been proven to be efficient, high reliability and faster dynamic response [108], shown from earlier sections.

The AC voltage output from the inverter is controlled by varying the PWM ratio and this varies with the power delivered where higher power corresponds with higher PWM ratio. In this thesis the (VSI) will be used to connect the PV system to the grid [109].

3.5.2.2(a) Pulse Width Modulated (PWM) Inverters:

Pulse width modulation inverter has constant dc voltage as input. Diode rectifiers are used to rectify the voltage, and the inverter controls the magnitude and the frequency of the ac output voltage [59].

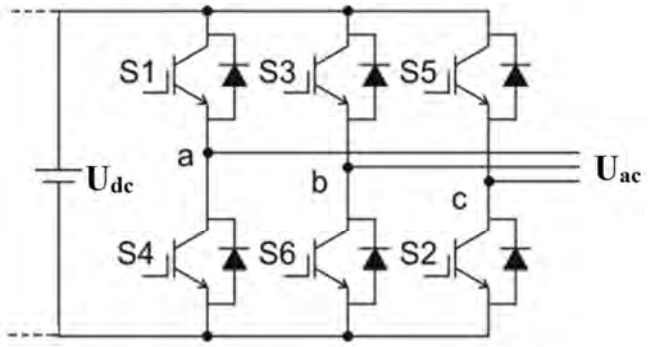

Figure 3-8: Equivalent Circuit PWM converter model in DigSilent [1]

Figure 3-7 shows the PWM model available in DigSilent which is to be used in this study, where U_{DC} is the input voltage across the inverter and the Capacitor DC-link is in parallel with input terminals of the inverter. The DC link is to reduce voltage spikes at the busbar during the operation of the inverter which may deteriorate the sinusoidal voltage. The DC link also helps improve the inverter life span.

The modulation index between $0<m<1$ is for linear modulation / operation range as seen on Figure 3-8, and for $m>1$ is known as over modulation or saturation and this point is not recommended.

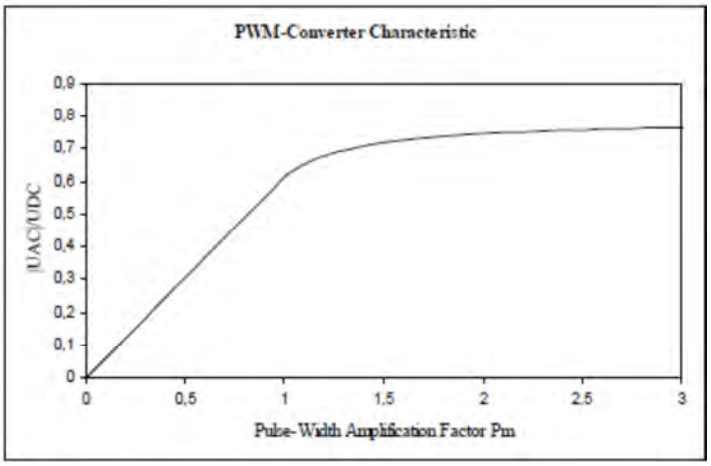

Figure 3-9: PWM converter saturation [80]

The DigSilent PWM converter has a number of built in options to enable steady and stability studies. Therefore the built in inverter is sufficient for use and only the capacitor will be externally added on to act as the DC link. The DigSilent PWM is a self-commutated, voltage sourced AC/DC converter. The circuit uses GTO's or IGBT's for switching.

Losses

The losses are no load losses resulting from switching, and these losses are just V^2-losses and can be modelled as resistance between the Dc terminals as shown in Figure 3-9.

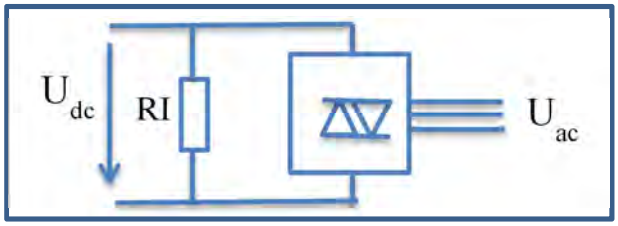

Figure 3-10: PWM equivalent resistance for switching losses [1]

Load flow

The load flow analyses show the controlled variables as a result of load flow calculation. In DigSilent there are preferred control conditions supported by the built in PWM converter as shown below. The chosen control mode for this study is the V_{DC}-Q.

Meaning and typical application of the various control modes are the following:

- Vac-phi: Specifies magnitude and phase of the AC-terminal. Typical control modes for motor-side converters in variable speed drive applications.
- PWM-phi: Load-flow setup without control. The pulse-width modulation factor is directly set in magnitude and phase.
- Vdc-Q: Specifies DC-voltage and reactive power output/flow. Typical applications: STATCOM, shunt converter of UPFC, grid-side converter of doubly-fed induction machines, VSC-HVDC applications.
- Vac-P: Specifies AC-voltage magnitude and active power. This is equivalent to a "PV" characteristic of conventional synchronous machines. Typical applications: Grid-Side converter of converter driven synchronous machines, VSC-HVDC.
- P-Q: Specifies P and Q at the AC-side. This control mode is equivalent to a "PQ"-characteristic of synchronous machines. Typical applications: Same as "Vac-P".
- Vdc-Vac: Specifies DC- and AC-voltage. Typical applications similar to the control mode 'Vdc-Q': STATCOM, grid-side converter of doubly-fed induction machines, VSC-HVDC applications.

For remotely controlled flow quantities (P, Q), the controlled cubicle can be selected. In case of voltage control, the controlled bus-bar needs to be specified.

S**tabilit**y

The stability model can be defined in different ways, depending on the application:

- Pmr, Pmi: Real and imaginary part of the pulse width modulation index. Reference system is here the global Reference-frame, which is usually defined by a reference-machine, external network or voltage source (or even a PWM-converter) why this set of inputs must always be used in combination with phase measurement devices (e.g. PLL) and reference-frame transformations.
- Pmd, Pmq, cosref, sinref: This set of input variables is convenient in grid-connected applications. It allows specifying a pulse-width modulation index-vector, with reference to a reference-system that is defined by cosref and sinref. A very common application is to measure the voltage angle using a PLL and to connect the output of a dq-current controller to Pmd and Pmq. The output of the PLL must be connected to cosref, sinref. This set of input variables avoids the explicit definition of reference-frame transformations.

- id_ref, iq_ref, cosref, sinref: as input variables reference values for the d- and q-axis currents can be used, when an internal current controller is defined on the RMS-simulation page (see also Figure 3-14). Similar to the previous set of input variables, the currents are defined with reference to a reference-system that is defined by cosref and sinref. Also here the explicit definition of transformation from local to global reference-frame is not needed.
- Pm_in, dphiu: Magnitude and phase of the pulse-width modulation index. This representation is fully equivalent to Pmr and Pmi (dphiu is expressed with reference to the global reference-frame).
- Pm_in, f0 (F0Hz): Pm_in defines the magnitude of the pulse-width modulation index. The frequency f0 allows varying the frequency of the output voltage. This is especially useful in variable speed-drive applications, in which a PWM-converter is used for driving an induction machine. The variable F0Hz can be used alternatively to f0 and defines the frequency in Hz (f0 is in p.u.).

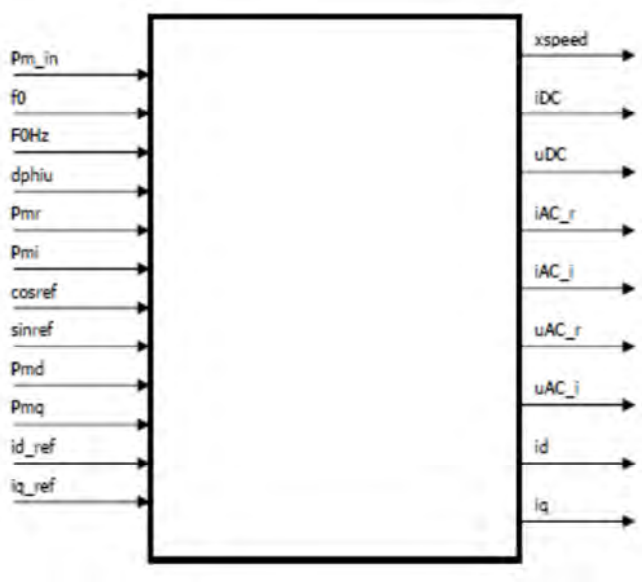

Figure 3-11: Input/Output Definition of the PWM converter model for stability analysis [80]

For this study the option control mode used will be inputs of id_ref, iq_ref, sinref, cosref to determine the modulation index and Figure 3-11 [110] is illustrating the dq-frame current control

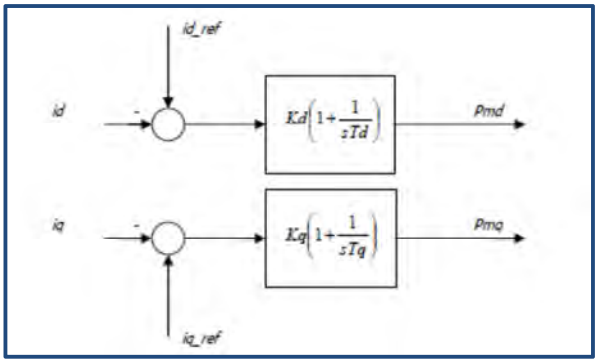

Figure 3-12: Built-in current controller

where $k_i=sT_d$ which is integral gain and K_d is the proportional gain and τ_i is the time-constant usually it is in the range of 0.5 to 5ms depending on the design speed then this can be expanded as shown below:

$$K_i = \frac{R}{\tau_i} \tag{3.24}$$

$$K_d = \frac{L}{\tau_i} \tag{3.25}$$

3.5.2.3 DC link calculation

Since the single stage inverter only has one power processing stage, the energy storage in needed to be placed in front of the inverter as shown in Figure 3-8.

The output AC voltage of the inverter is 400 V. The voltage value at dc bus is 700 V. This voltage is seen across the DC link capacitance. In this design the ripple voltage is taken as 10% of the specified bus voltage.

$$C = \frac{P_{pv}}{2\pi \cdot f \cdot V \cdot \Delta v} \approx 180mF \tag{3.26}$$

The approximated value will be used as is, not taking to consideration standardized values.

3.6 Model analysis and case studies

A comparison between the generic PV model and the developed model is presented for several case studies to validate the developed model and draw advantages from the increased accuracy modelling are evaluated.

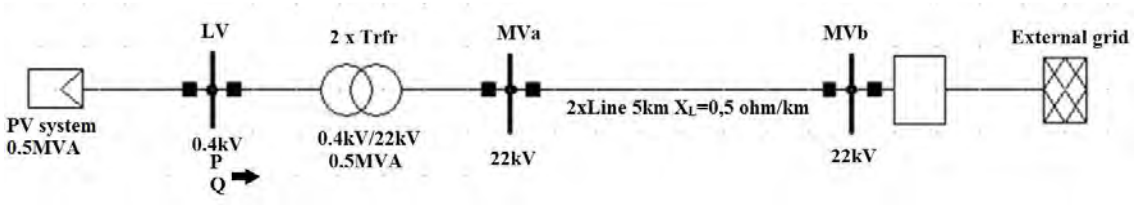

Figure 3-13: Single line diagram of power system

The power system has a PV system as the source of power rated 0.5 MVA connected to the LV busbar of 0.4 kV and a step up transformer from 0.4 kV to 22 kV rated 0.5 MVA off the shelves in line with the inverter rating where at 0.9 pf gives 0.45 MW neglecting active power losses. The short transmission lines are identical at a distance of 5 km. the measurements of voltage, active power and for PLL are taken from the LV busbar.

A comparison of the developed model and the PowerFactory model is tabled below.

Table 3-3: Comparison of PV system functions

Developed PV model in PowerFactory	**Generic PV model in PowerFactory**
Referenced scientific equations used for modelling	Undefined equations of the model
five parameter model	four parameter model (no shunt resistance)
MPPT block	No MPPT control

The testing of these two models in PowerFactory is compared below with each other. Each model will be connected independently to a power system shown in single line diagram below.

The case studies to test the developed PV system in comparison with generic model will give a good indication to validate the developed model since the generic model in PowerFactory gives basic understanding of the working principle of the PV system. Table 3- 4 show PV array parameters used.

.

Table 3-4: PV system parameters at STC

PV module Parameters	

Short circuit current	5 A
Open circuit voltage	43.8 V
Current at MPP	4.58 A
Voltage at MPP	35 V
K_i	0.0004
K_v	-0.0039
No. of series modules	20
No. of parallel modules	140

3.6.1 PV response due to weather conditions (Irradiance change)

The irradiance input is changed from 1000W/m2 to 500W/m2 and back to 1000W/m2. The graph results are shown below for: DC voltage (Uarray), DC current (i0dc), Active power and AC voltage at LV busbar and explained below.

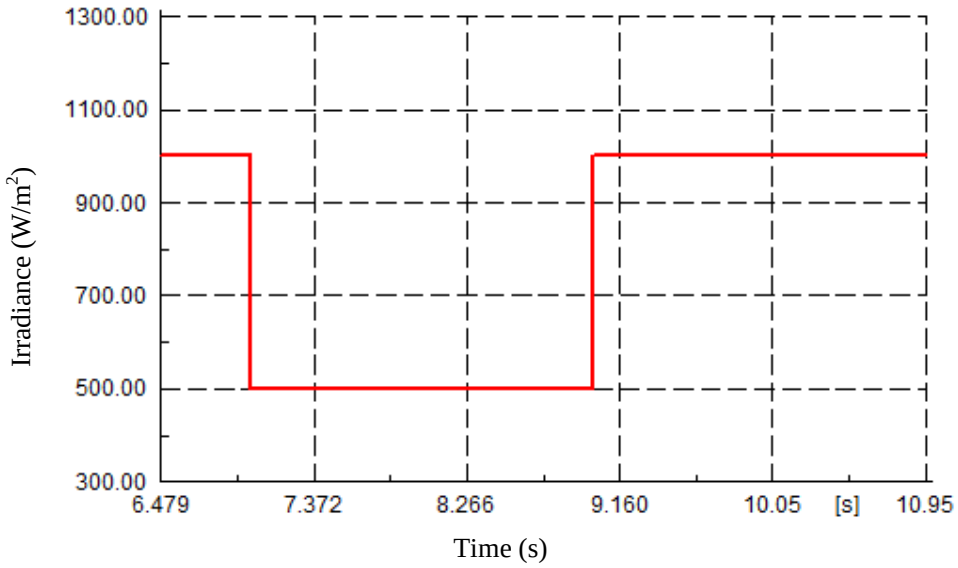

Figure 3-14: Input irradiance change (W/m^2)

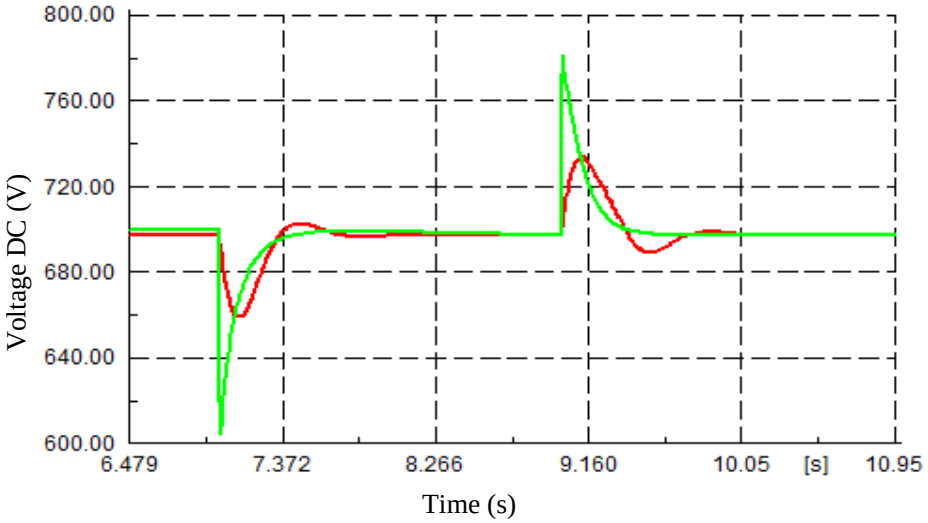

Figure 3-15: DC voltage (V)

Figure 3-15 shows the DC voltage change due to change in irradiance from Figure 9. The response in comparison show similar results from both models the green graph being a model from PowerFactory and the red is the developed PV.

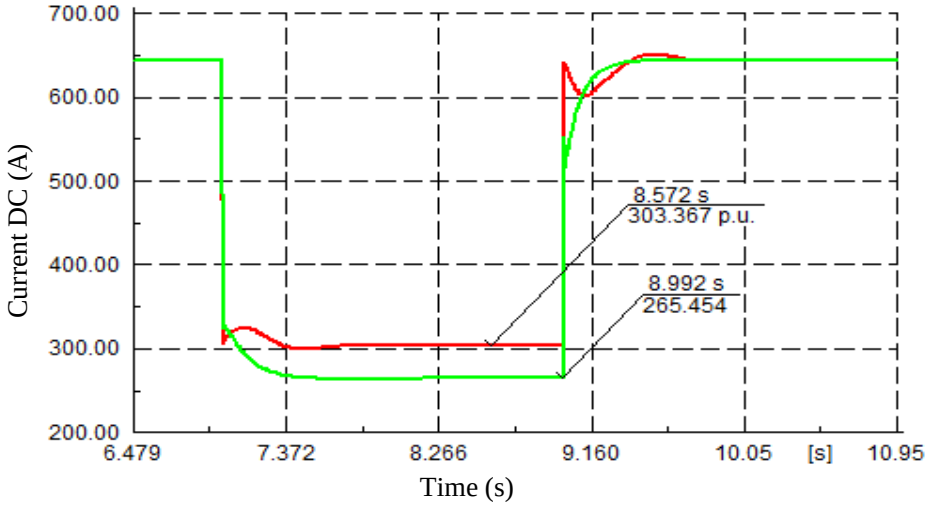

Figure 3-16: DC current (A)

Figure 3-16 shows the DC current response of the two models (green being the model from PowerFactory and red the developed PV model). In comparison the DC current has a slight different in the dynamic behavior due to the modelling method and mathematical equations used. From [21] & [88] indicated through equation (3.2) that the current output is directly proportional with irradiance therefore current at 500 W/m^2 is expected to be half.

From the graph the developed model has given a better estimate as the expected output current, from calculation is 140 x 4.58A / 2 = 320.6 A, the losses can be accounted by the leakage losses in the solar cell.

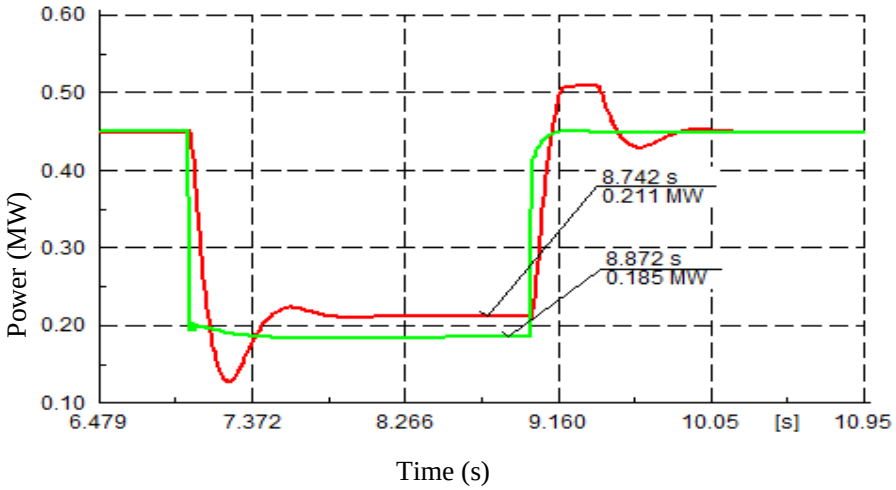

Figure 3-17: AC power of PV in (MW)

Figure 3-17 show the active power response is similar the slight different is the dynamic behavior for the developed model having an initial dip and overshoot at the changes. The prediction of the power generated once irradiance change is different by a margin of about ΔP_{pv} = 0.026 MW. This can be accounted for the extra control of MPPT included for the developed model to track maximum power point. The PV array response noted above Figure 3-16 12 is very instant at point of 1000 W/m^2 solar irradiance to 500 W/m^2 the PV array vertically moves down, whereas the inverter reaction is delayed by its controller delay. Thus, generic controller is faster than developed controller concluding from overshoot response of developed model requiring controller tuning.

Figure 3-18 show the AC voltage busbar response and for both models show similar behavior with the developed model showing transient behavior but overall response is negligence. The transients are influenced by controller and size of DC-link.

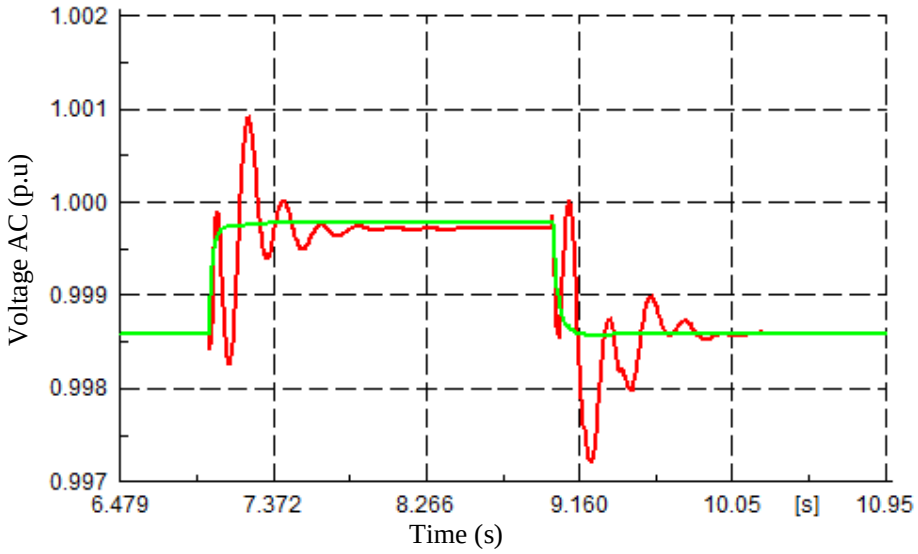

Figure 3-18 AC voltage @ LV busbar (p.u)

The response of the two model PV systems are very similar only differ in the dynamic behavior and transients from the developed model but similar results have also been seen from author [111] & [112]

3.6.2 PV response due to grid voltage change (AC side voltage change)

In this case the grid side has a disturbance where the external grid voltage will change from 1pu to 0.98pu permanently. Both models have similar controller therefore same output is expected. The DC voltage is seen to behave in a similar manor for both models same with the DC current as well as the LV busbar voltage. The results are shown below for: DC voltage (Uarray), DC current (i0dc) & AC voltage.

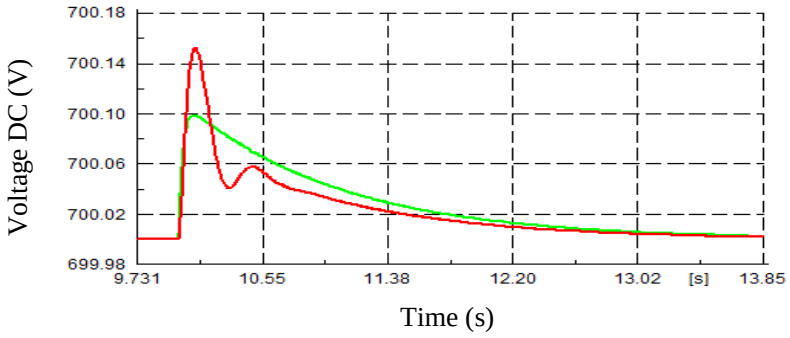

Figure 3-19: DC voltage (V)

Figure 3-shows the comparison of DC voltages for both models and the two models show similar behavior but the developed show transients. The increase is forced by the power transfer from the PV system to the grid which is the natural operation of the PV to maintaining a higher voltage then the grid for power flow.

Figure 3-20 shows the DC current response for both model and show similar behavior in comparison with slight different as the developed model show some transients.

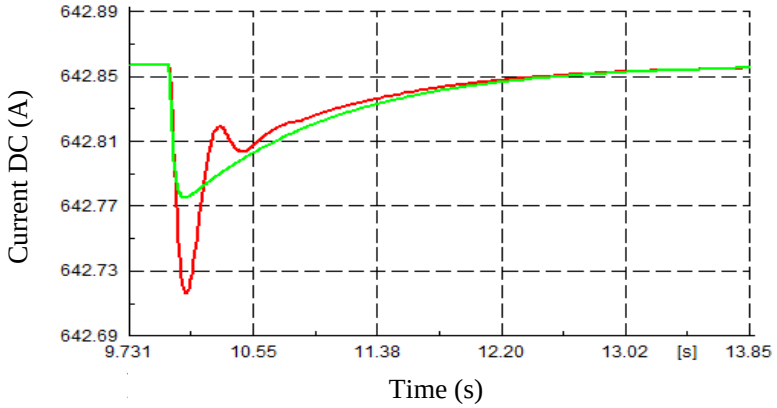

Figure 3-20 DC current (A)

Figure 3-21 shows the AC voltage (LV busbar) response and it can be seen the voltages are gradually decreasing towards 0.98pu the new voltage value from the grid voltage. For the reactive power no change was observed due to the control setting as the deadband was not violated therefore no control triggered.

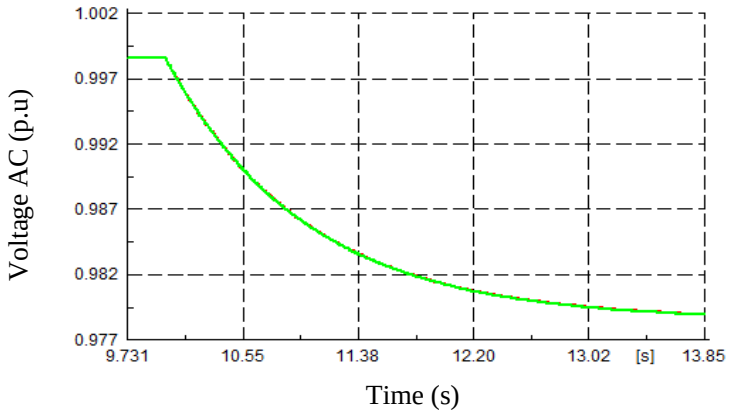

Figure 3-21 AC voltage at the LV bus

3.6.3 PV response due three phase fault (Fault applied at the grid connection)

A three phase short circuit is applied to the point of connection (MVa busbar) POC located after the step up transformer busbar, which has the highest impact out of all the faults [113]. Under these abnormal conditions both models will be observed to see similarities in behavior and the correlation will further validate the developed model. The fault will last for 1s which is extreme as the typical maximum fault duration is around 150ms.

The models will be compared for the following measurements DC voltage, DC current, Active power, AC voltage at LV busbar and reactive power.

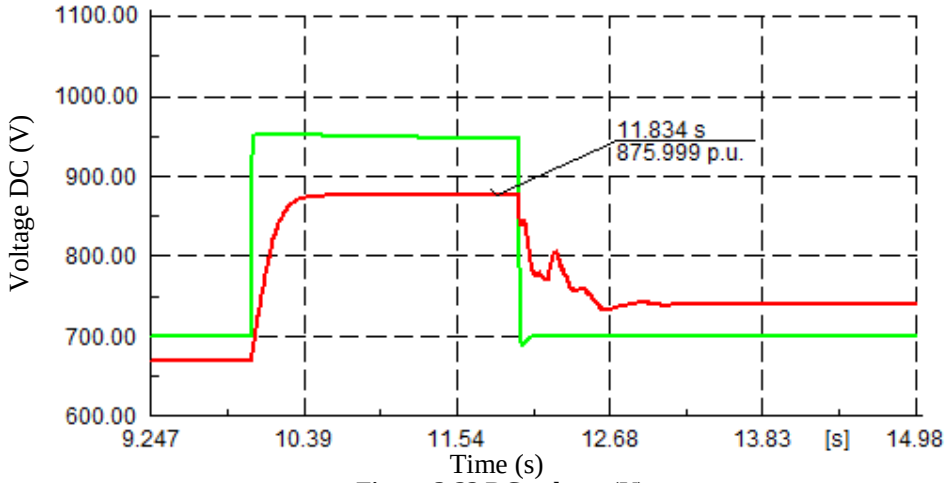

Figure 3-22 DC voltage (V)

Figure 3-21 shows the DC voltage response during a three phase fault for both the models the behavior is similar but for the developed model the voltage during a fault reaches the rated open circuit voltage 43.8V * 20 = 876V of the array and transients just after the fault is cleared and settles on the new higher value this behavior can also be seen from author [113].]. The rise in voltage is due to the active power from PV array dumped in the capacitor.

Figure 3-22 the DC current decreases for both models but the generic model decreases sharply than developed model and the delay is assumed to be caused by PV inverter controller and some transients can be seen after fault is cleared.

Figure 3-23 shows the active power and both models decrease to zero and as soon as the fault is cleared returns to the initial values. There are transients seen after fault is cleared and similar behavior can be realized from [114]. Even though the AC side faults current increases (not

shown) but the drop on the voltage at the point of connection side outweighs resulting to the output power drop [115].

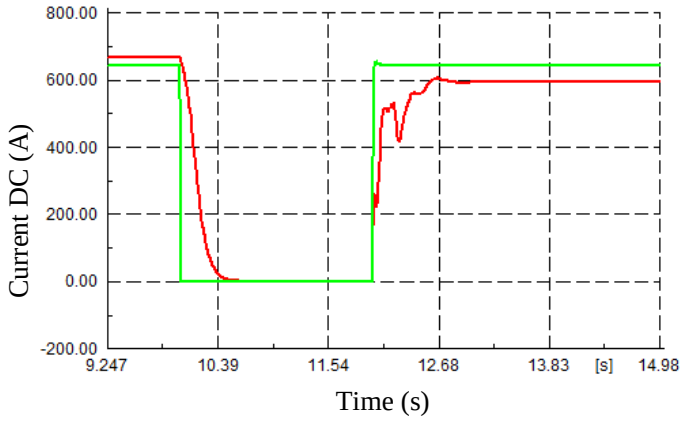

Figure 3-23 DC current (A)

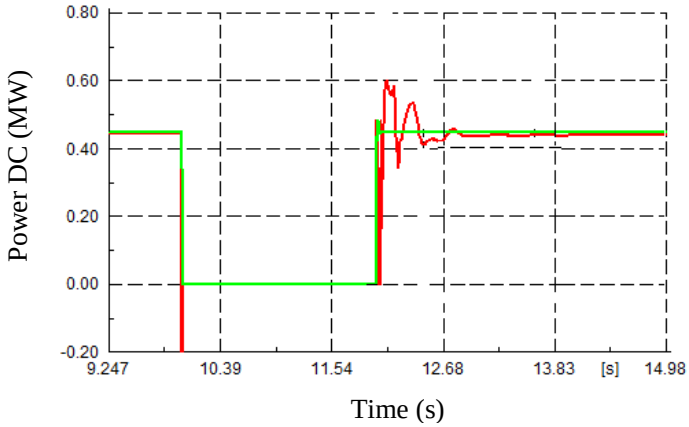

Figure 3-24 Active power (MW)

Figure 3-24 & Figure 3-25 show reactive power and AC voltage respectively. The response is similar for both cases where for reactive power for both models slightly increase during fault and decrease back to zero after the fault is cleared and some transients is seen for the developed model the reactive control reacts to keep up the oscillating voltage and to help the system network to stabilize. And for the AC voltage both models decrease close to absolute zero and returns back to initial value after fault is cleared. Due to the reactive power injection during a fault the voltages do not reach zero.

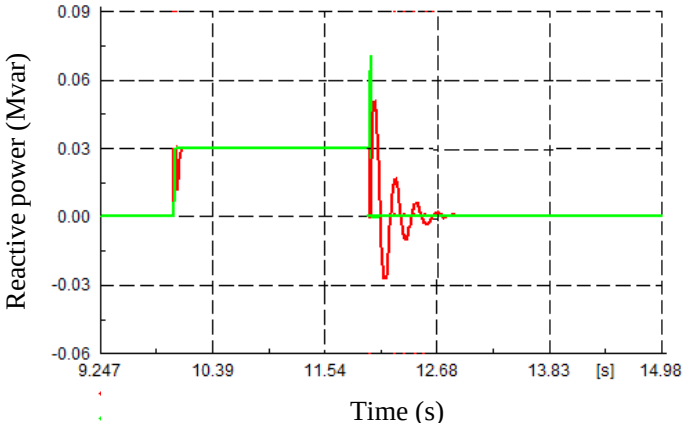

Figure 3-25 Reactive power (MVar)

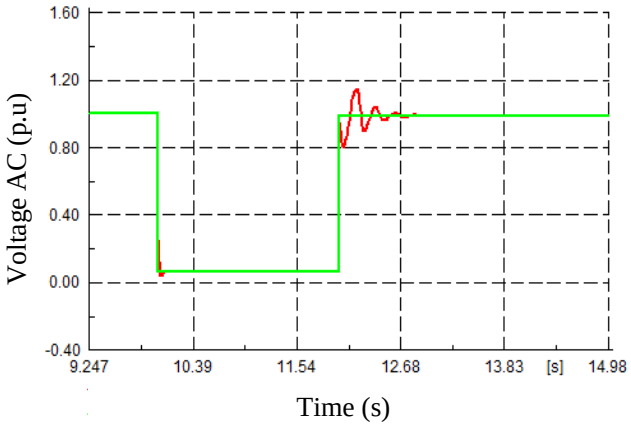

Figure 3-26 AC voltage in p.u (LV busbar)

PV generation relative simulation results of developed and PF model are consistent with each other. The voltage dip depth and recovery curve of PV generation grid-connected point is basically the same. During and after fault the output current, active power and DC voltage of PV generation is also basically the same. The observed fluctuations can be due to reactive power injected algorithm and inverter control characteristics.

3.7 Discussion

A number of available mathematical models for PV systems corresponding determination methods have been established and a few have been mentioned. The five-parameter model is the employed in this study and solved using analytical method which is simple and rapid convergence. The validation of the model is done by comparing simulation results produced by other methods. The results show that the chosen model can accurately simulate the entire I-V characteristic curves. The detailed mathematical model is implemented in simulation tool

PowerFactory DigSilent incorporated with control scheme for the grid-connected PV system. Since the proposed model of the PV array uses theoretical and empirical equations together with data provided by the manufacturer and atmospheric data enhances the accuracy of predicting the PV cell characteristic curve. The controls established for dynamic active power and reactive power also included the MPPT algorithm. The results demonstrate the validation of the proposed model and the effectiveness of the model control. Therefore, from the results obtained it can be concluded that the developed model in comparison with PowerFactory model is similar and the observed differences are due to the differences in PV modelling method. These similarities verify the developed model.

CHAPTER 4
MPPT AND GRID REGULATIONS

This chapter evaluates the developed PV model for integration impact and South African grid codes compliance. Several requirements that are important are examined for PV system modelled connected to a typical power station electrical auxiliary network where the load flow, fault level and contingency analysis are done with and without the PV system connected to the 11 kV busbar. The various testing to validate the established controls are performed for frequency response requirement tested for the active power reduction during the event of an over-frequency, the Low Voltage Ride Through (LRVT) which require that the PV plant continues to operate through periods of low voltages and must not disconnect from the grid and similar with the High Voltage Ride Through (HVRT) requirement. The results indicate the PV model capabilities to remain compliance to the requirements of (SAGC) at the Point of Connection (POC). A steady state analysis is conducted with the PV plant to evaluate any violation with the voltages at all busbars for typical power station distribution network. Scenarios for an n-1 contingency are tested for voltages variations and must be within allowable limits. The PV plant fault contribution is also evaluated load following characteristic of the PV plant and local generator.

Overall activities completed in this chapter are:

- MPPT implemented in PF and tested (P&O and IncCond)
- Testing SAGC compliance
- Steady state analysis of PV model connected to PS reticulation network
- Dynamic loading characteristic of PV model analysis

4.1 Maximum power point tracking

The MPPT algorithms incremental conductance and perturb & observe are first tested by introducing a disturbance to evaluate how the two techniques track the maximum point. And lastly ramping capabilities of local generator are evaluated. Finally, the adequacy of these grid codes to guarantee the safe and reliable operation of electrical grids is discussed.

The two MPPT techniques implemented are namely P&O and IncCond algorithm and shown in Figure 4-1 & Figure 4-2 as discussed in section 2.5. The design value of the threshold which considers operating exactly at the MPP and possible oscillation around the MPP is shown by equation (4.1) below.

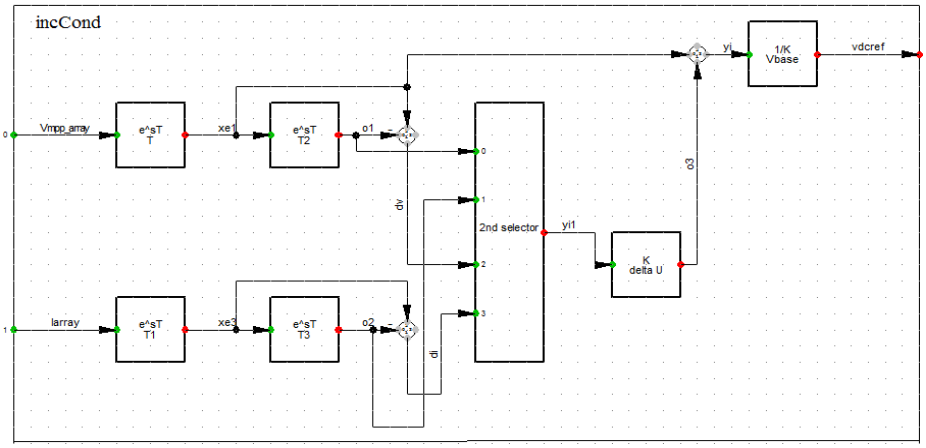

Figure 4-1: Incremental conductance in PowerFactory

Selecting optimal K-delta is important [116] and manually guessing the scaling factor is tedious so can be given by:

$$K_{deltaU} = V_{mpp} / \left(freq_{MPPT} \times step \right) \tag{4.1}$$

where V_{mpp} is the voltage at the maximum power point, $freq_{MPPT}$ is the frequency of the MPPT algorithm and the step is the perturbation step design. The frequency of the MPPT is typically in the range of 15-20 Hz. Different step sizes of 0.5, 0.05 and 0.005 were considered and all step sizes track the maximum point but for a step size of 0.5 the tracking is faster and oscillates more and the step size of 0.005 is slowest therefore tradeoff choosing 0.045 step size producing acceptable tracking speed and oscillations. Using the appropriate design parameters Figure 4-3 & Figure 4-4 shows results of MPPT.

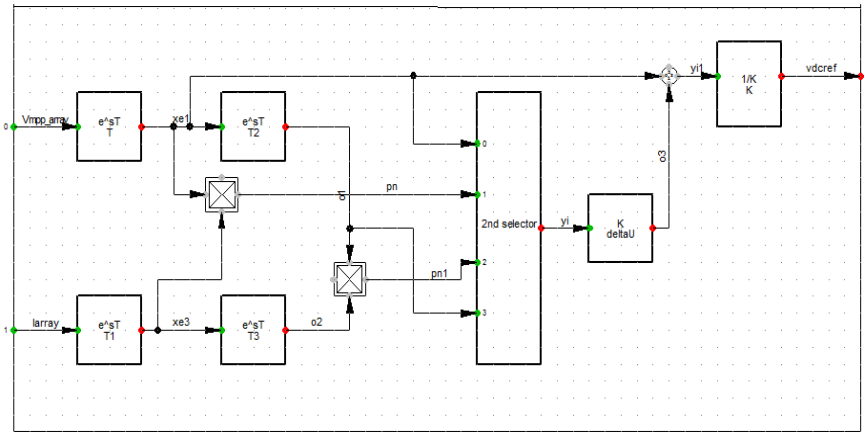

Figure 4-2: P&O in PowerFactory

The comparison of both MPPT algorithms is done by plotting results and noting the number of perturbation and oscillations. A large change in irradiation (1000 W/m^2 to 500 W/m^2) is created, with an expectation that both techniques will be able to track the maximum power point of the P-V curve. and the results are shown in Figure 4-3 and Figure 4-4. The simulation results show the incCond has no oscillations and can be seen climbing the P-V curve in order to get MPP hence more efficient then P&O algorithm.

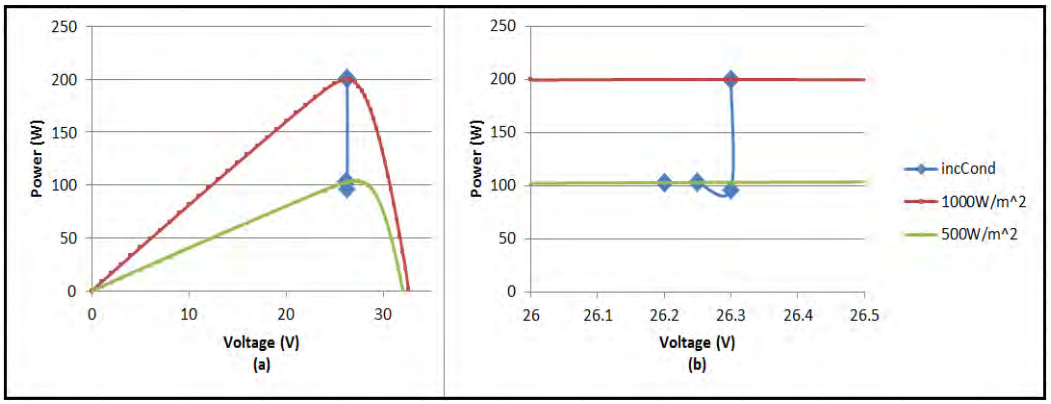

Figure 4-3: (a) PV characteristics and incCond response (b) zoomed in

Figure 4-3 initially at 1000 W/m^2 the blue dot is at the maximum power point and as soon as the irradiance changes to 500 W/m^2 the incCond checks the current and voltage and senses only current has changed from high to low therefore make the appropriate perturb which in this case decreasing the voltage one step and checks again then perturbs until reaches the maximum point in which is 26.2 V seen from Figure 4-3 (b). To overcome oscillations for incCond once the maximum point has been reached is the extra decision box is added which checks if $di_{pv} / dv_{pv} + i_{pv} / v_{pv} < \varepsilon$ where ε is the absolute value chosen depending on level of sensitivity the user desires and once this equation holds therefore maximum point has been reached and the voltage is kept unchanged [117].

In Figure 4-4 initially at 1000 W/m^2 the two blue dots show oscillations around the maximum point and then after the irradiance changes to 500 W/m^2 the algorithm finds a new maximum point and oscillates on the right side of the optimum voltage point. This makes the P&O technique less efficient and less stable. It has been shown that the P & O can exhibit unreliable results under rapid change in irradiance level and one of the simplest solution to overcome this which is implemented in the study entails the addition measurement of power *P1* at array voltage *V1*, perturbing the voltage and again measuring the power *P2* at voltage *V2*, and from the two measurements the algorithm can determine whether the irradiance has changed but the

extra measurement slows down the algorithm. From Figure 4-3 & Figure 4-4 results it can be concluded the MPPT algorithms work correctly as expected and implemented on the simulation circuitry.

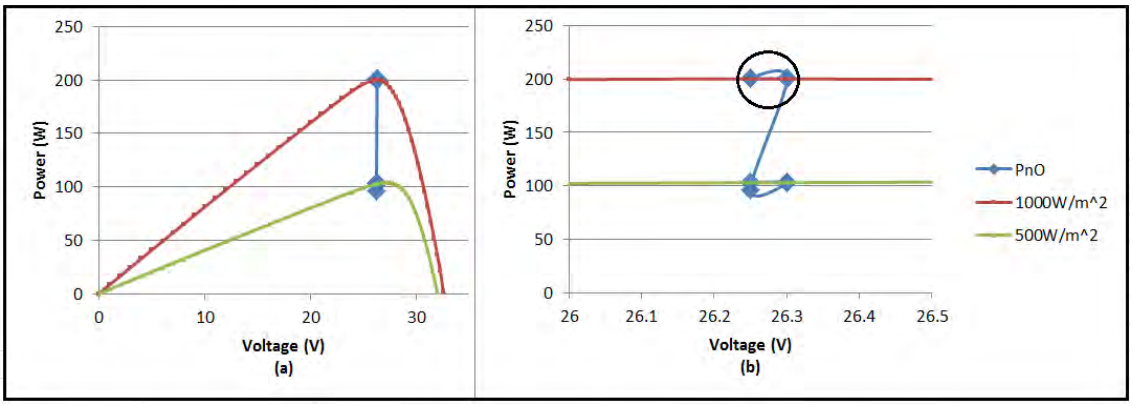

Figure 4-4: (a) PV characteristic and P&O response (b) zoomed in

4.2 Grid connection compliance for PV model

The renewable penetration must not jeopardize the normal operations of the system grid. Thus, technical specifications shall be enforced to ensure safe interconnection of renewables onto the grid. The grid connection code objective is to specify minimum technical and design grid connection requirements for Renewable Power Plants (RPPs) connected to or seeking connection to the South African electricity transmission system (TS) or distribution system (DS). An appropriate point of connection shall be recognized on the basis of secure network operation taking the generating plant into consideration, and at which the requested power can be received and transferred. The behavior of the renewable plant will determine the secure point of connection. Thus, assessment of the connection possibility under disturbances at the network connection be tested for short-circuit power, and operation mode of the renewable plant. Several renewable plants connected to the same voltage network, their overall impact must be taken into consideration. The following section presents the essential aspects to be taken into consideration for the connection of renewable plant to the grid so to maintain the security and reliability of network operation and evaluate requirements in accordance with SAGC.

4.2.1 Connection points

For this study a short conductor connecting the PV plant to the power station auxiliary load at different busbar levels is tested and at these different positions steady state analyses is done evaluating for any violations. A small difference at all the various connections is seen when

comparing all bus node voltages. The voltage at lower voltage ratings tends to rise at the connected bus node but within acceptable limits. This can be avoided by having multiple point of connection. However depending on the connection point the daily variations in solar irradiance can cause reverse flow in reticulation system that could course error in operation of protection relays thus, care should be taken when choosing connecting point. In this case the final connection point suitable is the 11 kV busbar which is the next voltage level stepped down from generator output voltage of 22kV, therefore the flow of power is in one direction and enhances the impact of PV plant to the generator for the purpose of the study. Further analyses are to be done to provide knowledge of any operational risk with PV plant connected.

With the PV system connected to an 11kV bus shown by Figure 1, grid code compliance will be tested at this connection point for various topics discussed below as per the requirements from SAGC.

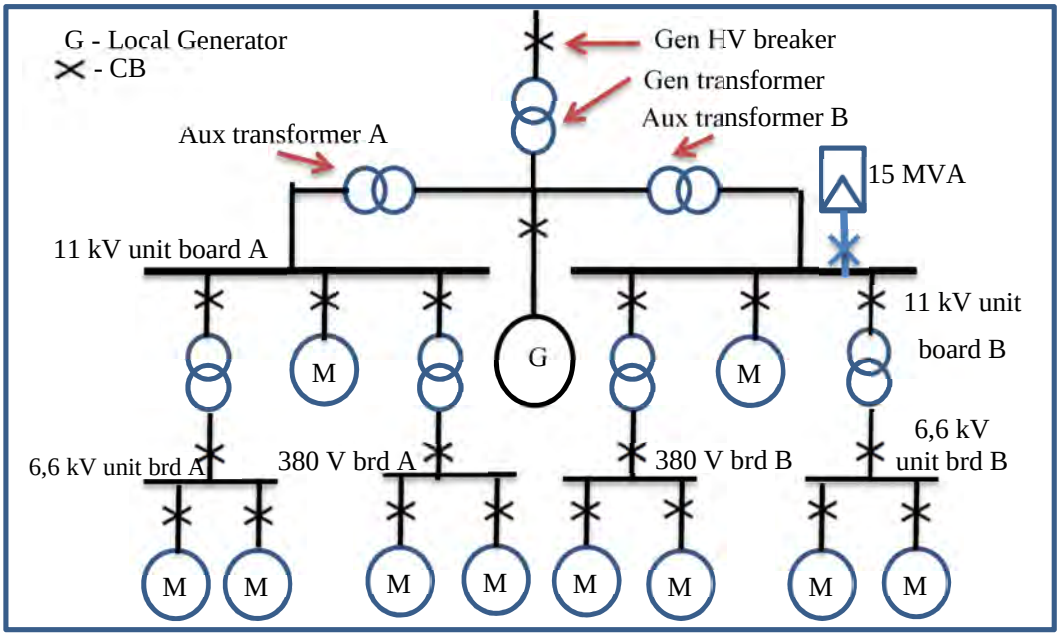

Figure 4-5: Auxiliary system for testing the PV system [77]

4.2.2 Grid code compliance for PV plant

The grid code integration requirement is an essential guideline for the design, control and operation of grid connected with PV energy system. In normal operation, the PV system is required to produce maximum within satisfactory injection currents e.g. IEC 61000 specification. For high PV penetration level scenario, grid connected PV systems will impose new challenges to the distributed electrical network. The challenge lies in the atmospheric

nature fuelling the PV sources and the response of PV systems from abnormal grid conditions. Thus, may induce instability on the network. To overcome the above issues, the grid requirements act as guard line. The SAGC requires that the systems connected to the medium or high-voltage networks should be capable of riding through voltage sag and at the same time to provide reactive current to the faulted grid [79]. When the grid voltage level is higher than the specified ones defined in Fig. 3, the PV systems should maintain connected to the distributed grid and inject reactive power to support the grid.

For RPP to be in compliance with the South African grid code relevant controls are established to meet the requirements. This paper will only focus on the requirements for category B & C of the SAGC, renewables rated in the range 1-20 MVA and above respectively [79].

PV model specification

The PV plant will consist of 5 feeders and each feeder with 6 inverters rated 0.5 MVA, power factor = 0.95 with maximum power P=0.475 MW each. Dispatched at P=0.45 MW therefore, 13.5 MW total power output. The inverter is connected through a step up transformer 0.4/11 kV 0.5 MVA, YNyn, 5%.

4.2.2.1 Frequency response

- When the frequency on the NIPS is higher than 52 Hz for longer than 4 seconds, the RPP shall be disconnected from the grid.
- When the frequency on the NIPS is less than 47.0 Hz for longer than 200ms, the RPP may be disconnected.
- The RPP shall remain connected to the NIPS during rate of change of frequency of values up to and including 1.5 Hz per second, provided the network frequency is still within the minimum operating range indicated in Figures 4-6.

For the nature of the power station electrical auxiliary network and RPP the PV plant will not be participating in the frequency control but will have the controllability to reduce its power output in the event of higher frequency limits exceeded as seen in figure 4-6 [79].

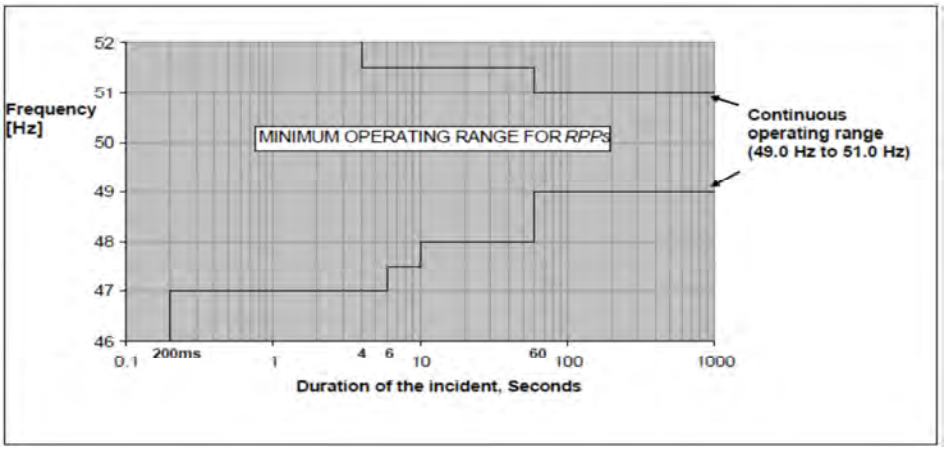

Figure 4-6 Minimum frequency operating range of a RPP (during a system frequency disturbance)

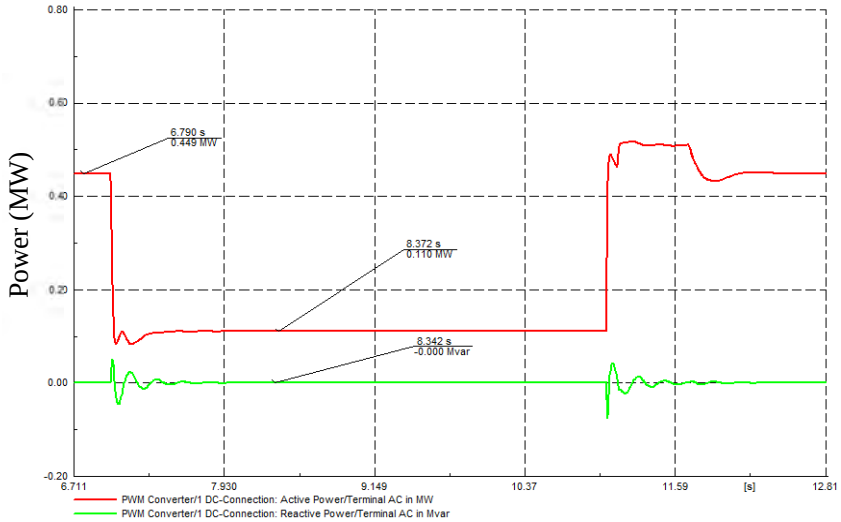

Figure 4-7: Active power frequency response

4.2.2.2 Voltage response

4.2.2.2(a) LVRT & HVRT capabilities

In order to demonstrate the LVRT capability of a RPP, dynamic simulation studies based on the established model are performed. And the results of these simulation studies shall demonstrate:

- The the RPP is capable of staying connected as long as voltage is above the lower limit curve (and below the upper limit curve) according to Figure 4 of SAGC (area A, B and D)
- The RPP injects reactive current as specified Figure 4-8.

This requirement shall apply to all types of faults (symmetrical and asymmetrical, i.e. one-, two- and three – phase faults).

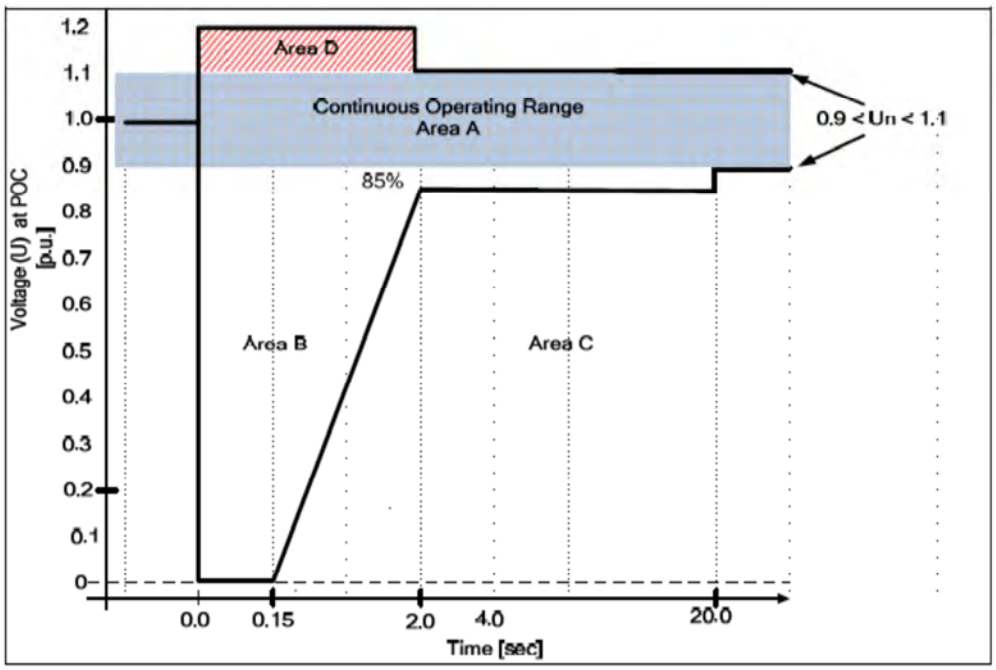

Figure 4-8: Voltage ride through capability for RPP of category A3, B and C

Disconnection is only allowed once Area C in Figure 4 is reached. The control of reactive current should follow the characteristics of Figure 6 with a tolerance of ±20% after 100ms. The supply of reactive power has first priority in area B, while active power has second priority. If possible maintain active power supply during voltage drop but a drop is allowed. To test the Low Voltage Ride Through (LVRT) capabilities, worst case operating conditions of RPP is assumed for:

- Operation at maximum active power output (P=Pn)
- Operation at max. voltage which leads to maximum voltage dips (ΔUmax)
- Operation at max. or min. reactive power (Q=Qmin, Q=Qmax)

To test the High Voltage Ride Through (HVRT) capabilities, worst case operating conditions of RPP is assumed for:

- Operation at maximum active power output (P=Pn)
- Operation at min voltage which leads to maximum voltage rise (ΔUmax)
- Operation at max or min reactive power (Q=Qmin, Q=Qmax)

The results are tabled below and shown in Figure 4-9 and Figure 4-10 where a three phase fault is applied at 7 second. The reactive current is tabled and marked in Figure 4-10 in red circles. The High Voltage Ride Through (HVRT) results are also tabled below Table 4-1.

Table 4-1: Voltage ride through capabilities

Voltage (p.u)	Fault duration (s)	Active Power (p.u)	Reactive current (p.u)	Stable (Y/N)
0	0.15	0	-1	Y
0.2	0.59	0	-1	Y
0.5	1.24	0.15	-0.801	Y
0.7	1.67	0.46	-0.409	Y
0.85	20	0.86	-0.018	Y
1.2	2	1	0.182	Y

The results obtained in Table 4-1 show the active power is reduced to zero for a bigger voltage drop and maximum reactive current is injected to the point of connection. The reactive current negative sign denotes that reactive power leaves the PV plant and positive absorbs reactive power. In Figure 4-9 the voltage does not reach absolute zero this is due to the reactive current support.

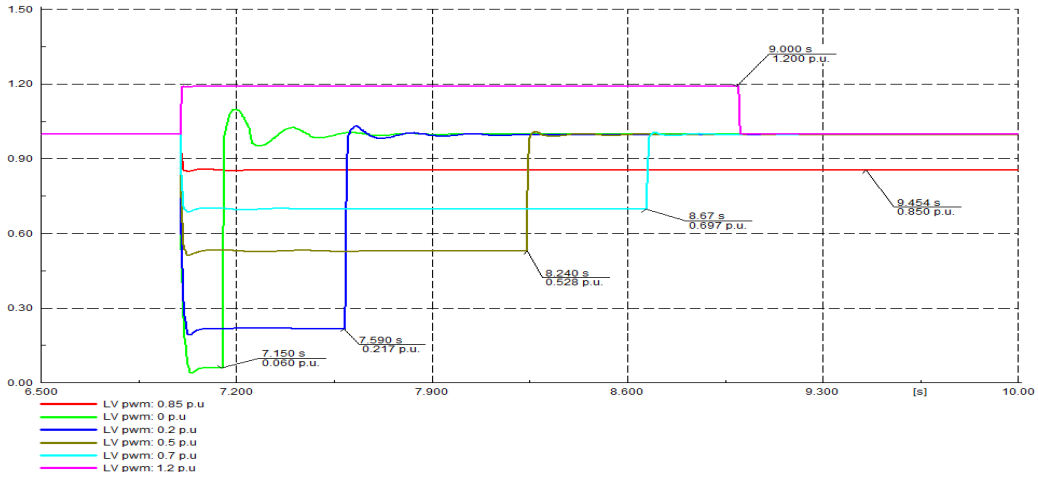

Figure 4-9: Voltage Ride Through capability of PV farm

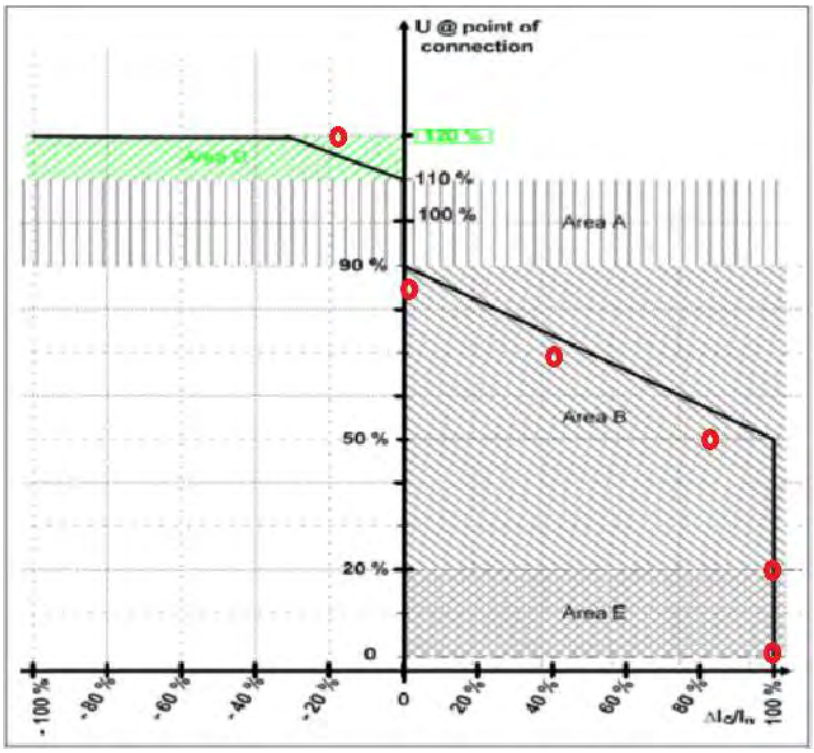

Figure 4-10: Requirements for reactive power support, I_Q during voltage drops or peaks at the POC

4.2.2.3 Reactive power capabilities

4.2.2.3.1 Requirement for category B

RPP shall be designed to supply rated power (MW) for power factors ranging between 0.975 lagging and 0.975 leading for a PV plant rated 15MVA and must be available from 20% of rated power measured at the point of connection as shown in Figure 4-11. The RPP must be capable to operate in the hatched area as shown in Figure 4-11 & Figure 4-12 [79].

Figure 4-11 point A and B are equivalent in (Mvar) to -5% and 5% respectively and point C is equivalent in MW to 5% rated MW output and the reactive power requirement over full generation range 22.8% corresponds to 0.975 pf for leading and lagging.

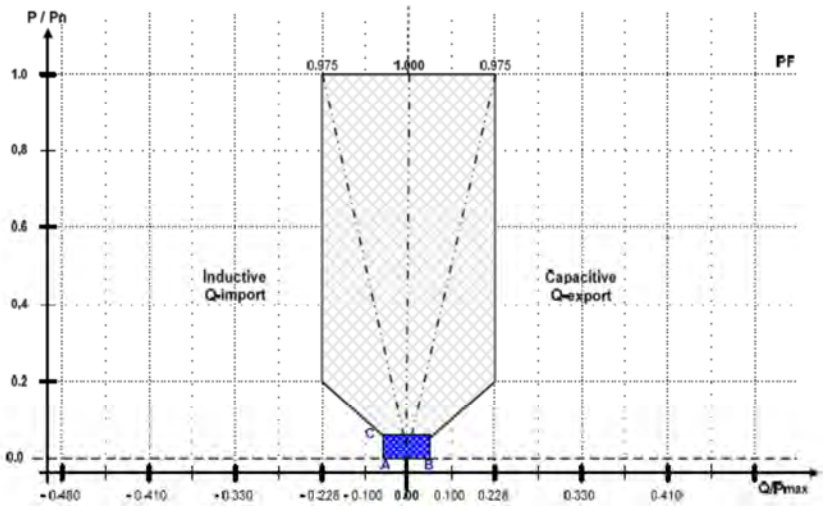

Figure 4-11 Reactive power requirements for RPPs of category B

The exercise to check if the PV plant complies with reactive power requirement is done for every point of operation of the PV plant. Aided by the power factor station controller to set the power output and reactive set points. The grid code requires at least 0.975 lagging and 0.975 leading and voltage to be within the range ±10%. The control is at the point of connection. Table 2 show results of PV plant at point of connection to meet all requirements without violations from the PV inverter. Observation for leading pf the PV inverter voltage rises within the limits considering the cable length from the last PV array inverter will not be expanded. Since the PV inverter manufacture recommends voltage operation should be within ±10%. So care should be taken when expending the PV plant:

Table 4-2 Results of PV farm connected

Power	Required Q @ POC	Required Q @ POC	Reactive power met? (Y/N)	Voltage @ POC	Voltage @ Inverter	Actual Q @ POC
P=5%	Q=5% (ind)	0.65Mvar	Y	1.02	1.02	0.5
P=5%	Q=5% (cap)	0.65Mvar	Y	1.01	1.01	0.5
P=20%	Q=22.8% (ind)	3Mvar	Y	1.01	1	3
P=20%	Q=22.8% (cap)	3Mvar	Y	1.02	1.04	3
P=100%	Q=22.8% (ind)	3Mvar	Y	1.01	1	2.99
P=100%	Q=22.8% (cap)	3Mvar	Y	1.03	1.04	3

Now to test for voltage control capabilities of the PV plant against grid code requirements shown by Figure 4-12 [79]. An external grid connected to the PV plant aids changing the voltage of the point of connection and a station control is to be used to control the power factor at the point of connection.

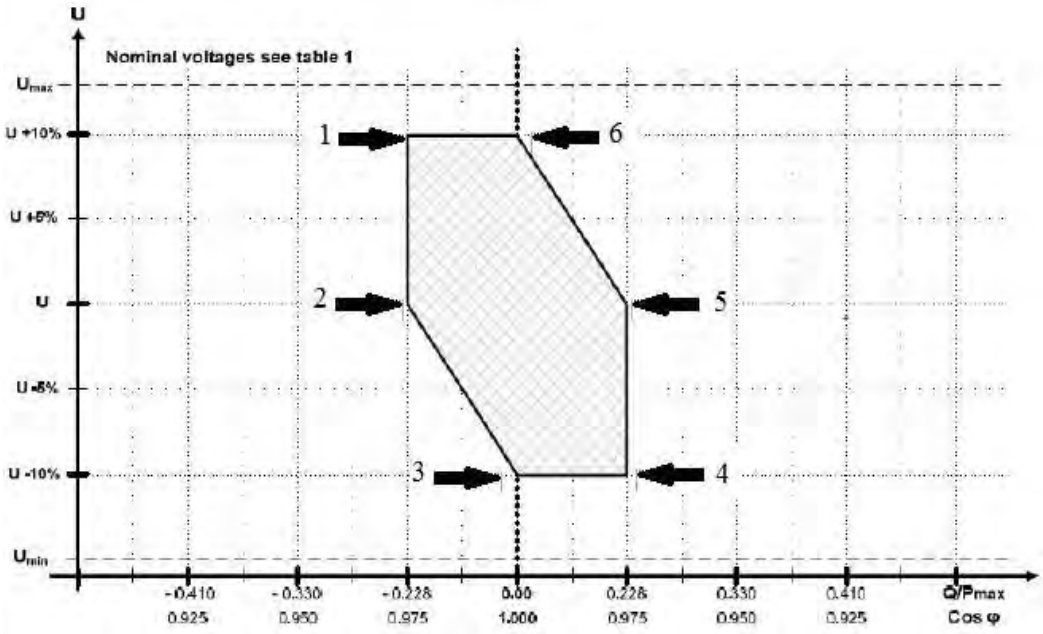

Figure 4-12 Requirements for voltage control range for RPPs of category B

Table 4-3 Results of PV farm at various voltages and power factor

Point	V @ POC	PF @ POC	Q @ POC	Actual PF @ POC	Voltage @ inverter	Grid Compliant (Y/N)
1	1.1	0.975 (lag)	3 Mvar	0.975	1.11	Y
2	1	0.975 (lag)	3 Mvar	0.975	1.02	Y
3	0.9	1	0	1	0.9	Y
4	0.9	0.975 (lead)	-3Mvar	0.975	0.89	Y
5	1	0/975 (lead)	-3Mvar	0.975	0.99	Y
6	1.1	1	0	1	1.1	Y

From the table 3 the obvious voltage violation are at the maximum and minimum voltage limits of the PV inverter when operated at 1.1p.u and pf is 0.975 lagging the maximum voltage limit is exceeded, and also when operated at voltage 0.9p.u. and pf is 0.975 leading the minimum

voltage limit is exceeded. Therefore compensation is needed. Where a minimum shunt reactor rating of 2.1 Mvar when modelled show improvement and the PV inverter voltages stay within limits specified by manufacture.

4.2.2.4 Reactive power and voltage control functions

The requirements of reactive and voltage control only applies to category B and C. The RPP must be equipped with reactive power control function, and voltage control function capable to controlling reactive power and voltage at the point of connection. But one control function can be activated at a time: Voltage control, Power factor control & Reactive power control. In this study only voltage control function is used [79].

4.2.2.4(a) Voltage control

The voltage control requirement is such that the voltage setpoint shall be commenced two seconds and completed no later than 30 seconds after receipt of an order to change the setpoint. The accuracy of the voltage setpoint shall be within ±0.5% of nominal voltage and the accuracy of the control must not deviate by more than ±2% of the required reactive power according to the droop characteristic as shown in Figure 4-13 [79]. The control shall not be limited to perform the control within its dynamic range and voltage limit with the droop configured. The droop is the voltage change in p.u caused by the change in reactive power (p.u). When the voltage control has reached the RPP's dynamic design limit, the control function shall await possible overall control from the tap changer or other voltage control functions [79]. Overall voltage coordination shall be handled by the network service provider in collaboration with the system operator. The voltage control function has been displayed above to be working in accordance to the requirements and shown in the appendix figure 8-14 where the upper is active power control and the lower for reactive power controller.

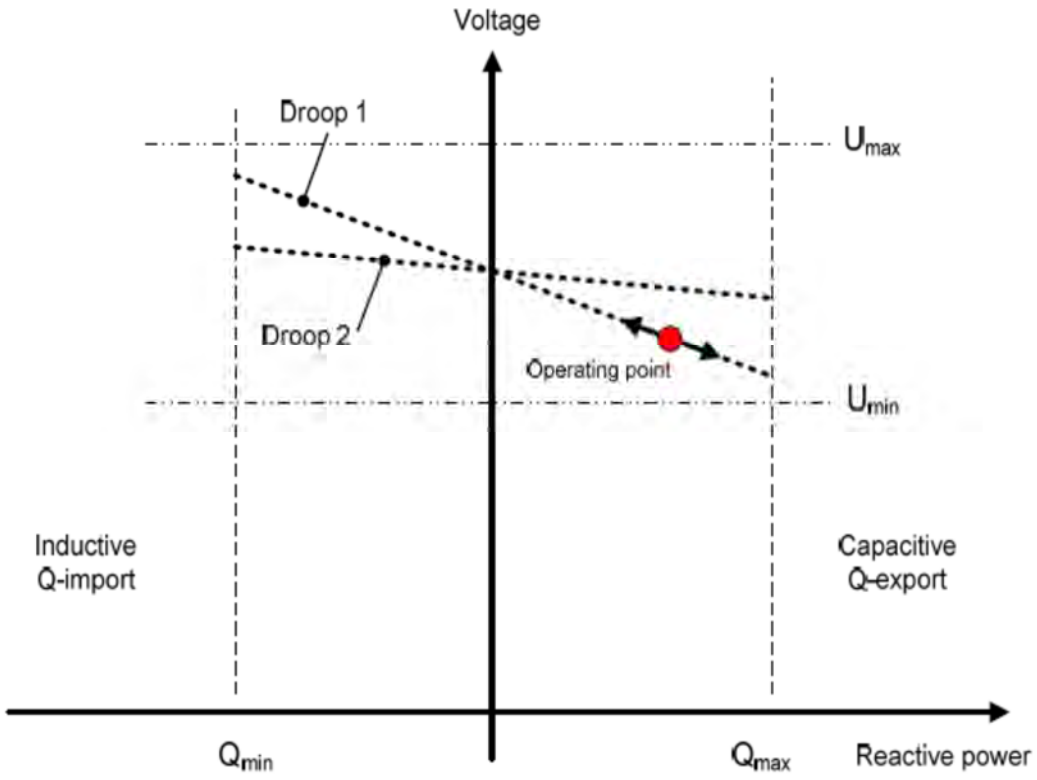

Figure 4-13 Voltage control for the RPP

The regulation method of the voltage at the connection point of the PV system is employed by reactive power with voltage as input. Therefore, the consumption of reactive power is dependent by voltage variation. The general relation between reactive power of a PV system and the grid voltage is defined as follows:

$$droop = \frac{\Delta Q}{V - V_n} \tag{4.1}$$

where droop is the slope factor (kVar/V) and V_n is the nominal voltage ΔQ is the required reactive power limit.

4.3 Power system analysis of auxiliary network

Steady state of RPP and local generator testing is performed to evaluate any possible electrical risks associated with PV system to ensure secure network operation taking all possible cases into consideration. The analysis results of the auxiliary network shown below.

4.3.1 Case: N-1 transformer contingency

An n-1 case where the aux unit transformer feeding 11 kV Unit Board A is isolated /disconnected and the tie link between busbar 11 kV board A and 11 kV board B is closed to maintain supply on the other rest of the auxiliary network and load flow showing busbar voltages is tabled below and show the PV plant improves the voltage in a situation for an n-1 contingency

Table 4-4: Voltages at aux transformer n-1 contingency

Busbar (voltage)	Local generator (p.u)	Local gen & PV farm (p.u)
0.38kV	1.04	1.05
6.6kV	1.01	1.02
11kV	0.99	1
22kV	1.02	1.02

4.3.2 Case: Fault and voltage analyses

A load flow and fault level analysis is tabled below with busbars results.

Table 4-5: Fault levels

	Local generator		Local gen & PV plant	
Busbars	3-phase fault (kA)	1-phase fault (kA)	3-phase fault (kA)	1-phase fault (kA)
0.38kV	34.777	33.32	34.779	33.317
22kV	214.92	0.01054	214.92	0.01054
6.6kV	22.366	0.327	22.371	0.3273
11kV	25.97	0.308	26	0.8258

Table 4-6: Busbar voltages different loading

Busbar	Local generator (p.u)		Local gen & PV plant (p.u)	
	50% aux load	Max aux load	50% aux load	Max aux load
0.38kV	1.09	1.07	1.09	1.07
6.6kV	1.06	1.04	1.06	1.04
11kV	1.04	1.02	1.04	1.02
22kV	1.02	1.02	1.02	1.02

The tabled results show the PV plant contribution is significant for single phase fault at the point of connection. The single phase fault is increased to 0.825kA from 0.308kA. Since the dq-

axis based current control scheme enables the current control in a balanced condition, the three phase fault current generated by the PV inverter is limited by the q and d axis reference values of the current controller, but for unbalanced fault, a single line to ground fault is not effectively controlled during the fault condition but limited to 120% of the inverter-rated current [118], which is also seen in this case [91] [113].

The PV plant shows no contribution to voltage violation as seen in Table 4-6 but for a low auxiliary loading, with the PV plant connected the voltage of 0.38 kV boarders around the boundary of low voltage limit of ± 10 % reaching 1.09 p.u. at half load.

4.4 Load following characteristic of PV farm

The ability of the PV system to supply the auxiliary load is tested under load changing scenarios, the table below shows case 1 with only the power station generator supplying the auxiliary system. Case 2 is the load flow when both the Generator and PV plant supplying the auxiliary load. Case 3 an equivalent load to PV supply power is added. Case 4 the added load is reduced and Case 5 the auxiliary load is reduced by 50% of full load.

Table 4-7: Load following characteristic

Case	**description**	**Local Gen (MW)**	**PV plant (MW)**	**Load added (MVA) 0.9 pf**
1	Gen only	544.88	0	0
2	Gen & PV farm	531.33	13.47	0
3	Gen, PV farm & Load	544.81	13.477	15
4	Added Load in case 3 reduced	544.855	13.477	7.5
5	Auxiliary load reduced	510.36	13.476	-50% aux load

From table 4-7 shows different case of loading and results are shown in Figure 4-14 to Figure 4-16. Figure 4-14 shows the loading event created; Figure 4-15 shows the generator power response to the loading event and the generator shows ability to follow the load closely and Figure 4-16 show the PV power output response to the loading event and from obtained results the load following characteristic is not possible with the PV system. Note: as the graph does not show a straight line but on the y-axis its showing one value of 13.48 MW.

From the table the connection of PV system decreases the generating output capacity which increases the ramping margin to follow the load. Therefore running the generator at lower capacity reduces costs and emissions.

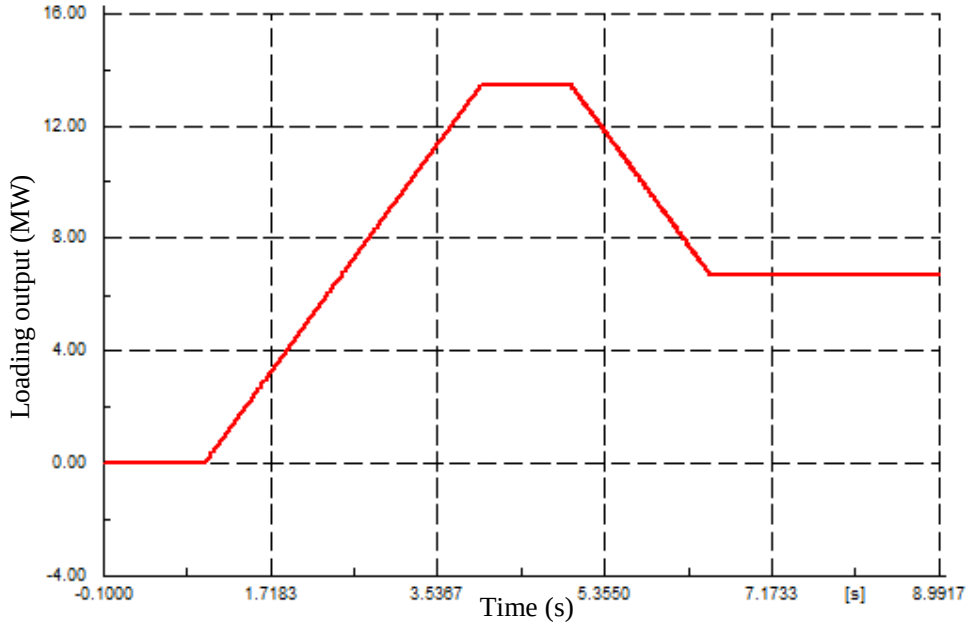

Figure 4-14: Load ramp event

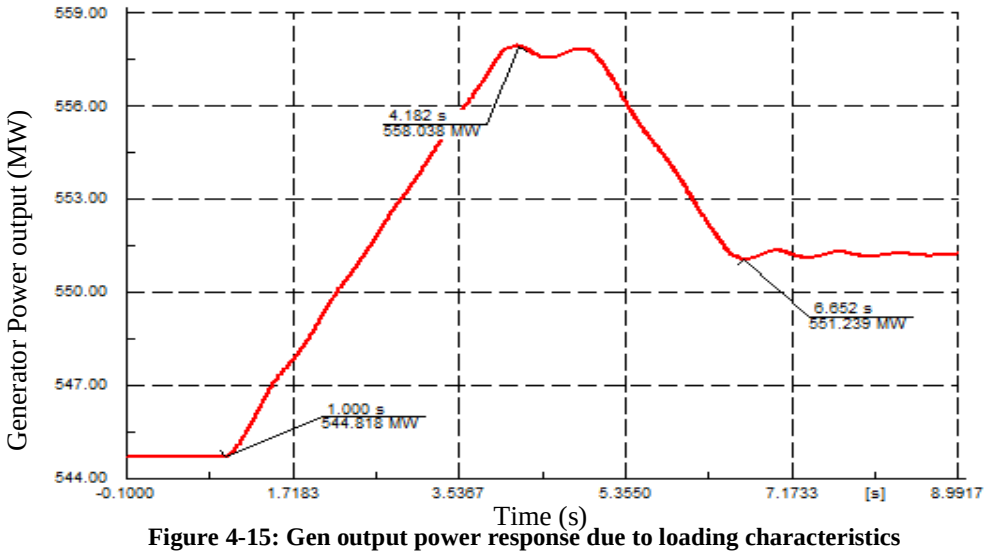

Figure 4-15: Gen output power response due to loading characteristics

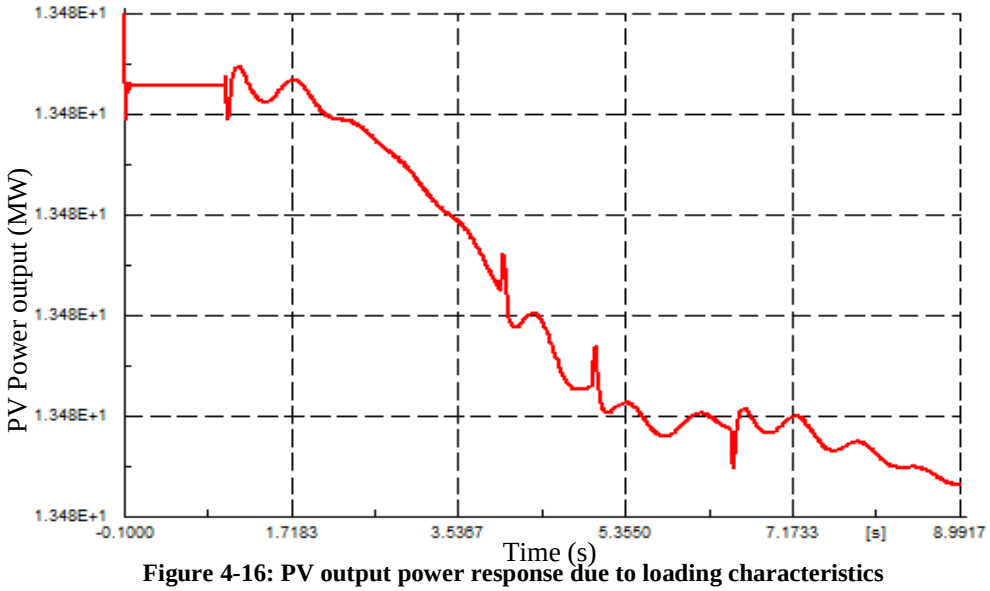

Figure 4-16: PV output power response due to loading characteristics

4.5 Discussion

In this chapter the integration of the PV plant and power station electrical auxiliary network has been successfully tested utilizing the developed controllers of MPPT and voltage control. The dynamic behavior is investigated according to SAGC for category B & C. the LVRT & HVRT were tested under various voltage dips to satisfy the requirements. The results displayed the capabilities of the PV model to remain connected and supply desired reactive power to the point of connection thus, assisting in grid stability. The frequency response requirement effectively adjusted in case of over frequency event. Thus, encouraging high PV penetration level without compromising much on the network operations and stability. A steady state analysis revealed no major concerns with only the low busbar voltages rising close to limit when the PV plant is connected thus, the PV plant voltage control must consider such variation to suit the requirements of the specific auxiliary network. The rating limit of the PV plant is dependent to both load following and spinning reserve capacity to take over the maximum output power of the PV plant. If the variations are large and not properly followed by the generator they may cause system stability issues. The optimum PV penetration level may depend on several of other factors such as cost per unit of electric energy and size of the local power station generation.

CHAPTER 5
STABILITY ANALYSIS

The previous chapters conducted load flow and dynamic studies to evaluate the PV system and the analyses showed stable results meeting all the grid codes. This chapter presents the results of transient stability due to an impact from a solar plant connected to the power station reticulation system. The rapid variation in power injection by PV system due to changing weather events and other factors such as tripping out the PV system will introduce power fluctuation in the reticulation system and frequency instability. Thus need to evaluate the impact of rapid power variation of the PV system due to changes of irradiance and temperature, also tripping the PV system and simulating a three phase fault. This will illustrate the stability impact of the PV system and the responses of high PV penetration level therefore will relatively reduce the local generator power output. In particular, the PV impact on the transient stability is expected to be more serious considering close proximity of the connected PV system to the generator.

5.1 Stability Case studies

Two different levels of penetration are to be considered in the study one with a penetration of 15 MVA and 7.5 MVA which is supplying 24 % & 12 % respectively of the auxiliary load for an 810 MVA rated machine. Various case studies are looked at with the two PV penetration level. At higher penetration of the PV the local generator is expected to oscillate more.

The output power of the PV system varies every minute due to weather changes which is a negative impact on the stability especially if the variations are large e.g. sharp drop rate of irradiance from 1000 to 200 W/m2 in just a few seconds which is a huge generation loss in a short space of time. The objective of the ramping rate test is for the cloud effect over the PV panels. The PV system penetration level is demonstrated at cases where the PV plant will be subject to internal fault and short circuit faults which is inevitable to any engineered components and safety measures to protect against further damage is to trip out the faulted part therefore both the scenario when the PV plant is tripped out is evaluated at different penetration levels as mentioned. And when the PV plant is subject to short circuit fault lasting for 0.15 sec and then cleared located at the PV plant busbar.

The generator power, load angle, frequency and PV power output of the generator are monitored and analyzed. The PV system is connected on the 11 kV busbar board B which is the closest point to the generator to simulate the case studies and view the various impacts on the

local generator stability. The generator power, load angle, frequency and PV power output of the generator are monitored and analyzed.

5.1.1 Effect of irradiance change in stability

The effect of a large cloud suddenly covering 80% sunshine for the PV panels dropping the irradiance from 1000 W/m^2 to 200 W/m^2 in less than a minute is investigated at different irradiance ramping rates (-1000 W/m^2, -400 W/m^2, -200 W/m^2) per second to determine impact on stability. A drop of the magnitude 10 MW within a short time can have significant impact on the local generator stability.

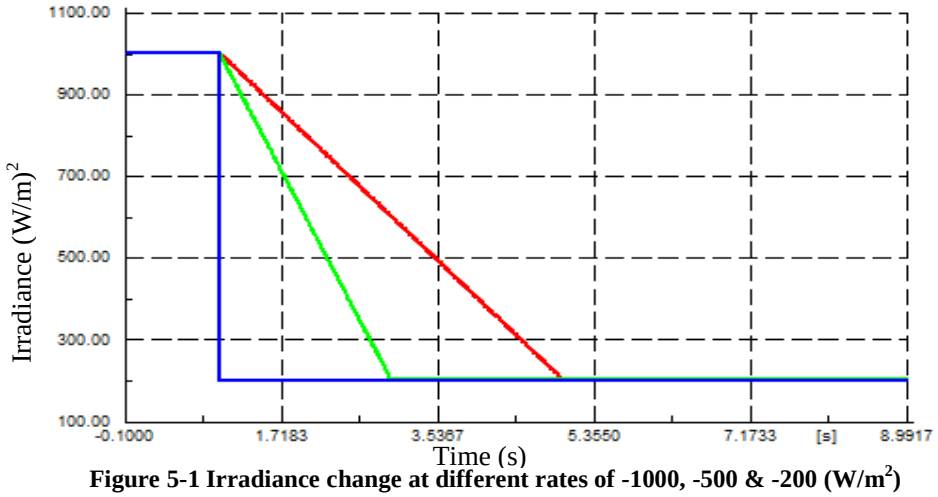

Figure 5-1 Irradiance change at different rates of -1000, -500 & -200 (W/m^2)

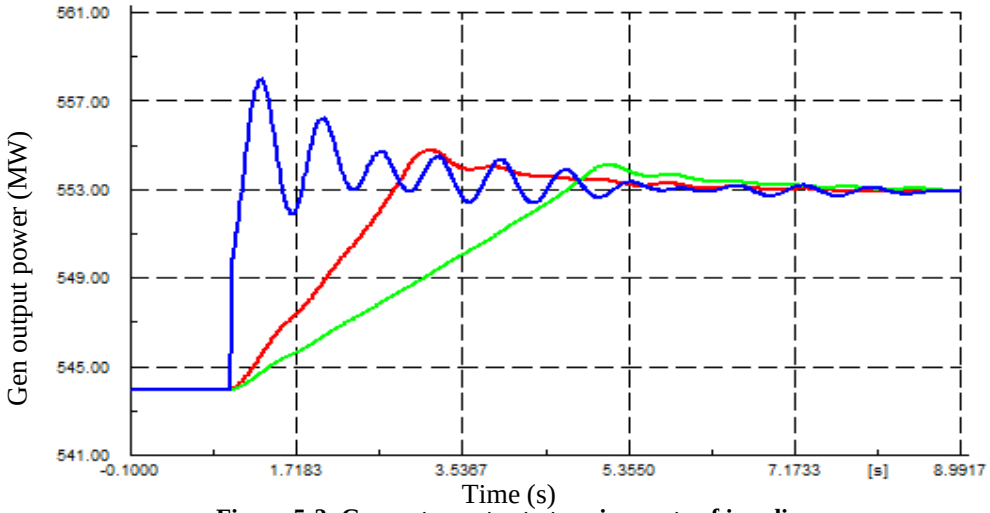

Figure 5-2: Generator output at various rate of irradiance

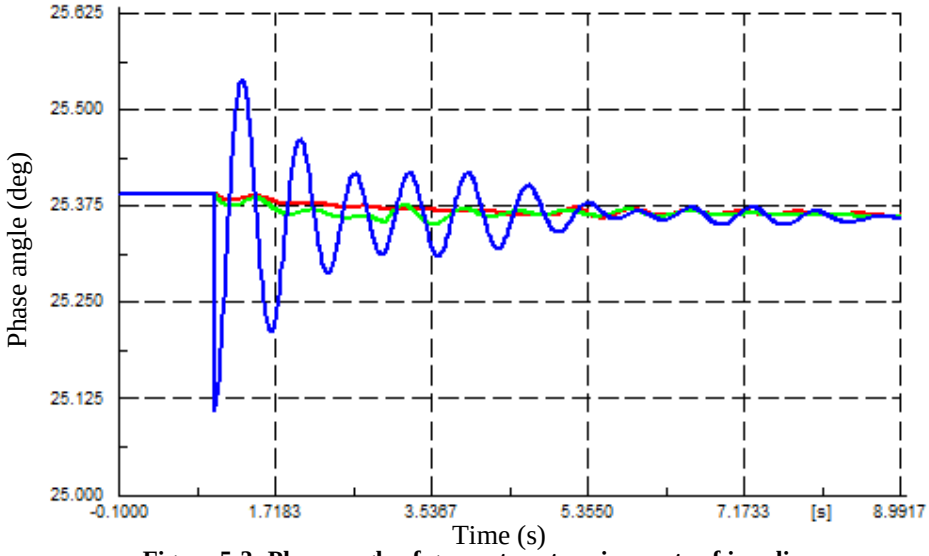

Figure 5-3: Phase angle of generator at various rate of irradiance

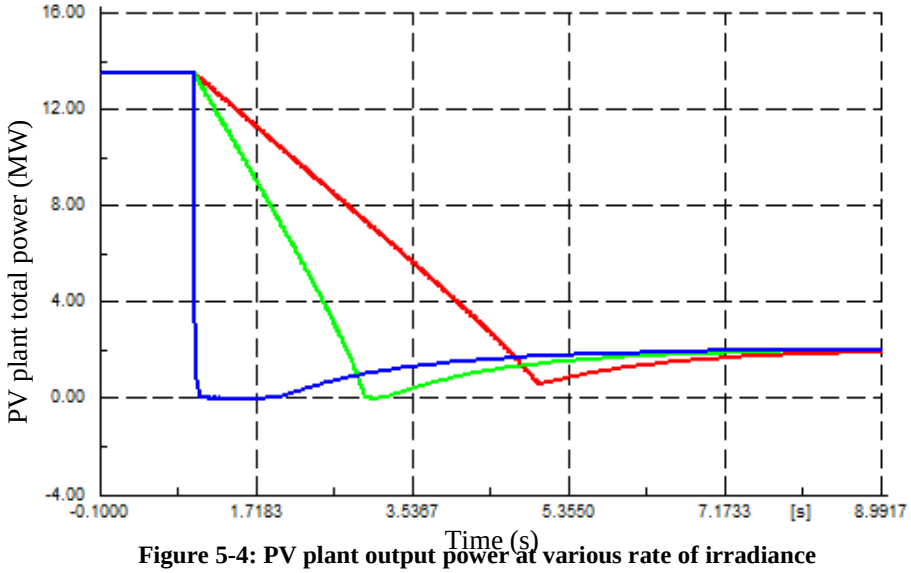

Figure 5-4: PV plant output power at various rate of irradiance

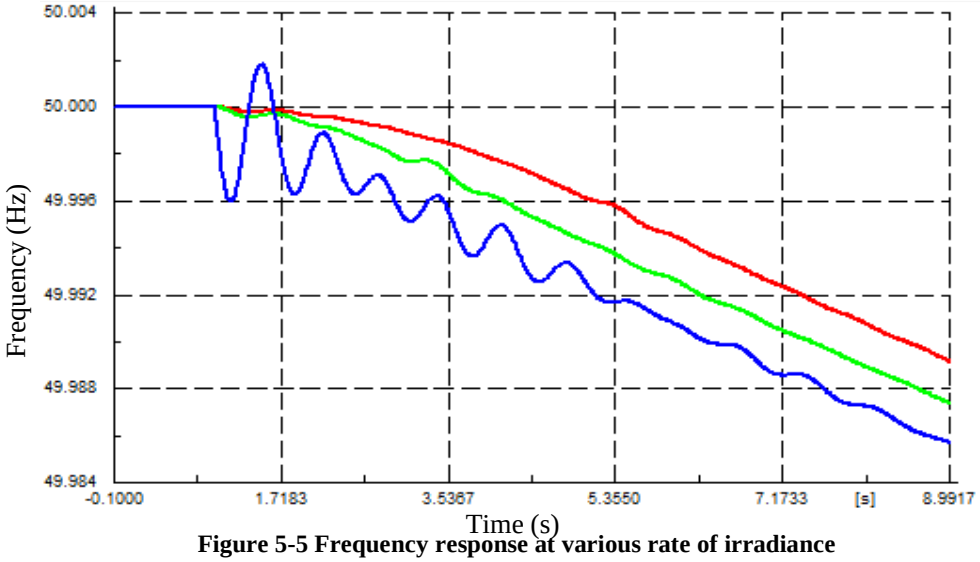

Figure 5-5 Frequency response at various rate of irradiance

Figure 5-1 shows the change of irradiance from 1000 W/m^2 to 200 W/m^2 at different ramping rates, change in generator power output is shown in Figure 5-2, generator load angle on Figure 5-3, PV plant output power changes and frequency response are shown in Figure 5-4 and Figure 5-5 respectively.

The local generator output power shown in Figure 5-2 can be seen picking up the PV plant lost generation load at different ramping rates and for a quick drop rate (blue curve) the output power is seen to oscillate and eventually settles to a level which compensates the difference of the lost and available PV generation. But for slower irradiance drop rate (red curve) trivial oscillations are seen. Load angle shown in Figure 5-3 show the significant of drop rate which is seen for a quick drop rate irradiance the oscillations are severe when compared with slower drop rate. But in reality outside of simulation a big cloud will not instantly cause a sudden drop of irradiance for a 15 MVA PV plant considering the size of a cloud and the speed the cloud can travel with. Therefore, the drop will not be as quick as indicated on simulation. Therefore, Changes in atmospheric conditions will not cause severe oscillation that can impose stability threats as suggested by obtained results. Figure 5-4 show the PV plant drops to zero for a second for quickest drop rate and due to the available irradiance the PV plant steadily picks up and continues to produce power according to the available 200 W/m^2 of irradiance and the PV system does not oscillate as it does not have rotary machinery. Figure 5-5 shows the frequency response, and oscillations are seen for quickest drop rate and the significant is that the frequency drops quicker to a lower level for higher drop rate which is undesired but other control mechanism such as the governor will respond and maintain the frequency to be stable.

5.1.2 Effect of tripping a PV farm

This case study is considering worst case scenario by disconnecting the PV plant operating at full capacity 13.5 MW at the closest possible point of connection to the generator and the effect of the change in loss of the PV plant at various penetration levels is to be observed below. The PV plant output power suddenly drops from 13.5 to 0 MW but at that time the local generator continues to supply power and in the event the PV plant is tripped the generator is subject to sudden load increase and must compensate the sudden increase in load that was supplied by the PV plant. The output power and frequency of the local generator is shown on figure 5-6 and Figure 5-7 respectively where the red curve is local generator output supply when the PV plant is supplying 13.5 MW and green curve is local generator output supply when PV plant supplying 6.75 MW.

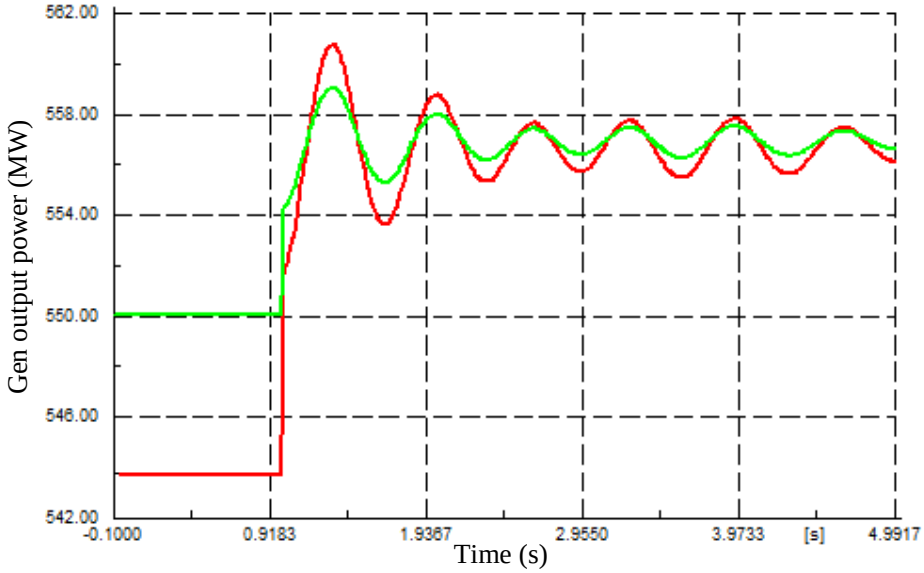

Figure 5-6: Generator output power at different PV plant penetration level

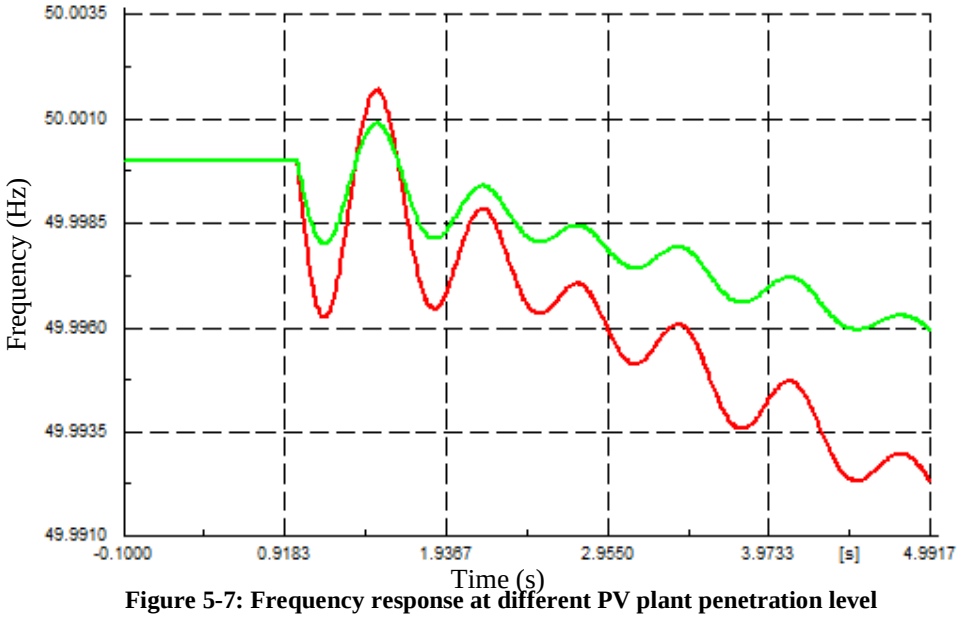

Figure 5-7: Frequency response at different PV plant penetration level

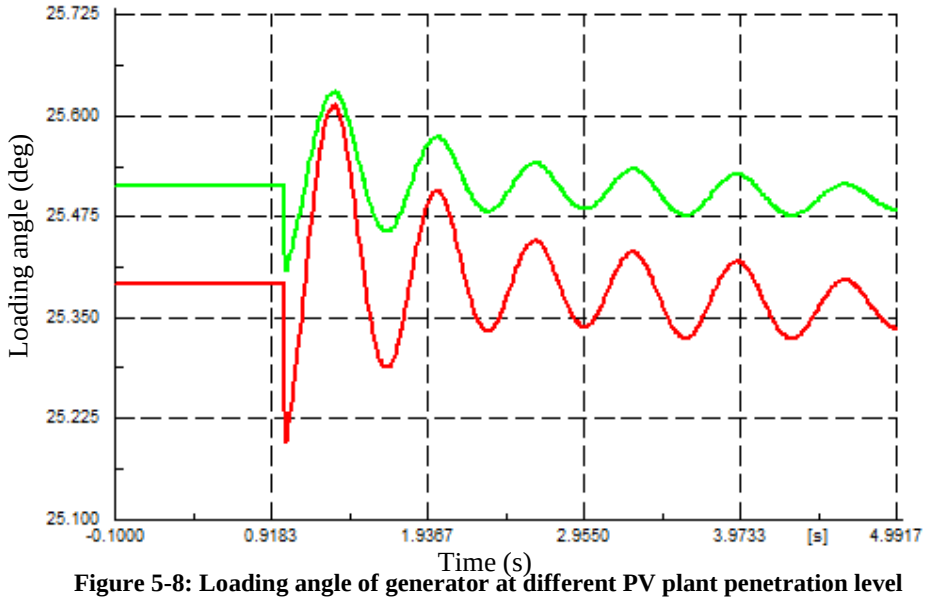

Figure 5-8: Loading angle of generator at different PV plant penetration level

Figure 5-6 shows power from the local generator and the quick loading increase change due to the Plant disconnecting results in oscillations as observed and the generator power output power settles at the new level. The local generator has produced the extra power of the lost PV generation therefore total generation is increased at a short space of time. It is also observed that at a higher penetration level the higher the magnitude of oscillations in comparison with less penetration level as seen with the red (Higher MW) & green (Lower MW) curves.

Figure 5-7 shows that penetration level of PV plant has a significant impact on the generator frequency. With the increase in PV penetration level the more severe the impact on the system stability as the frequency decays faster. Therefore increased PV penetration may make system to be unstable at the presented conditions.

The governor reaction function is to correct any frequency deviation but the response time is slow therefore not adequate for such a quick disturbance therefore PV penetration level should be a guidance limit considering the reserve margin of each local generator unit to take over the total PV plant power output. Specifically the operating point of generator in terms of load angle should consider the PV plant output power for example shown in Figure 5-8 the first swing (red curve) is high when PV plants is disconnected but the margin of the electrical inertia is high enough to bring the swing back and dampen the oscillations.

5.1.3 Effect of a fault at the PV bus

In this case study a three phase short circuit fault is applied at the PV bus. The fault is applied through a small R/X ratio and lasted for 0.15 s. The solar irradiance is maintained constant at 1000 W/m^2 therefore maximum power output from the PV plant. Due to the fault the voltage shoots down to zero till fault is cleared in 0.15 sec so does the PV power output but after the fault the PV system maintain supply at full capacity.
Figure 5-9 show the PV power drops to zero until the fault is cleared. When the fault is cleared the output power went back to produce maximum capacity. During the fault Figure 5-10 shows the output power from the local generator drops and when the fault is cleared it shows oscillations but dampens after some time. The PV power response does not oscillate as it does not have rotary machines and it settles faster than the local generator.

Figure 5-11 shows the frequency response of the local generator oscillates within the limits and then damping out after some time.

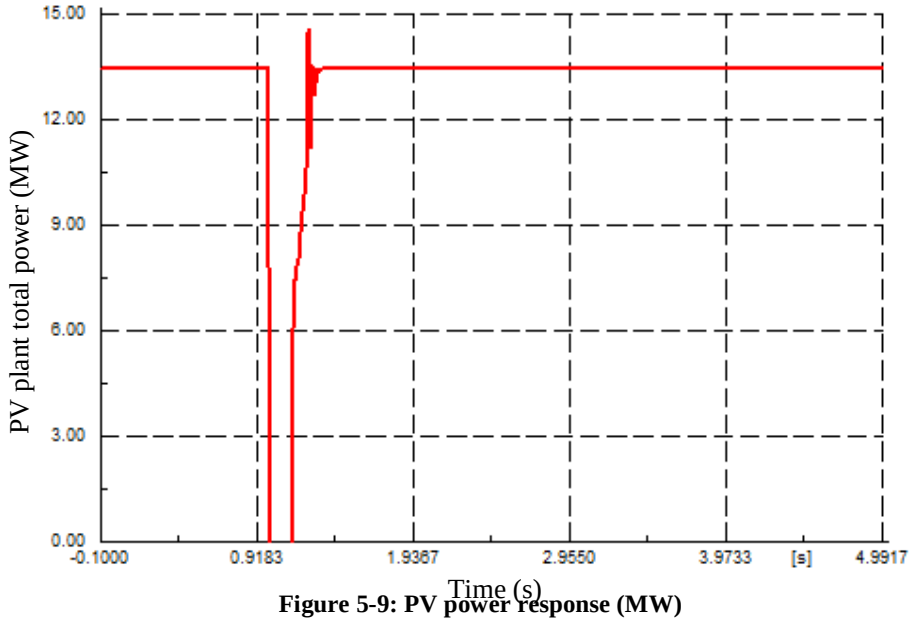

Figure 5-9: PV power response (MW)

Figure 5-10: Generator output power after three phase fault

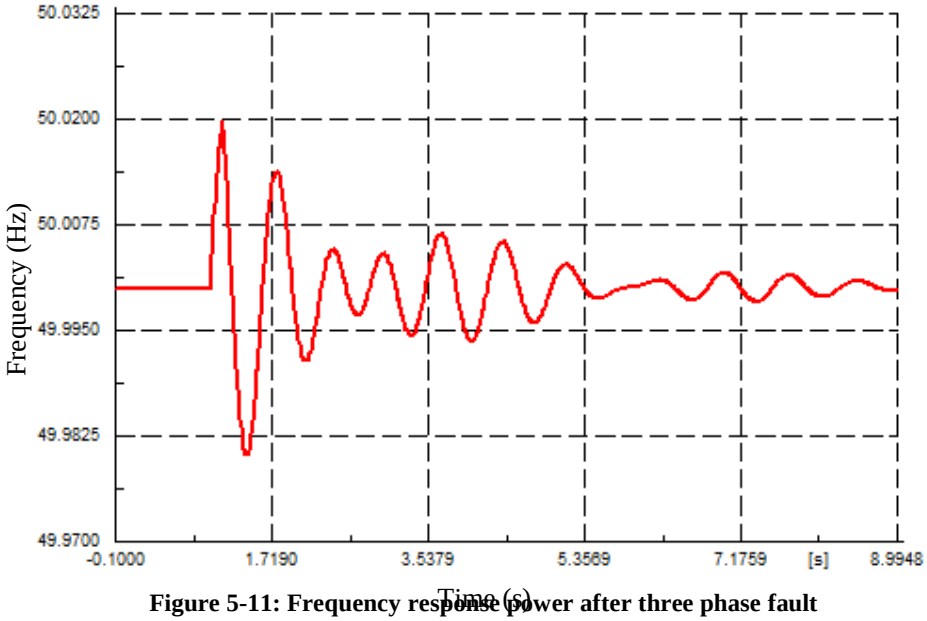

Figure 5-11: Frequency response power after three phase fault

5.2 Discussion

A significant increase in the penetration of PV generation has a significant impact on the stability of the local generator. The more PV penetration level connected to the auxiliary network the more susceptible to stability problems. This can be counteracted by having enough reserve generation margin of the local generator to avoid unstable condition due to PV plant. The evaluated scenarios demonstrate that in such cases the integration of PV system does contribute to transient problems but assist in running the generator at lower capacity, saving costs and reduced emissions. The connection of PV plant to a load busbar does help in reducing frequency oscillation as seen to be not severe and oscillates within limits for worst case of tripping out the PV plant. The PV system had minimal impact on the voltage as it did not violate any limits but if penetration level is increased the voltage control and compensation shall be considered. However, based on observations from results, changes in irradiation will not cause stability problems as the power station governor may respond quicker than irradiance drop. The benefits of integrating PV plant on power station distribution to be beneficiary in terms of running the generator at lower capacity and negative results are drawn from transient results corresponding to PV plant inconstant power output.

CHAPTER 6
DISCUSSION AND CONCLUSION

This work has presented the development of PV model, the effects of integrating a PV plant into a typical power station electrical auxiliary network, performance during normal plant operations and how the variation of power output from solar affects the voltage stability of the auxiliary network and local generator stability. The methodology described in this thesis intended to help system operators to understand the changes in PV generation caused by moving cloud shadows.

The literature completed the following task:

PV system modelling

A number of analytical methods to determining the parameters (I_{ph}, I_0, n, R_s, R_p) that characterize the solar cell with sufficient degree of precision in a simple manner were evaluated and compared. The chosen method for photovoltaic modelling in PowerFactory was based on accuracy and degree of complex. The method used has been validated mathematically and in simulation tool. The results displayed expected behavior for all created cases compared with other equivalent methods.

The developed PV model is based on classical equations and maximum power point tracking (MPPT) implemented, using pulse width modulation (PWM) as the interfacing in PowerFactory and is compared with the generic model using similar controls. Further validation of the model was conducted by simulating different types of disturbances and comparing the behavior of the developed model against the generic model which is constrained by assumptions, such as: no MPPT and uses static generator as the interfacing converter but gives basic understanding of PV operation results displayed were similar in both developed and generic models. The prediction of produced energy from harvested solar in a large scale is under estimated by the generic model in comparison with established model which influences decision making to invest on the PV technology. The simple generic model is based on the 4-p model implying more approximations to the system than the developed model which is based on 5-p model. The inclusion of MPPT control increased the efficiency of the system. After establishment and validation, the two techniques, P&O and IncCond were implemented and compared against each other. IncCond displayed better results as the P&O method displayed some oscillation around the maximum point and the IncCond did not oscillate resulting in better efficiency.

PV model (South Africa Grid Code) compliance

The control of reactive power and active power were established to be in accordance with the requirements from the South African Grid Code. Various testing to validate the controls were performed. Frequency response requirement was tested and displayed the active power reduction during the event of an over-frequency. The LRVT require that the PV plant continue to operate through periods of low voltages and must not disconnect from the grid. The Low Voltage Ride Through (LVRT) requirement was verified under five voltage dips and for all scenarios the PV plant complied effectively. The High Voltage Ride Through (HVRT) requirement was tested for 1.2 p.u voltage and displayed complying results. The durations of the voltage dip for each scenario were in line with the SAGC for category B & C. The results indicated that the PV model is capable to remain connected during a voltage dip and simultaneously provide reactive current to the Point of Connection (POC). Therefore, the grid stability is improved through the reactive support by the PV plant at the POC.

Steady state analyses

A steady state analysis conducted with the PV plant connected to the power station reticulation network revealed no major concerns with the only exception on the low voltage busbars at 50% reduced loading. The voltages at 380 V rise close to operating limit of 1.1 p.u when the PV plant is connected and participating in voltage control. The observation suggests the voltage limit at low voltage level may be exceeded if voltage control set point be changed. The PV plant was found to improve the voltage in a situation for an n-1 contingency (one aux transformer operating). The PV plant fault contribution was found to be limited by PV inverter to 120% of nominal current of inverter thus a proposition that the inverter has controllability of fault current and only positive sequence current was notably injected during fault contribution. Load following characteristic was evaluated and obtained results showed ramping ability is not possible with the PV system. But the generator shows ability to follow the load closely.

PV system stability analyses

The developed PV model was then subject to transient studies on the existing power station reticulation system with various solar PV sizes ranging from 7.5 MVA to 15 MVA. The effects were analyzed for mainly voltage stability and local generator behavior. It was discovered that increasing PV penetration level connected to the auxiliary network, the greater the risk of

becoming unstable. The frequency decreased quicker for high penetration of PV plant and generation power output oscillated more.

Increasing the PV capacity in the power stations reticulation system suggests the capacity of conventional synchronous generator will be reduced relatively. The trade off to size the PV plant for a typical power station reticulation system is determined by the reserve margin of the local generator in order to avoid unstable conditions due to PV plant impact. Changes in atmospheric conditions were found not to impose any stability threat as the response did not cause severe oscillations.

6.1 Recommendations on variation issue

The variations of solar plant introduce stability problems in the network where connected, therefore mitigations are to be established at the system level. The variation from the generation point of view is nothing new as the variation of PV plant is similar to load variation. But allowable variations are to be determined by the ability of generator control equipment to follow sharp variations. The generator control (governor) will see these variations as sudden change in load and response accordingly. For very large sharp variations the generator may not successfully follow the load rate closely thereby causing stability problems. The Open Cycle Gas turbine (OCGT) can counteract these sharp variations since they have very fast ramping rate capabilities whenever available on standby, However they are expensive to operate and therefore are usually used at certain times like during peak. The mismatch can then be picked up by pumped storage unit, if none of these are sufficient, changes on the PV generation can be made. Thus a large amount of PV penetration levels could be allowable as long as generator ramping rate for worst case scenarios can be achieved. During overcast and cloudy days the PV can be limited or disconnected to protect against stability risks. Centralized PV penetration increases the significance of stability effect; while dispersed PV will reduce the effect since a damping effect is created by different cloud conditions at different locations. Another mitigation solution which is expensive is installing storage technology which is able to store instantaneous variable power and produce steady power output. It can be recommended that a weather and insolation forecasts be made available to make proper prediction of the variability of PV generation in the system. The system operator would be able to ensure that enough voltage and frequency control are in place and available.

In summary the project targets were completed successfully and discovered the following conclusion listed below, the case studies revealed that during operation:

- local generation was reduced relatively
- Ancillary services generations demand increase in terms of load reduction.
- Total spinning reserves increased meaning the availability of generators synchronized to the grid, that can increase output power immediately in response to a major disturbance and can reach full capacity.
- production costs will reduce, and
- the worst situation will occur when the demand is decreased, and at the same time, PV generation increases

The advantages and disadvantages with regards to completed activities to interconnecting the PV system onto the Eskom power station reticulation system:

Advantages

- The developed model improved the prediction of photovoltaic plant in PF
- The inclusion of MPPT control increased the efficiency of the PV system
- The PV model is SAGC compliance thus the grid stability is improved at the POC.
- The PV plant improves the voltages in situations of n-1.
- The inverter limits the fault current injected.
- Increasing the PV capacity suggests the capacity of local generator will be reduced relatively, thus, reduce fuel consumption of local generator as well as emissions of carbon dioxide and directly saving costs (emission fees)

Disadvantages

- Load following characteristic is not possible with the PV system
- The increasing PV penetration level connected to the auxiliary network, the greater the risk of becoming unstable

6.2 Recommended Future Work

- The development of a detailed radiation solar model taking into consideration cloud modelling, shading effect and angle of incidence of sun light.

- The islanding behavior of the PV system under proposed control strategy is worth investigating in a future research. Thus, the adoption and incorporation of a suitable islanding detection scheme may be necessary in a practical system;
- Research studies should be done for power quality. The harmonic distortion or possible flicker effects that the PV inverter can cause. If it is in accordance to the IEEE Recommended Practice for Utility Interface of Photovoltaic (PV) Systems (IEEE Std 929-2000) with appropriate design of the filter.

- Develop Ramp-rate controls to ensure that the plant output does not ramp up or down faster than a specified ramp-rate limit and statistic for availability factor of the PV plant.

REFERENCES

[1] G. Parkinson, "RenewEconomy," 4 february 2013. [Online]. Available: http://reneweconomy.com.au/2013/the-top-solar-countries-past-present-and-future-96405. [Accessed 10 may 2015].

[2] R. Secretariat, "Rnewables 2014 Global status report," Paris REN21 Secretariat, Paris, 2014.

[3] J. Allan, B. Antonich, A. Bisiaux, E. Kosolapova, K. Kulovesi, M. Luomi and A. Savaresi, "A Reporting Service for Environment and Development Negotiations," *International Institute for Sustainable Development (IIS D),* vol. 12, no. 594, pp. 1-32, 26 11 2013.

[4] "Department of energy Republic of South Africa," [Online]. Available: http://www.energy.gov.za/files/renewables_frame.html. [Accessed 12 06 2015].

[5] J. Duffie and W. Beckman, Solar engineering of thermal processes, New Jersey: John Wiley & Sons, 2013.

[6] V. Quaschning, Understanding Renewable Energy Systems, UK and USA: Earthscan, 2005.

[7] M. Casaro and D. Martins, "Grid-connected PV system using a three-phase modified dual-stage inverter," *IEEE,* vol. 978, no. 1, pp. 167-173, 2009.

[8] G. M. Masters, Renewable and Efficient electric power systems, New Jersey: John Wiley & Sons, 2004.

[9] J. Nelson, The physics of Solar Cells, Imperial College Press, 2003.

[10] M. A. Green, Solar Cells, The University of New South Wales, 1998.

[11] R. A. Messenger and J. Ventre, Photovoltaic Systems engineering, Florida: CRC Press LLC, 2003.

[12] W. X. e. al, "Real time identification of optimal operating point in photovoltaic power system," *IEEE transaction power electronics,* vol. 53, no. 4, pp. 1017-1026, 2006.

[13] Z. S. e. al, "An improved two-diode photovoltaic PV model for PV system," *in Proc. Joint int. Conf. power electronics drives and energy,* pp. 1-5, 2010.

[14] W. S. e. al, "Improvement and validation of a model for photovoltaic array perfomance," *Solar energy,* vol. 80, pp. 78-88, 2006.

[15] T. Ma.n, HongxingYang and LinLu, "Solar photovoltaic system modelling and perfomance prediction," *ScuenceDirect,* vol. 36, pp. 304-315, 2014.

[16] H. Bellia, R. Youcef and M. Fatima, "A detailed modelling pf photovoltaic module using Matlab," *National Research Institutie of Astronomy and Geophysics,* no. 3, pp. 53-61, 2014.

[17] L. Han, N. Chiba and T. Mitate, "Modelling of an equivalent circuit for dye-sensitized solar cells," *Appl Phys Lett,* vol. 5, no. 84, pp. 24-33, 2004.

[18] M. P. A, A. Mellit and V. Lughi, "Explicit empirical model for general photovoltaic devices: expirimental validation at maximum power point," *Sol Energy,* no. 16, pp. 101-105, 2014.

[19] A. Celik and N. Acikgoz, "Modelling and experimental verification of the operating current of mono-crysalline photovoltaic modules using four and five parameter models," *Applied Energy,* no. 84, pp. 1-15, 2007.

[20] S. Dongue, D. Njomo, J. Tamba and L. Ebengai, "Modelling of electrical response illuminated crystalline photovoltaic modules using four and five parameter models," *International Journal of Emerging Technology and Advanced Engineering,* no. 9, pp. 2-612, 2012.

[21] R. Chenni, M. Makhlouf, T. Kerbache and A. Bouzid, "A detailed modelling method for photovoltaic cells," *Energy,* no. 32, pp. 1724-1730, 2007.

[22] Q. Kou, S. Klein and A. Beckman, "A method for estimating the long term perfomance of direct-coupled PV pumping systems," *Elsevier Science,* vol. 64, pp. 33-40, 1998.

[23] A. Ghoneim, "Design optimization of photovoltaic powered water pumping systems," *Energy conversion & Management,* vol. 47, pp. 1449-1463, 2006.

[24] M. Karamirad, M. Omid, R. Alimardani and H. Mousazadeh, "ANN based simulation and experimental verification of analytical four and five parameters models of PV modules," *ELSEVIER,* vol. 34, pp. 86-98, 2013.

[25] J. Gow and C. Manning, "Development of a photovoltaic array model for use in power electronics simulation studies," *IEEE proceedings,* vol. 146, no. 2, pp. 193-200, 1999.

[26] E.Saloux, A.Teyssedou and M.Sorin, "Explicit model of photovoltaic panels to determine voltages and currents at the maximum power point," Natural Sciences and Engineering Research Concil of Canada, 2010.

[27] S. Daniel, H. Chan, C. Jacob and H. Phang, "Analytical Methods for the extraction of solar cell single and double diode model parameters from I-V characteristics," *IEEE*

Transactions, vol. 34, no. 2, pp. 286-293, 1987.

[28] K. Nishioka, N. Sakitani, K. Kurobe, Y. Ishikawa, Y. Uraoka and T. Fuyuki, "Analysis of the temperature characteristics in polycrystalline Si Solar cells using modified equivalent circuit model," *Japanese journal of applied physics,* vol. 42, 2003.

[29] K. Ishaque, Z. Salam and H. Taheri, "Simple, fast and accurate two diode model for photovoltaic modules," *Solar energy materials & solar cells,* vol. 95, pp. 586-594, 2011.

[30] M. d. Blas, J. Torres, E. Prieto and A. Garcia, "Selecting a suitable ,odel for characterizing photovoltaic devices," *Renewable energy,* vol. 25, pp. 371-380, 2002.

[31] P. Wurfel, Physics of Solar Cells from Principles to New Concepts, British Library, 2005.

[32] H. Tia, F. Mancilla-David, K. Ellis and E. Muljadi, "A cell to module to array detailed model for photovoltaic panels," *ScieVerse ScienceDirect,* vol. 86, pp. 2695-2706, 2012.

[33] K. Hussein, I. Muta, T. Hoshino and M. Osakada, "Maximum photovoltaic power tracking: an algorithm for rapidly changing atmospheric conditions," *IEEE proc. of generation, transmission and distribution,,* vol. 142, pp. 59-64, 1995.

[34] T.Ma and L. H.Yang, "Development of a model to simulate the perfomance characheristics of crystilline silicon photovoltaic modules/strings/arrays," *ScienceDirect,* vol. 100, pp. 31-41, 2014.

[35] S. Tarak, M. Bouzguenda, A. Gastli and A. Masmoudi, "Matlab/Simulink Based Modelling of Solar Photovoltaic Cell," *International journal of renewable energy research,* vol. 2, no. 2, pp. 1-6, 2012.

[36] B. Marion, B. Kroposki, K. Emery, J. d. Cueto, D. Myers and C. Osterwald, "Validation of Photovoltaic Module energy ratings procedure at NREL," National Renewable Energy Laboratory, Colorado, 1999.

[37] E. Koutroulis, K. Kalaitzakis and N. Voulgaris, "Development of a microcontroller-based photovoltaic maximum power point tracking control system," *IEEE transactions on power electronics,* vol. 16, no. 1, pp. 46-59, 2001.

[38] D. Hohm and M. Ropp, "Comparison study of maximum power point tracking algorithms using an experimental, programmable, maximum power point tracking test bed," *IEEE,* pp. 1699-1702, 2000.

[39] R. Cullen, "Blue sky energy," Oct/Nov 2000. [Online]. Available: www.blueskyenergyinc.com. [Accessed 15 Nov 2014].

[40] M. Shan and C. W. Tan, "A study of maximum power point tracking algorithm for stand-alone photovoltaic systems," *IEEE applied power electronics colloquium,* vol. 8, no. 11, pp. 22-27, 2011.

[41] C. Hau and C. Shen, "Comparative study of peak power tracking techniques for solar storage system," *IEEE,* vol. 98, no. 9, pp. 679-685, 1998.

[42] T. Esram and P. Chapman, "Comparison of photovoltaic array maximum power point tracking techniques," *IEEE transaction on energy conversion,* vol. 22, no. 2, pp. 439-449, 2007.

[43] K. Surya and M. V. Prasad, "PV cell based five level inverter using multicarrier PWM," *International Journal of Modern Engineering Research,* vol. 1, no. 2, pp. 545-551.

[44] F. Liu, S. Duan, F. Liu, B. Liu and Y. Kang, "A variable step size INC MPPT method for PV system," *IEEE transactions on industrial electronics,* vol. 55, no. 7, pp. 2622-2628, 2008.

[45] A. Al-Diab and C. Sourkounis, "Variable step size P&O MPPT algorithm for PV system," *OPTIM,* vol. 10, no. 12, pp. 1097-1102, 2010.

[46] M. Yamaguchi, K. Kawarabayashi, T. Takuma, Y. Ueda and Y. Yamano, "Development of a new utility-connected photovoltaic inverter LINE BACK," *Proc. of the 16th international telecommunications energy conference (INTELEC'94),* pp. 676-682, 1994.

[47] Y. Hsiao and C. Chen, "Maximum power tracking for photovoltaic power system," *IEEE proc of the 37th annual industry application conference (IAS'02),* vol. 2, pp. 1035-1040, 2002.

[48] B. Liu, S. Duan, F. Liu and P. Xu, "Analysis and improvement of maximum power point tracking algorithm based on incremental conductance method for photovoltaic array," *IEEE,* vol. 7, no. 5, pp. 637-641, 2007.

[49] J. Schoeman and J. v. Wyk, "A simplified maximal power controller for terrestrial photovoltaic panel arrays," *IEEE power electronic specification conference,* vol. 13, pp. 361-367, 1982.

[50] G. Hart, H. Branz and C. Cox, "Expirimental tests of open loop maximum power point tracking techniques," *Solar Cells,* vol. 13, pp. 185-195, 1984.

[51] B. Bekker and H. Beukes, "Finding an optimal PV panel maximum power point tracking method," *IEEE AFRICON,* pp. 1125-1129, 2004.

[52] F. Schimpf and L. E. Norum, "Grid connected converters for photovoltaic state of the art, ideas for improvement of transformerless inverter," *Nordic Workshop on Power and*

Industrial Electronics, pp. 9-11, 2008.

[53] G. Boyle, Renewable energy power for a sustainable future, New York: Oxford Unirvesity Press, 2004.

[54] A. Falk, C. Durschner, K. Remmers and A. Solapraxis, "Photovoltaic for professionals - solar electric system - marketing and installation," in *Design and installation, Beuth Verlag GmbH in association with Earthscan*, Berlin, 2007.

[55] N. Henze, A. Engler and B. Sahan, "Perfomance of a novel three-phase photovoltaic inverter for module intergration," in *photovoltaic solar energy conference and exhibition*, Milan, 2007.

[56] F. Schimpf and L. Norum, "Grid connected converters for photovoltaic state of the art, ideas for improvement of transformerless inverters," in *NORPIE*, Norway, 2008.

[57] T.V.Thang, N.M.Thao, J.-H. Jang and J.-H. Park, "Analysis and Design of Grid-connected photovoltaic systems with multiple-intergrated converters and pseudo DC-Link inverter," *IEEE Transactions on industrial electronics,* vol. 61, no. 7, pp. 3377-3386, 2014.

[58] B. Karanayil, V. Agelidis and J. Pou, "Evaluation of DC-link Decoupling using electrotytic or polypropylene film capacitors in three-phase grid-connected photovoltaic inverters," *IEEE,* pp. 6980-6986, 2013.

[59] V. Vodovozov, "Inverters," in *Introduction to power electronics*, Valey Vodovozov & Ventus Publishing ApS, 2010.

[60] S. Azmi, K. Ahmed, S. Fnney and B. Williams, "Comparitive analysis between voltage and current source inverters in grid-connected application," *Renewable power generation IET Conference,* pp. 1-6, 2011.

[61] A. Meulen and J. Maurin, "Current source inverter vs Voltage source inverter topology," White paper WP020001EN, Cleveland, 2014.

[62] G. Hingorani and L. Gyugyi, Understanding FACTS: Concepts and technology of flexible AC transmission systems, Florida: Wiley-IEEE Press, 1999.

[63] S. Kjaer, J. Pedersen and F. Blaabjerg, "A review of single-phase grid connected inverters for photovoltaic modules," *IEEE transaction on industry application,* vol. 41, no. 5, pp. 1292-1306, 2005.

[64] R. Attanasio, M. Cacciato, F. Gennaro and G. Scarcella, "Review on single-phase PV inverters for grid-connected applications," in *Internation conference on energy,*

environment, ecosystem and sustainable development, portugal, 2008.

[65] J. Myrzik and M. Calais, "String and module intergrated inverters for single-phase grid connected photovoltaic systems - a review," in *IEEE Bologna powerTech conference*, Bologna, 2003.

[66] N. Mohan, T. Undeland and W. Robbins, Power electronics converters, applications and design, Danvers: John Wiley & Sons, 2003.

[67] S. Jeon and G. Cho, "A zero-voltage and zero-current switching full bridge DC-DC Converter with transformer isolation," *IEEE on power electronics,* vol. 16, no. 5, pp. 573-580, 2001.

[68] M. Salcone and J. Bond, "Selecting Film Bus Link Capacitors Selecting Film Bus Link Capacitors," *IEEE,* pp. 1692-1699, 2009.

[69] S. Kjaer, J. Pedersen and F. Blaabjerg, "A Review of Single-Phase Grid-Connected Inverters for photovoltaic modules," *IEEE TRANSACTIONS ON INDUSTRY APPLICATIONS,* vol. 41, no. 5, pp. 1292-1306, 2005.

[70] C. Meza, D. Biel and J. Negroni, "Considerations on the control design of DC-link based inverters in grid-connected photovoltaic systems," *IEEE,* vol. 6, no. 2, pp. 5067-5070, 2006.

[71] S. Mekhamer, A. Abdelaziz and S. Ismael, "Technical comparison of harmonic mitigation techniques for industrial electrical power systems," 2012. [Online]. Available: http://works.bepress.com/almoataz_abdelaziz/54. [Accessed 26 02 2015].

[72] G. Sandoval and J. Houdek, "A review of harmonic mitigation techniques," 2005. [Online]. Available: http://www.artchepq.com/assets/files/AReviewOfHarmonicMitigTech.pdf. [Accessed 26 09 2014].

[73] k. Kaiser, "operational cost avoidance through harmonic mitigation in industrial environment," Schneider electric white paper, Austria, 2013.

[74] S. Mekhamer, A. Abdelaziz and S. Ismael, "Design Practices in Harmonic Analysis Studies Applied to Industrial Electrical Power Systems," *Engineering, Technology & Applied Science Research,* vol. 3, no. 4, pp. 467-472, 2013.

[75] M. Martinson, "Harmonics and Noise in Photovoltaic (PV) Inverter and the Mitigation Strategies," Solectra renewables.

[76] M. Zeman, "Photovoltaic systems," in *Solar cells*, pp. 9.1-9.17.

[77] P. Smit and G. Coetzee, "Power station electrical plant-auxiliary power system training manual," Eskom Generation Group, 2008.

[78] G. Castleberry, "Power plant electrical distribution system," PDH-Course E184, 2008. [Online]. Available: www.PDHcenter.com.

[79] N. E. R. o. S. A. (NERSA), "Grid connection code for renewable power plants (rpps) connected to the electricity transmission system (ts) or the distribution system (ds) in south africa," Eskom Transmission Division, Germinston, 2012.

[80] D. GmnH, "DigSilent PowerFactory 15 user manual," DigSILENT GmbH, Gomaringen, 2013.

[81] F. Almonacid, C. Rus, L. Hontoria and F. Munoz, "Characterisation of PV CIS module by artificial neural networks. a comperative study with other methods," *Renewable energy,* vol. 35, pp. 973-980, 2010.

[82] C. Carrero, D. Ramirez, J. Rodriguez and C. Platero, "Accurate and fast convegence method for parameter estimation of PV generators based on three points of the I-V curve," *renewable energy,* vol. 36, pp. 2972-2977, 2011.

[83] S. Dongue, D. Njomo and L. Ebengai, "An improved nonlinear five-point model for photovoltaic modules," *Photoenergy,* vol. 2013, p. 11, 2013.

[84] I. Houssamo, M. Sechilariu, F. Locment and G. Friedrich, "Identification of photovoltaic array model parameters. modelling and experimental verification," in *International conference on renewable energy and power quality*, Granada (Spain), 2010.

[85] S. Lineykin, M. Averbukh and A. Kuperman, "An improved approach to extract the single-diode equivalent circuit parameters of a photovoltaic," *Renewable and sustainable energy reviews,* vol. 30, pp. 282-289, 2014.

[86] J. Phang, D. Chan and J. Philips, "Accurate analytical method for the extraction of solar cell model parameters," *Electronics letters,* vol. 20, no. 10, pp. 406-408, 1984.

[87] M. Chegaar, Z. Ouennoughi and A. Hoffmann, "A new method for evaluating illuminated solar cell parameters," *Solid-state electronics,* vol. 45, pp. 293-296, 2001.

[88] T. Ma, H. Yang and L. Lu, "Solar photovoltaic system modeling and perfomance prediction," *Renewable and sustainable energy reviews,* vol. 36, pp. 304-315, 2014.

[89] W. D. Soto, S. Klein and W. Beckman, "Improvement and validation of a model for photovoltaic array perfomance," *Solar energy,* vol. 80, pp. 78-88, 2006.

[90] M. d. Blas, J. Torres, E. Prieto and A. Garcia, "Selecting a suitable ,model for characterizing photovoltaic devices," *Renewable energy,* vol. 25, pp. 371-380, 2002.

[91] S. Kim, J. Jeon, C. Cho, E. Kim and J. Ahn, "Modeling and simulation of a grid-connected PV generation system for electromagnetic transient analysis," *Solar Energy,* vol. 83, pp. 664-678, 2009.

[92] M. Bashahu and P. Nkundabakura, "Review and tests of methods for determination of the solar cell junction ideality factors," *Solar energy,* vol. 81, pp. 856-863, 2007.

[93] T. Ma, H. Tang and L. Lu, "Developement of a model to simulate the perfomance characteristics of crystalline silicon photovoltaic modules/strings/array," *Solar energy,* vol. 100, pp. 31-41, 2014.

[94] M. Villalva, J. Gazoli and E. Filho, "Comprehensive approach to modelling and simulation of photovoltaic arrays," *IEEE transaction on power electronics,* vol. 24, no. 5, pp. 1198-1208, 2009.

[95] F. Almonacid, C. Rus, L. Hontoria, M. Fuentes and G. Nofuentes, "Characterisation of Si-crystalline PV modules by artificial nearal networks," *ELSEVIER Renewable Energy,* vol. 34, pp. 941-949, 2009.

[96] J. Hernandez, G. Gordillo and W. Vallejo, "Predicting the behaviour of a grid-connected photovoltaic system from measurements of solar radiation and ambient temepreature," *Applied energy,* vol. 104, pp. 627-537, 2013.

[97] K. Lam, T. Lai, W. Lo and W. To, "the application of dynamic modelling techniques to the grid-connected PV (photovoltaic) systems," *Energy,* vol. 46, pp. 264-274, 2012.

[98] Y. Xu, X. Kong, Y. Zeng and X. Xiao, "A modeling method for photovoltaic cells using explicit equations and optimization algorithm," *Electrical power and energy systems,* vol. 59, pp. 23-28, 2014.

[99] D. Sera and P. Rodriguez, "PV panel model based on datasheet values," *IEEE,* vol. 9, no. 7, pp. 2392-2396, 2007.

[100] M. Molina and E. Espejo, "Modelling and simulation of grid-connected photovoltaic energy conversion systems," *ScienceDrirect,* vol. 39, pp. 8702-8707, 2014.

[101] X. Zhu, Z. Fu, X. Long and Xin-Li, "Sensitivity analysis and more accurate solution of

photovoltaic solar cell parameters," *Solar Energy,* vol. 85, pp. 393-403, 2011.

[102] Y. Xu, X. Kong, Y. Zeng, S. Tao and X. Xiao, "A modelling method for photovoltaic cells using explicit equations and optimization algorithm," *Electrical power and energy systems,* vol. 59, pp. 23-28, 2014.

[103] J. Cubas, S. Pindado and A. Fassahi, "New method for analytical photovoltaic parameter extraction," in *Renewable energy research and applocations*, Madrid, 2013.

[104] M. G. Villalva, J. Gazoli and E. Filho, "Modelling and circuit-based simulation of photovoltaic arrays," *IEEE,* vol. 09, no. 4, pp. 1244-1254, 2009.

[105] *KC200GT high efficiency multicrystal photovoltaic.*

[106] D. GmbH, "DigSilent PowerFactory Application Guide," DigSILENT GmbH, Gomaringen, 2013.

[107] S. Kim, J. Jeon, C. Cho, E. Kim and J. Ahn, "Modelling and simulation of a grid-connected PV generation system for electromagnetic transient analysis," *Solar energy,* vol. 83, pp. 664-678, 2009.

[108] Z. Chen and E. Spooner, "Voltage source inverters for high power variable coltage DC power sources," *IEE,* vol. 148, no. 5, pp. 439-447, 2001.

[109] N. Mohan, M. Undeland and W. Robbins, Power electronics: Converters, Applications, and Design, John Wiley & Sons Inc, 1989.

[110] A. Yazdani and P. Dash, "A control methodology and characterization of dynamics for a photovoltaic (PV) system interfeced with a distribution network," *power delivery,* vol. 24, no. 3, pp. 1538-1551, 2009.

[111] A. Yahya, H. Fadil, F. Giri and H. Erguig, "Advanced control of three-phase grid connected," *IEEE,* pp. 753 - 758, 2014.

[112] A. Cuprtino, J. d. Resende, H. Pereira and S. S. Junior, "A grid-connected photovoltaic system with a maximum power point tracker using passivity-based control applied in a boost converter," *IEEE,* pp. 1-8, 2012.

[113] I. Banu and M. Istrate, "Study on three-phase photovoltaic systems under grid faults," *electrical and power engineering,* vol. 8, pp. 1132-1137, 2014.

[114] K. Manohar and P. Rani, "Mppt and simulation for a grid-connected photovoltaic system and fault analysis," *The international journal of engineering and science,* vol. 1, no. 2, pp.

158-166, 2012.

[115] S.-K. Kim, J.-H. Jeon, C.-H. Cho, E.-S. Kim and J.-B. Ahn, "Modeling and simulation of a grid-connected PV generation system for electromagnetic transient analysis," *Solar Energy,* vol. 83, pp. 664-678, 2009.

[116] Y. Tian, B. Xia, Z. Xu and W. Sun, "Modified asymmetrical variable step size incremental conductance maximum power point tracking method for photovoltaic systems," *Power electronics,* vol. 14, no. 1, pp. 156-164, 2014.

[117] A. Yazdani, A. D. Fazio, H. Ghoddami, M. Russo, M. Kazerani, J. Jatskevich, K. Strunz, S. Leva and J. Martinez, "modelling guidlines and a benchmark for power system simulation studies of three-phase single-stage photovoltaic systems," *IEEE Trnsactions on power delivery,* vol. 26, no. 2, pp. 1247-1263, 2011.

[118] T. Neumann and I. Erlich, "Short circuit contribution of a Photovoltaic power plant," *Institute of electrical power systems.*

[119] S. S. Mohammed, "Modelling and Simulation of Photovoltaic module using Matlab/Simulink," *International Journal of Chemical and Environmental Engineering,* vol. 2, no. 5, 2011.

[120] Anne, Labouret, Michel and Villoz, Energie photovoltaıque 3rd edition, Dunod, 2006.

[121] B. Karanayi, V. Agelidis and J. Pou, "Evaluation of DC-link Decoupling Using Electrolytic Evaluation of DC-link Decoupling Using Electrolytic Evaluation of DC-link Decoupling Using Electrolytic," *IECON,* pp. 1-7, 2013.

[122] B. Alexis, Rey-Boue, R. Gaecia-Valverde, A. d. Francisco, Ruz-Vila and M. Jose, "An intergrative approach to the design methodology for 3-phase power conditioners in photovoltaic grid connected systems," *Energy Conversion and management,* vol. 56, pp. 80-95, 2012.

[123] K. Kennerud, "Analysis of perfomance degradationin Cds solar cells," *Aerospace and electronic systems,* vol. 5, no. 6, p. 6, 1969.

APPENDIX A

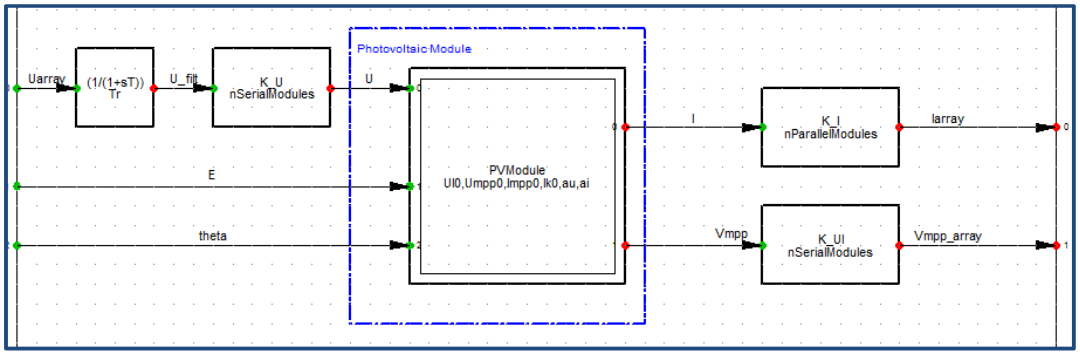

Figure 8-1 PV array block in PF

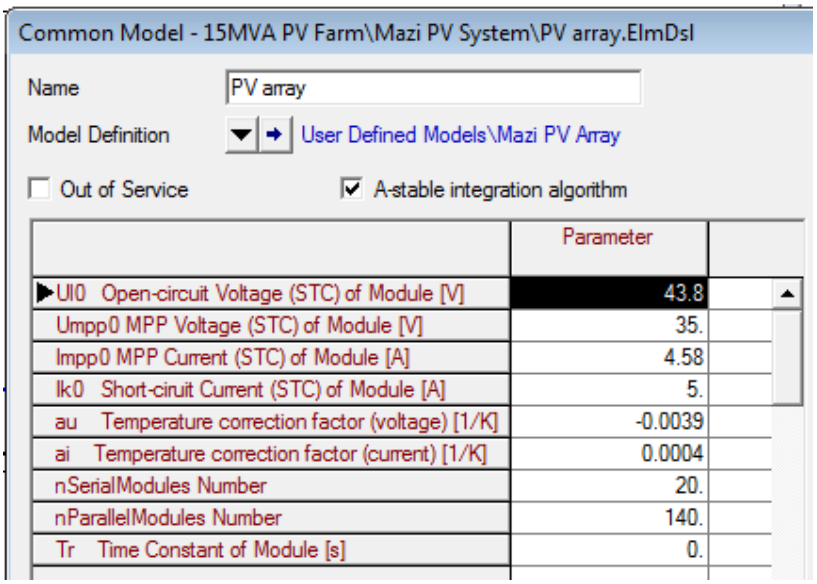

Figure 8-2: Modelling parameters

DSL code: modelling PV module

```
!-----------------------------------------!
!  Model of a Photovoltaic Module         !
!     - Current Voltage Characteristic    !
!     - Dependency of Solar Radiation,    !
!       valid for E >> 1 W/m²             !
!     - Dependency of Module Temperature  !
```

```
!----------------------------------------!
!vardef(Ul0)   = 'V';   'Open-circuit Voltage (STC)'
!vardef(Ik0)   = 'A';   'Short-ciruit Current (STC)'
!vardef(Umpp0) = 'V';   'MPP Voltage (STC)'
!vardef(Impp0) = 'A';   'MPP Current (STC)'
!vardef(au)    = '1/K'; 'Temperature correction factor (voltage)'
!vardef(ai)    = '1/K'; 'Temperature correction factor (current)'
!vardef(Ul)    = 'V'; 'Open-circuit Voltage'
!vardef(Ik)    = 'A'; 'Short-ciruit Current'
!vardef(Umpp)  = 'V'; 'MPP Voltage'
!vardef(Impp)  = 'A'; 'MPP Current'
!vardef(Pmpp)  = 'W'; 'Power at MPP'
!vardef(U)     = 'V'; 'Voltage'
!vardef(I)     = 'A'; 'Current'
!vardef(P)     = 'W'; 'Power'
inc(E)=1000
! Constants / Konstanten
! inc(lnEstc) = ln(1000)                    ! ln of E at STC
! inc(ImppIk) = ln(1-Impp0/Ik0)
! !---------------------------------
! Temperature Dependency:
tempCorrU = 1+au*(theta-25)                 ! Voltage Correction Factor
tempCorrI = 1+ai*(theta-25)                 ! Current Correction Factor
! Open-circuit voltage:
! E_help  = max(E, 1.0)                     ! to avoid ln(0) in next equation
! lnEquot = select(E>1.0, ln(E_help)/lnEstc, 0.0) ! ln(E)/ln(1000W/m²), if E > 1W/m²
Ul = Ul0*E/1000*tempCorrU                   ! Open-circuit voltage dependent from E and theta
! Short-circuit current:
!Ik = Ik0*E/1000*tempCorrI                  ! Short-circuit current dependent from E and theta
Ik = Ik0*E/1000*tempCorrI     ! Current generation only if E>1 (limitation of model)
Vmpp = U
P = U * I
Vth=1.3806*pow(10,-23)/(1.6022*pow(10,-19))*theta
ng = (Ul - Umpp0 - Vth) / (Vth * ln(Ik / (Ik - Impp0)))
```

```
ns = (Ul - Umpp0) / (Vth * ln(Umpp0 / Vth))
np = (Ik - Impp0) * (Umpp0 - Vth) / (Ik * Vth)
n = min(ng, ns, np)
Rs = (1 / Impp0) * (Ul - Umpp0 - n * Vth * ln(Umpp0 / (n * Vth)))
Rsh = ((Umpp0 - Impp0 * Rs) * Umpp0 - n * Vth * Umpp0) / ((Umpp0 - Impp0 * Rs)
& * (Ik - Impp0) - n * Vth * Impp0) - Rs
alpha = (Umpp0 + n * Vth - Impp0 * Rs) / (n * Vth)
beta = (Ik * (Rs + Rsh) - Ul) / (Ik * (Rs + Rsh) - 2 * Umpp0)
ng1 = (Ul - Umpp0 - Impp0 * Rs) / (Vth * ln((Ik * (Rs + Rsh) - Ul) /
& ((Ik - Impp0) * (Rs + Rsh) - Umpp0)))
np1 = ((Ik - Impp0) * (Umpp0 - Impp0 * Rs)) / (Vth * Ik)
ns1 = (Ul - Umpp0) / (Vth * ln(alpha * beta))
n1 = min(ng1, np1, ns1)
alpha1 = (Umpp0 + n1 * Vth - Impp0 * Rs) / (n1 * Vth)
beta1 = (Ik * (Rs + Rsh) - Ul) / (Ik * (Rs + Rsh) - 2 * Umpp0)
Rs1 = (1 / Impp0) * (Ul - Umpp0 - n1 * Vth * ln(alpha1 * beta))
Rsh1 = ((Umpp0 - Impp0 * Rs1) * Umpp0 - n1 * Vth * Umpp0) /
&((Umpp0 - Impp0 * Rs1) * (Ik - Impp0) - n1 * Vth * Impp0) - Rs1
ng2 = (Ul - Umpp0 - Impp0 * Rs1) / (Vth * ln((Ik * (Rs1 + Rsh1) - Ul) /
& ((Ik - Impp0) * (Rs1 + Rsh1) - Umpp0)))
np2 = ((Ik - Impp0) * (Umpp0 - Impp0 * Rs1)) / (Vth * Ik)
ns2 = (Ul - Umpp0) / (Vth * ln(alpha1 * beta1))
n2 = min(ng2, np2, ns2)
alpha2 = (Umpp0 + n2 * Vth - Impp0 * Rs1) / (n2 * Vth)
beta2 = (Ik * (Rs1 + Rsh1) - Ul) / (Ik * (Rs1 + Rsh1) - 2 * Umpp0)
Rs2 = (1 / Impp0) * (Ul - Umpp0 - n2 * Vth * ln(alpha2 * beta1))
Rsh2 = ((Umpp0 - Impp0 * Rs2) * Umpp0 - n2 * Vth * Umpp0) /
&((Umpp0 - Impp0 * Rs2) * (Ik - Impp0) - n2 * Vth * Impp0) - Rs2
ng3 = (Ul - Umpp0 - Impp0 * Rs2) / (Vth * ln((Ik * (Rs2 + Rsh2) - Ul) /
& ((Ik - Impp0) * (Rs2 + Rsh2) - Umpp0)))
np3 = ((Ik - Impp0) * (Umpp0 - Impp0 * Rs2)) / (Vth * Ik)
ns3 = (Ul - Umpp0) / (Vth * ln(alpha2 * beta2))
n3 = min(ng3, np3, ns3)
alpha3 = (Umpp0 + n3 * Vth - Impp0 * Rs2) / (n3 * Vth)
```

Rs3 = (1 / Impp0) * (Ul - Umpp0 - n2 * Vth * ln(alpha3 * beta2))

Rsh3 = ((Umpp0 - Impp0 * Rs3) * Umpp0 - n3 * Vth * Umpp0) /

&((Umpp0 - Impp0 * Rs3) * (Ik - Impp0) - n3 * Vth * Impp0) - Rs3

n4 = (Ul - Umpp0 - Impp0 * Rs2) / (Vth * ln((Ik * (Rs2 + Rsh2) - Ul) /

& ((Ik - Impp0) * (Rs2 + Rsh2) - Umpp0)))

IL = Ik*(Rs2+Rsh2)/Rsh2

I0=(Ik*(Rs2+Rsh2)-Ul)/Rsh2*exp(-Ul/(n4*Vth))

I=IL-I0*(exp((Vmpp+IL*Rs2)/(n4*Vth))-1)-(Vmpp+IL*Rs2)/Rsh2

! Limits

limits(Ul0) = (0,]

limits(Umpp0) = (0,]

limits(Impp0) = (0,]

limits(Ik0) = (0,]

limits(E) = [0,]

APPENDIX B

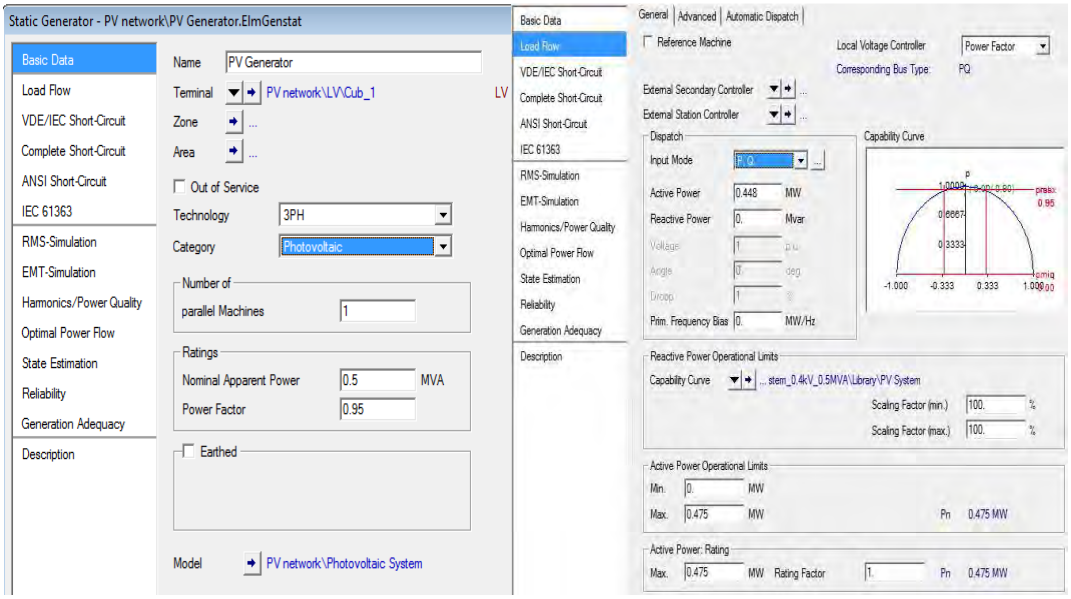

Figure 8-3: Static generator basic tab and load flow tab for steady state conditions

APPENDIX C

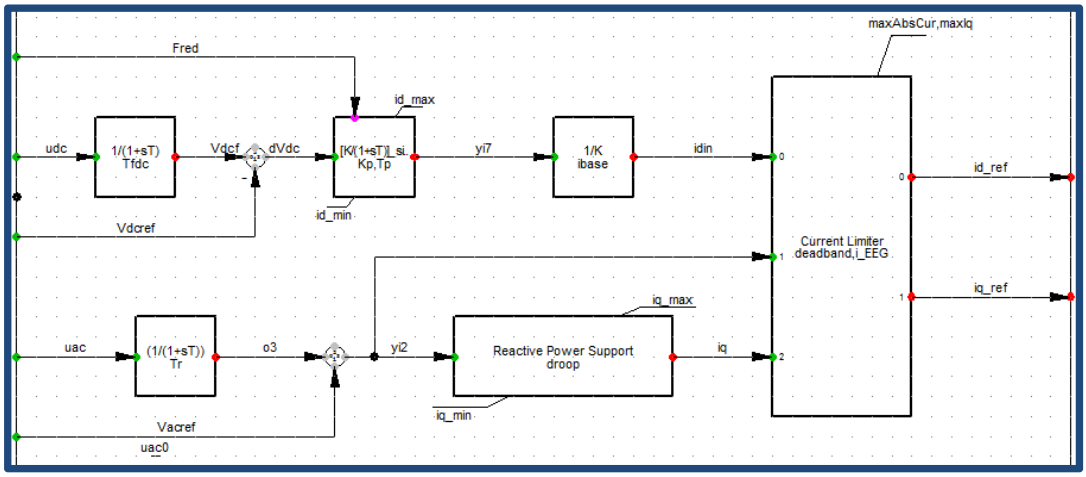

Figure 8-4: Controller on PF